THE ROLE OF OXYGEN VACANCIES IN THERMOLUMINESCENCE PROCESSES IN Al_2O_3:C

By

JERIMY CLIFFORD POLF

Bachelor of Science

Oklahoma State University

Stillwater, Oklahoma

1998

Submitted to the Faculty of the
Graduate College of the
Oklahoma State University
in partial fulfillment of
the requirements for
the Degree of
MASTER OF SCIENCE
May, 2000

THE ROLE OF OXYGEN VACANCIES IN

THERMOLUMINESCENCE

PROCESSES IN Al_2O_3:C

Thesis Approved:

Thesis Adviser

Dean of the Graduate College

ACKNOWLEDGEMENTS

I would like to think a number of people for helping me to realize my potential and helping me to reach this point in my life. First of all, I would like to thank Dr. McKeever for giving a clueless, slow-to-comprehend undergraduate a job. Over the years working in Dr. McKeever's research group, I have learned so many things, many of which have nothing to do with my research. Everything I have learned form Dr. McKeever and everyone in the research group, I believe will prove to be invaluable to me in the future. I would also like to think all of my professors that gave me too much homework, and test questions that seemed next to impossible to solve. It was during the long nights of problem solving and studying that I gained an understanding of Physics and an understanding to approach and solve any possible problem that I will ever face. Also, I would like to thank Dr. Martin and Mr. Charles Hunt for letting me use the spetrcophotometer, and the cutting and polishing equipment in the Crystal Growth Lab.

Also, I think that it is important to mention the importance of the 3M corporation for their continued production of Duct Tape, black electrical tape, and double sticky tape. Without these three items I believe that none of my experiments would have been possible. Whenever an experiment was not aligned correctly or light from an outside source was leaking into the sample chamber, the best fixes always involved some the use of some combination of these three items.

Next I would like to thank every member of my family for supporting me even when I was less than appreciative of it. I believe that without my father's example of hard work, determination, and perseverance, I never would have had the bull-headed, refusal to quit needed to reach this point in my life. Thank you to Trey, Hunter, Lyndsey, Carissa, Jessica, and Amanda for being there to give me someone to try and inspire to work hard for what they want. Whenever I was feeling beaten, I knew that if I worked harder and succeeded at what I was doing, that it might show my cousins and nieces that they can have whatever they if want they work hard and never quit

Finally, I would very much like to thank a group of men that may have just saved my life. To my brothers at the Beta Kappa chapter of the Phi Kappa Tau Fraternity, THANK YOU. You came into my life when I was headed in the wrong direction. Thanks to you guys, I had a reason to work hard and stay in school. You helped me when the classes were a little too hard, and taught me how to be a successful college student. Most importantly, you helped me to break my drug habits, and taught me to respect myself and my work. It was you guys that showed me how to be successful. I thank you for from the bottom of my soul for saving me from myself, and providing me with the support of a family when I needed it.

TABLE OF CONTENTS

LIST OF TABLES

LIST OF FIGURES

Chapter 1

Introduction

1.1 General History of Radiation Dosimetry

The field of modern radiation dosimetry had its beginnings in the late 1940's and early 1950's with the work of Randall & Wilkins, Garlick & Gibson, and Daniels as well as many others [1.1]. Research on luminescence produced during thermal stimulation of materials following their irradiation led Daniels and his research group at the University of Wisconsin to the observation that the intensity of luminescence produced by a material during heating increased with the dose of radiation absorbed by the material. This led them to suggest the use of the luminescence signal produced during heating as a tool for radiation dosimetry.

Since that time the application of luminescence techniques to the field of radiation dosimetry has grown immensely. Luminescence dosimeters have been produced for the measurement of heavy particles such as neutrons and alpha particles as well as high-energy photons such as X-rays and gamma rays [1.2]. This work has led to the advancement of two types of luminescence as dosimetry techniques. These are thermally stimulated luminescence known as thermoluminescence (TL) and optically stimulated luminescence (OSL). These two techniques have been widely used in the field of commercial radiation dosimetry and shall be discussed in greater detail in the chapter

two. For now we simply note the particular importance of TL and OSL to the field of radiation dosimetry as well as to the work presented in this thesis.

Through the years great effort has been expended in the search for suitable materials for application in TL and OSL radiation dosimetry. Although numerous materials have been studied, by far the most widely used material has been lithium fluoride (LiF). Since its first use in the 1950's in atomic bomb research LiF has been a popular material in both commercial and research applications of thermoluminescence dosimetry (TLD). However, the complicated nature of the TL signal of LiF has helped to fuel the search for alternative materials for use in dosimetric purposes. Over the years numerous materials have been suggested as alternatives. These materials include beryllium oxide (BeO), calcium sulphate doped with Dy and Tm ($CaSO_4$:Dy, $CaSO_4$:Tm), calcium fluoride (CaF) doped with several different types of impurities just to name a few of the more popular ones [1.3]. In particular, an increasingly popular material is aluminum oxide (Al_2O_3) which is the subject of the research presented in this thesis.

1.2 Aluminum Oxide for use in radiation dosimetry

The use of aluminum oxide (Al_2O_3) was suggested as an alternative to LiF as early as 1957 by Daniels, but was soon rejected because of its lack of sensitivity of the TL signal [1.3]. Over the years several forms of Al_2O_3, varying mostly in the type of dopants, have been tested and used with limited success in the area of TL dosimetry. It wasn't until the introduction of carbon-doped aluminum oxide (Al_2O_3:C) that this material began to see widespread use in the area of TL dosimetry [1.3].

Since then, Al_2O_3:C has been widely used in many forms in both the research and commercial arenas. Popular forms include single crystals consisting usually of a disk five millimeters in diameter and one millimeter thick cut directly from the as-grown crystal, and powders consisting of the as-grown crystal uniformly ground to grains of about 100 microns in size. Also, Al_2O_3:C has been grown with several types of additional dopants for the purpose of maximizing its efficiency. Several of these dopants include titanium, magnesium, chromium, silicon, yttrium, and nickel.

Al_2O_3:C is grown from the melt in the format of single crystal rods. The crystals produced by this method contain certain intrinsic impurities that are unintentionally introduced during the growth process, as well as those intentionally introduced as dopants. Common intrinsic impurities include iron, silicon, calcium, chromium, and titanium [1.4]. These impurities are products of the growth process and are present in a dosimetry quality crystal only in trace amounts. The added dopants are added in controlled amounts, and are found in concentrations ranging from as little as ten parts per million to as much as several thousand parts per million [1.4]. Crystal growth is carried out in a highly reducing atmosphere in the presence of carbon as well as any other desired dopants added to the melt. As the growth proceeds, the presence of carbon in the process catalyses the production of oxygen vacancies in the crystal [1.5]. It is these vacancies that are responsible for the luminescence produced by Al_2O_3:C during a TL or OSL measurement.

Since the introduction of carbon-doped aluminum oxide, it has been used in several types of TL and OSL dosimeters. In particular, it has proven to be a quite versatile material for application to the measurement of dose from high-energy photons.

Al_2O_3:C dosimeters are now commercially available for measurement of absorbed dosed of gamma rays, beta particles, X-rays and UV light.

1.3 This Thesis

In order to develop a material for the application of thermoluminescence dosimetry (TLD) or optically stimulated luminescence dosimetry (OSLD) it is necessary to understand the nature of its defects. It is important to know the changes in the properties of these defects during thermal or optical stimulation to clearly understand the processes that produce the luminescence signal. Knowledge of the behavior of these defects will give us the understanding necessary to better engineer Al_2O_3:C for luminescence dosimetry, as well as design OSLD and TLD techniques better tailored to the luminescence signal of the material.

In the case of Al_2O_3:C, the defects of interest are the oxygen vacancies produced in the crystal growth process. An oxygen vacancy leaves the crystal lattice with a 2+ charge imbalance in the local region around the vacancy. This leads to the vacancy being filled with two electrons to restore the local charge balance. A vacancy filled with two electrons is known as an F center. A vacancy filled with one electron (leaving an overall 1+ charge imbalance) is known as an F+ center. This process would involve either the recombination of an electron with an F+ center to produce an excited F center, or the recombination of a hole with an F center to produce an excited F+ center. Either of the excited vacancies will relax to lower state of energy via a radiative process producing luminescence [1.5].

Exposure of Al_2O_3:C to radiation causes electrons to be ionized into the conduction band and holes to be ionized into the valence band. The ionized electron and

hole are then free to move around the crystal lattice where they may encounter a defect center that has the ability to trap the ionized charges (electron/holes). The energy level of a charge trapped at a defect site will be less than the energy of a free charge. The difference in energy of these two states is known as the activation energy of the site. A charge can be trapped at a defect site by the coulumbic potential of the site. The trapped charge will then relax into the ground state of the site possibly producing luminescence. Stimulation (typically by thermal or optical means) comparable to the activation energy of the defect site may release the charge from the trap site where it is again free to move about the lattice. The charge may then encounter an F or F+ center where recombination will take place. This process gives the basis for the TL and OSL process observed in irradiated Al_2O_3:C. A detailed discussion of TL and OSL processes will be given in Chapter 2.

The position and shape of the TL signals, which is known as the TL glow curve, has been studied in great detail and these properties are well known for Al_2O_3:C. However, it is not well known whether the trapped charges released during thermal stimulation are electrons or holes. The purpose of this research is to gain a deeper understanding of the luminescence processes in Al_2O_3:C through the monitoring of the changes in F and F+ center concentrations while the sample is heated during a TL measurement. For this research the following experimental techniques were used to obtain information about the charge processes involved in TL (each of these experiments will be explained in greater detail in chapter 3). The optical absorption (OA) spectrum of irradiated Al_2O_3:C was measured in the wavelength region of F and F+ center absorption as the sample was heated. From these measurements the concentrations of F and F+

centers will be determined as a function of anneal temperature. The OA data was then be compared to TL data, the TL emission spectrum, and thermally stimulated conductivity (TSC) data collected from the same samples. From comparison of these measurements, a better understanding of the nature of the recombination process in Al_2O_3:C will be gained.

Chapter 2

Background and Theory

2.1 Energy Bands and Charge Traps

During the formation of a solid, the overlap of atomic potentials due to the close packing of the atoms causes a splitting of the atomic energy levels. This results in the formation of a large number of closely packed energy levels. These levels combine to form continuous energy bands throughout the crystal. The uppermost filled energy levels form the valence bands and the lowest empty levels form the conduction band of the materials.

Electrons in the crystal will occupy energy states in these two bands. The occupancy of each band is given by the density of states function [6]

$$n(E) = Z(E) * f(E) \tag{2.1}$$

where $f(E)$ is the Fermi-Dirac distribution given by the equation

$$f(E) = \frac{1}{(\exp[(E - E_f)/kT] + 1)}. \tag{2.2}$$

From equation 2.1, the density of the occupied energy states is $n(E)$, the density of the available energy states in a particular energy band is $Z(E)$, and E_f is the Fermi level of the crystal. At absolute zero, all the energy states below the Fermi level are occupied, and above all energy states are empty. For non-conducting materials the Fermi level is above the top energy level in the valence band. This results in the valence band being completely filled, and no conduction of charge can take place in the valence band.

For conduction to take place in these materials, an electron must absorb enough energy to be excited into the unoccupied levels of the conduction band. The excitation must be large enough to overcome the energy gap from the top of the valence band to the bottom of the conduction band. A diagram of the band structure is shown in figure 2.1.

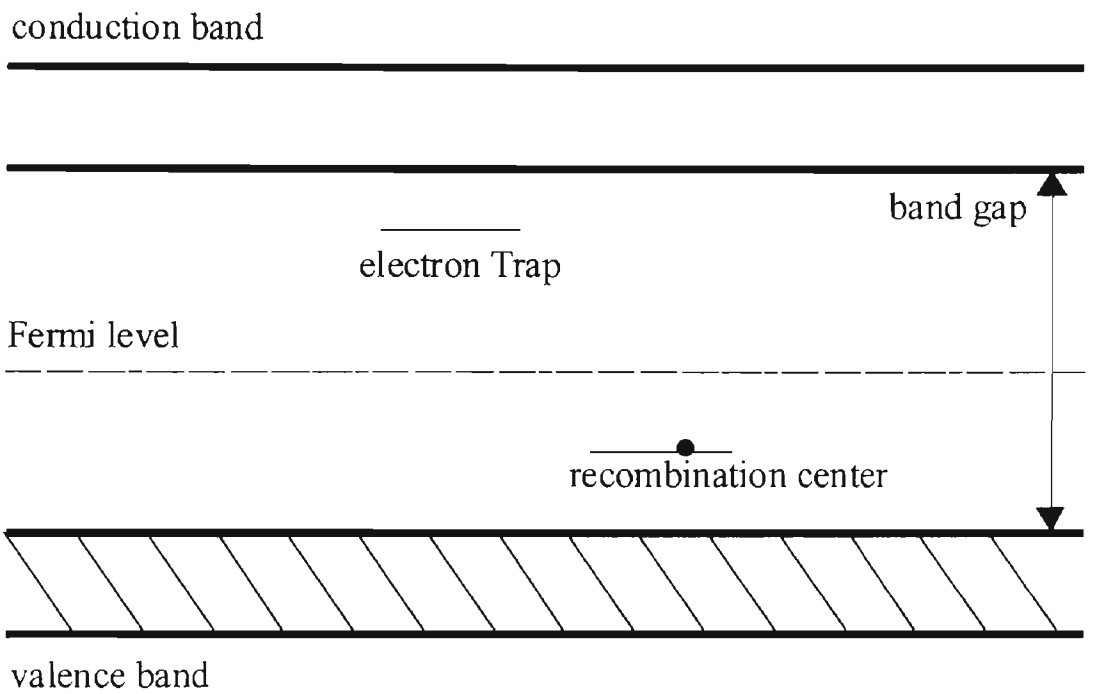

Figure 2.1: Energy band diagram for insulators and semiconductors representing the filled energy states of the valence band, the empty states of the conduction band, and the relation of electron traps and recombination centers to the Fermi level.

For an ideal crystal, the only allowed energy levels would be those contained in the valence and conduction bands. Energy levels in between these two bands are not allowed and are said to be "forbidden." In real crystals, the lattice will contain occasional defects. These defects include atoms displaced from a lattice site, or interstitial atoms, along with atoms missing from a lattice site, or vacancies, and also impurity atoms that substitute in place of the regular atoms in the lattice [2.1]. The occurrence of defects will

cause the creation of forbidden energy levels within the energy gap (or band gap). The forbidden energy level created by the defect is only present locally near the defect. Therefore the energy levels arising due to these defects are known as localized states.

For the case of wide band gap semiconductors and insulators the localized states can play two roles in the production of luminescence. These are the roles of charge trap, and recombination center. For the most part, a localized state with an energy level below the Fermi level will be considered a recombination center due to the high probability of a free charge recombining at this localized center. A localized state with an energy level above the Fermi level will be considered a trap due to the high probability of a free charge becoming trapped at this site. The relative locations of the traps and recombination centers in the band gap are shown in figure 2.1.

2.2 Concepts of Thermoluminescence in Solids

Luminescence in a material is produced following the absorption of energy from an external source. This luminescence takes place in the form of emission of light from the sample. Absorption of sufficient energy can excite charge carriers in the form of electrons (e) and holes (h) into the valence and conduction bands respectively. These charges are free to move about in the delocalized bands until they either recombine with each other or become trapped at some localized state with an energy level within the band gap. Emission from a material may be described as either fluorescence or phosphorescence depending on whether the excited state between absorption of energy and production of emission due to recombination involves the charge being trapped in a metastable state or not. If emission occurs due to the being excited to a higher energy state, but not ionized, then the emission due to relaxation of the center is known as

fluorescence [1.2]. If however, the return to the ground state is delayed due to the transition of the charge into and out of a localized state before recombination and emission occur, then this type of emission process is known as phosphorescence.

Emission in a phosphorescent process may be greatly delayed depending on the energy level of the localized state into which the charge makes a transition. If a transition into a localized state m occurs at a temperature T, where the energy ΔE (known as the activation energy of the trap) of separation between m and the excited state is greater than several $k_b T$ (k_b is Boltzmann's constant), then the charge is likely to stay trapped in m for an extended period of time. Given a Maxwellian distribution of trap energies, the probability p per unit time for thermal excitation from the trap is exponentially dependent on the temperature according to

$$p = s * \exp[\frac{-\Delta E}{k_b T}] \tag{2.3}$$

where s is a constant with units reciprocal time and ΔE is the activation energy of the trap [1.2]. Therefore it is seen that the key feature in the production of phosphorescence is the amount of time the charge spends in the localized trap. Then from equation 2.3, the lifetime of the trap can be seen to last as long as the temperature T is low enough to sufficiently slow down the thermal emission rate.

Taking from the work done by Randall and Wilkins [2.2] on the production of luminescence, the rate of thermal excitation of electrons from a trap can be written by the equation

$$-\frac{dn}{dt} = n * s * \exp[\frac{-\Delta E}{k_b T}] \tag{2.4}$$

with n equal to the concentration of trapped electrons, where the constant s is now known as the frequency factor with units of inverse seconds, and the negative sign indicating a loss of trapped electrons. Furthermore, the assumption is made that only one trap and one recombination center take place in the luminescence process and that released electrons can only recombine and cannot re-trap at the trapping site. Under these conditions, the intensity of the luminescence will be seen to depend upon the rate of recombination, which is equal to the rate of electron detrapping and can be given by the equation.

$$I(t) = -\frac{dn}{dt} = -\eta * n * s * \exp[\frac{-\Delta E}{k_b T}] \tag{2.5}$$

where η is the luminescence efficiency of the material and is often a constant.

Electrons trapped in a localized state with activation energy such that $\Delta E \gg k_b T$ will require an input of external energy to de-trap the electron. If that energy is supplied by raising the temperature of the sample at an arbitrary rate, the probability that the electron will be released from the trap will increase according to equation 2.3 producing an increase in the luminescence emission. Since this emission is due to the increase in temperature, it is called thermoluminescence (TL) (which should more appropriately be called thermally stimulated luminescence (TSL)). During such a TL measurement the luminescence will increase until the population of trapped electrons is depleted. After this point as the temperature is increased further, the luminescence will fall off producing a characteristic TL peak with a maximum at a temperature that is related to the activation energy ΔE of the trap, the frequency factor s, and the heating rate β [2.2].

A TL measurement requires the pertubation of the system from thermodynamic equilibrium by the absorption of energy usually in the form of ionizing radiation. This

ionizing radiation causes the trapping of electrons and holes in a metastable state lying above the Fermi level and are typically empty. This is then followed by the thermally assisted release and recombination of electrons and holes which is accompanied by the measurement of the emission produced in the sample during relaxation of the recombination centers back to their ground state [2.3].

In order to describe a simple TL process, we will make several definitions and assumptions. First of all we define that the heating of the sample during measurement be preformed at a linear rate according to the equation $T(t) = T_o = \beta t$, where T_o is the initial temperature. Also, we adopt the definition of trapping states to be those at which the probability of transition of the trapped charge into the delocalized band is greater than the probability of recombination of a free charge of opposite sign. Conversely, the definition of a recombination center is defined as a site with a greater probability of recombination occurring than thermal release from the site. Then we make the assumptions that all transitions out of the localized traps take place via the delocalized bands. Also, transitions of electrons from the conduction band into localized traps are nonradiative producing only phonons, and transitions of electrons from the conduction band into recombination sites (trapped holes) are radiative producing photons. Finally, assuming for this treatment of TL that the only type of charge that is released during heating are electrons. We note here that, it could have just as easily been assumed that only holes are released during heating.

From the above assumption that no trapped holes are released during heating, we see that the only way that the trapped hole concentration (n_h) changes is through

recombination. This allows us to define the luminescence intensity as the change in the recombination centers n_h. Using these assumptions, we can express the luminescence intensity as

$$I_{TL} = -\frac{dn_h}{dt}. \tag{2.6}$$

During irradiation, we see that electron-hole pairs are created which can be trapped at electron trap and hole trap (recombination) sites. After this, the sample is heated to release the trapped charges and produce the TL emission. The trapping, release, and recombination processes are shown in figure 2.2. We can develop a picture of the TL process by the development of expressions for the change in the number of trapped electrons, trapped holes and free electrons in the conduction band during heating. Expressions for the changes in these quantities can be expressed by the equations

$$\frac{dn}{dt} = -ns * \exp[\frac{-\Delta E}{k_b T}] + n_c(N_t - n)A_t \tag{2.7}$$

$$\frac{dn_h}{dt} = -n_c n_h * A_r \tag{2.8}$$

$$\frac{dn_c}{dt} = \frac{dn_h}{dt} - \frac{dn}{dt} \tag{2.9}$$

where n_c is the concentration of free electrons in the conduction band, n_h is the concentration of holes trapped at recombination sites, N_t is the total number of traps, A_t and A_r are the transition coefficients of free electron and free holes respectively, and all other quantities remain as previously defined. The transition coefficients A_r and A_t are defined as the product of the thermal velocities of the respective charge carriers and the capture cross section of the centers. Also, since electrons and holes are created in pairs, the total number of holes and electrons present in the sample will be equal and expressed

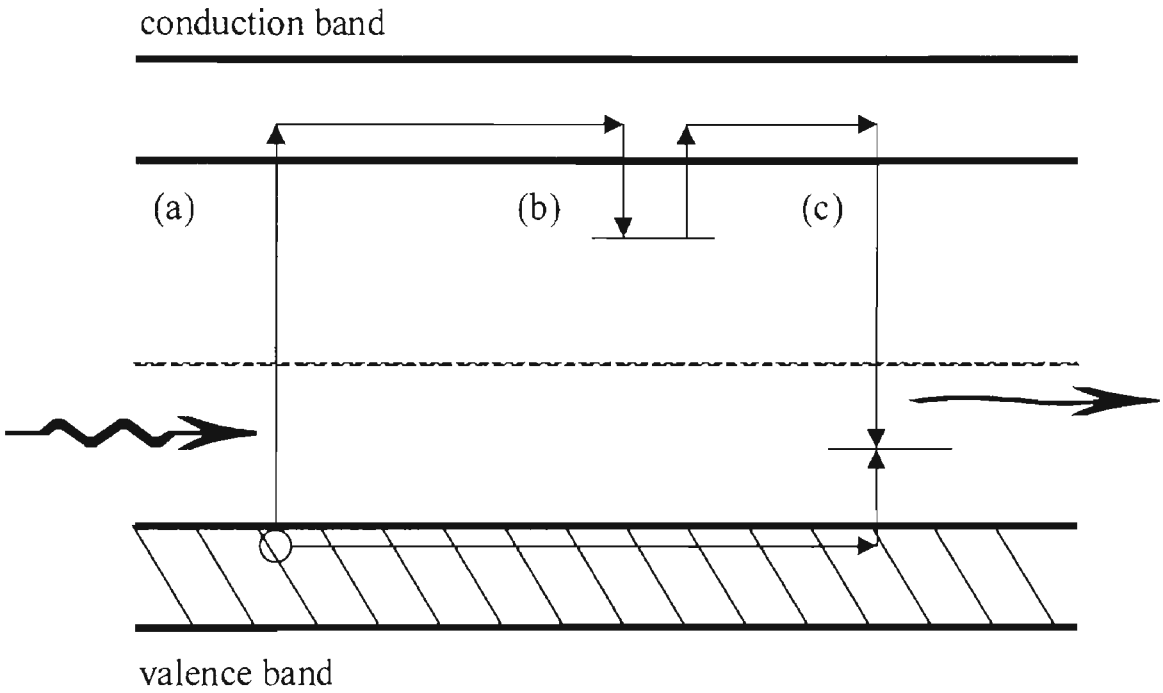

Figure 2.2: (a) Generation of electron-hole pairs by irradiation, (b) trapping of electrons, and (c) release of electrons and recombination of electron-hole pairs to produce emission.

by the equation

$$n + n_c = n_h . \tag{2.10}$$

Equations 2.7 – 2.9 are the rate equations representing the movement of charge during the heating cycle of a TL measurement. These equations are non-linear, coupled, first order differential equations and are in general analytically insoluble. To develop an analytic expression for the TL intensity as a function of temperature ($I_{TL}[T]$), several assumption must be made to further simplify the above differential equations.

One important assumption is that of "quasi-equilibrium" (QE). This assumption requires that the number of electrons in the conduction band be changing much slower than the number of trapped charges. This assumption is expressed by the equations

$$\frac{dn_c}{dt} \langle\langle \frac{dn}{dt}, \tag{2.11}$$

$$n_c \langle\langle n . \tag{2.12}$$

Applying the approximation made in equation 2.11 to equation 2.9 yields the relation

$$\frac{dn_h}{dt} \approx -\frac{dn}{dt} . \tag{2.13}$$

Substituting equations 2.7 and 2.8 into equation 2.13 and solving for n_c gives,

$$n_c = \frac{ns * \exp[\frac{-\Delta E}{k_b T}]}{n_h A_r + (N_t - n) A_t} \tag{2.14}$$

Substituting this result into equation 2.8 and using equation 2.6 for the TL intensity we get,

$$I_{TL} = -\frac{dn_h}{dt} = sn * \exp[\frac{-\Delta E}{k_b T}] \{ \frac{n_h A_r}{n_h A_r + (N_t - n) A_t} \} \tag{2.15}$$

For this equation to be useful for predicting TL intensities, one must still know the concentration of trapped electrons (n). In order to find this one can make the substitution from equation 2.13 into 2.15 to get,

$$I_{TL} = \frac{dn}{dt} = sn * \exp[\frac{-\Delta E}{k_b T}]\{\frac{n_h A_r}{n_h A_r + (N_t - n)A_t}\}. \tag{2.16}$$

Rewriting this expression gives,

$$I_{TL} = sn * \exp[\frac{-\Delta E}{k_b T}]\{1 - \frac{(N_t - n)A_t}{n_h A_r + (N_t - n)A_t}\} \tag{2.17}$$

Equations 2.16 and 2.17 is known as the general-one-trap (GOT) expression for TL emission [2.4], [2.5]. It is noted that the term in the square brackets if the probability that the thermally released electrons will not be re-trapped, and the ratio $(N - n)A_t/n_hA_r$ is the ratio of the retrapping probability to the recombination probability.

To find a first-order solution to equation 2.17, another approximation is often made regarding the size of the retrapping probabilities and the recombination probabilities. One assumption that is often made is that $n_hA_r \gg (N_t - n)A_t$. That is, the recombination probability is much greater than the retrapping probability. With this assumption equation 2.16 becomes,

$$I_{TL} = \frac{dn}{dt} = sn * \exp[\frac{-\Delta E}{k_b T}]. \tag{2.18}$$

This equation can now be integrated over the temperature range of the TL measurement. Using from the assumptions above a constant heating rate so that $T = T_o + \beta t$, the expression for n is given by,

$$n = n_o * \exp[-\frac{s}{\beta}\int_{T_o}^{T}\exp[\frac{-\Delta E}{k_b\theta}]d\theta] \tag{2.19}$$

where n_o is the initial concentration of trapped electrons. Substituting this value back into equation 2.18, the TL intensity is found to be,

$$I_{TL} = sn_o \exp[\frac{-\Delta E}{k_b T}] * \exp[-\frac{s}{\beta}\int_{T_o}^{T}\exp[\frac{-\Delta E}{k_b\theta}]d\theta]. \tag{2.20}$$

This is the well known Randall-Wilkins [2.2] equation for the TL intensity. Equation 2.20 represents a first-order expression for intensity since it depends on the first power of the carrier concentration. The first-order TL intensity equation 2.20 produces asymmetric peaks with the peak position depending on the activation energy and frequency factor. The shape of the first order TL intensity peak is shown in figure 2.3.

This first-order expression was derived using the assumption that recombination dominated over retrapping during heating. For the case when the opposite is true, that is, when retrapping dominates over recombination ($n_h A_r \ll (N_t - n)A_t$) along with the assumptions that the number of electron traps is much larger than the number of trapped electrons ($N_t \gg n$) and the number of trapped electrons equal the number of trapped holes ($n = n_h$), we se that equation 2.18 becomes,

$$I_{TL} = \frac{dn}{dt} = s(\frac{A_t}{N_t A_r})n^2 * \exp[\frac{-\Delta E}{k_b T}]. \tag{2.21}$$

Note that equation 2.21 depends on n^2 and represents a second-order expression for the TL intensity. Considering the additional assumption that $A_t = A_r$, equation 2.21 can be integrated to yield,

$$I_{TL} = (\frac{n_o^2}{N_t})s * \exp[\frac{-\Delta E}{k_b T}] * \{1 + (\frac{n_o s}{\beta N_t})\int_{T_o}^{T}\exp[\frac{-\Delta E}{k_b\theta}]d\theta\}^{-2}. \tag{2.22}$$

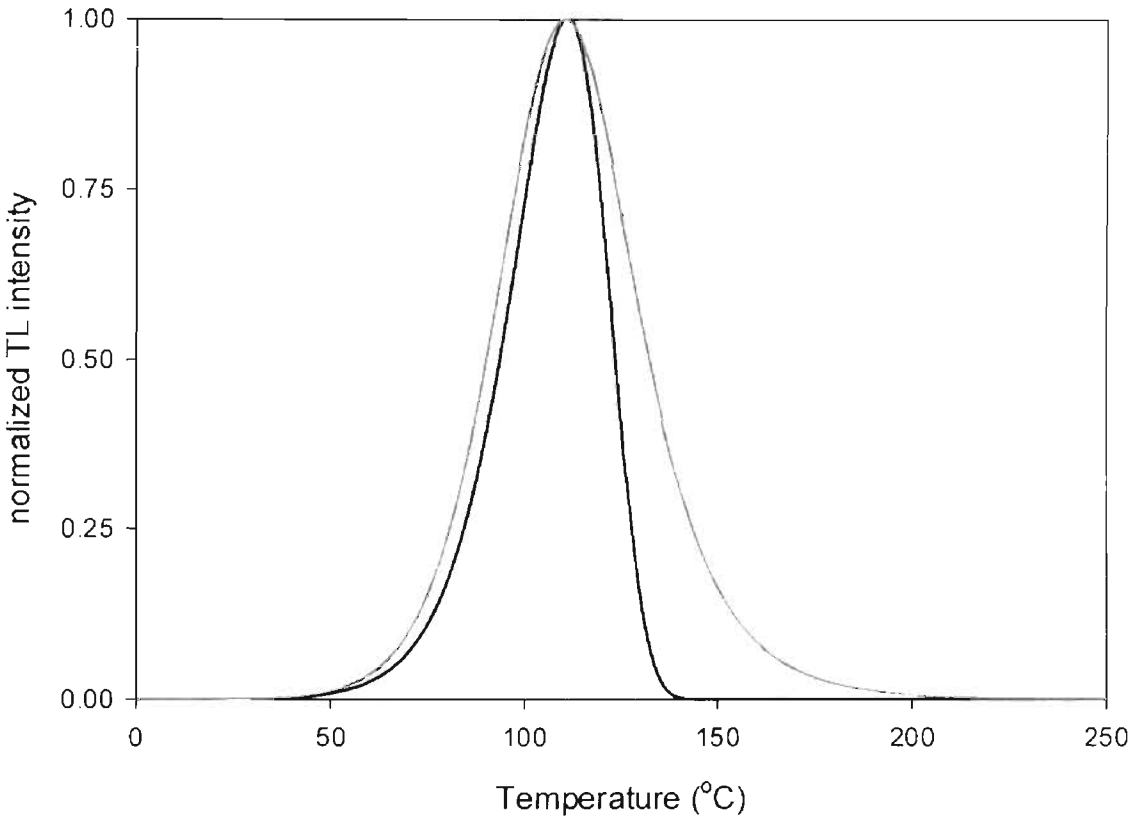

Figure 2.3: First order Randal-Wilkins TL peak generated using equation 2.20 (black) and second order Garlick-Gibson TL peak generated using equation 2.22 (gray).

This is the Garlick-Gibson [2.6] TL expression for second-order kinetics. The second-order expression produces a more symmetric peak shape. This can be understood from the assumption that retrapping dominates over recombination. Therefore large numbers of electrons in the conduction band are re-trapped and re-released before they recombine spreading out the luminescence over a larger temperature range. The shape of the second-order TL peak is shown in figure 2.3.

The Randall-Wilkins and Garlick-Gibson equations were both derived using specific assumptions about the relative recombination and retrapping probabilities. From the forms of equations 2.18 and 2.21 Rasheedy [2.7] proposed an equation for TL intensity of general-order with the form of

$$I_{TL} = \frac{dn}{dt} = (\frac{n^b}{N_t^{b-1}})s * \exp[\frac{-\Delta E}{k_b T}], \tag{2.23}$$

which clearly reduces to first order for the case of $b \rightarrow 1$.

An important assumption of the model presented above is that during heating electrons are ejected from charge traps into the conduction band where they recombine with hole traps. During this process, if an electric field is applied across the sample during heating a thermally stimulated conductivity (TSC) can be measured. Since both the emission an conductivity in the above model are dependent on the number of carriers released into the conduction band, they should be seen to exhibit the same general curve shape. The TSC intensity curve can be seen to follow the shape of a general TL intensity curve. As well as depending on the same parameters as the TL intensity, the TSC intensity will also depend on the applied electric field and the charge mobility of the electrons in the conduction band. A general equation for the TSC intensity can be given by,

$$I_{TSC} = Ae\tau\mu\{I_{TL}\} \tag{2.24}$$

where A is the area of the electrodes applied to the sample, e is the charge of an electron, τ is lifetime of the charge carrier in the delocalized bands, μ is the charge mobility and I_{TL} is the TL intensity given by equation 2.20. From this equation we see that the correlation between TL and TSC peaks is very prominent. It is therefore important to understand the relationship between TL and TSC curves. From equations 2.15 and 2.8 we see that

$$I(t) = -\frac{dn_h}{dt} = n_c n_h A_r . \tag{2.25}$$

At peak intensity for TL we must have that $\frac{dI(t)_{TL}}{dt} = 0$ and differentiating equation 2.25 we get

$$\frac{dI}{dt} = \frac{dn_c}{dt} n_h A_r + n_c \frac{dn_h}{dt} A_r = \frac{dn_c}{dt} n_h A_r - n_c^2 n_h A_r^2 = 0 \tag{2.26}$$

where the second equality follows by plugging equation 2.8 into the second term. For this equation to equal zero,

$$\frac{dn_c}{dt} = n_c^2 A_r > 0 . \tag{2.27}$$

This says that the change in the number of electrons in the conduction band is greater than zero, and therefore the TSC has not peaked yet. Therefore we expect to see the TSC peak at a higher temperature than the TL peak. This is not always the case however, if $\frac{dn_h}{dt} \gg \frac{dn}{dt}$, then $\frac{dn_h}{dt} \approx 0$ and the second term in equation 2.26 will equal zero, and the TL and TSC peaks will again be at the same temperatures. Also the charge mobility (μ) is seen to be temperature dependent in some materials. This will have the affect of

shifting the TSC peak either to higher or lower temperatures according its dependence on temperature.

The simple model described above gives a good basis for understanding TSC and TL kinetics, but real materials are much more complicated. A material described by this simple model would have traps with a single activation energy and would therefore have only one peak. In reality, a number of peaks are observed over the temperature range in the measurement. One extension to the simple model is the idea of a thermally disconnected trap. This trap is one in which the trapped electrons are thermally stable over the temperature range in which the TL or TSC peak is measured. The addition of this trap to the model causes a need to modify the rate equations (equations 2.7 – 2.9) for trap emptying and the charge neutrality equation (equation 2.10) to include its contribution. The important thing to consider when incorporating the thermally disconnected trap, is to remember that the number of electrons de-trapping from the deep trap is zero over the temperature range of the observed peak. It has been shown by Chen [2.5] that the kinetics of TL and TSC reduce to first order when the number of electrons trapped in thermally disconnected traps is much greater than the number trapped in non-disconnected traps. Also, when the number of electrons in the thermally disconnected traps is much less than the number in non-disconnected traps, the kinetics of TL and TSC tended to second order.

2.3 Optical Absorption

The optical absorption spectrum can provide a variety of information about the lattice defects within a material through the analysis of the optical transitions of these defects. The optical transitions are determined by the ground and excited energy states as

well as the oscillator strengths and influence of the surrounding lattice. These properties result in an absorption line with characteristics such as a specific central absorption energy, absorption strength, and line shape. Each of these absorption characteristics are due to certain fundamental properties of the lattice site. From these properties, information such as the type of defect, the type of transitions occurring, and the concentration of these defects in the material can be determined.

The absorption properties of the lattice defects can be best illustrated with a configurational coordinate diagram. A typical diagram for optical absorption at a localized charge center is shown in figure 2.4. In these diagrams, the total energy of the defect is plotted versus the displacement coordinate (Q) of the charge carriers from their equilibrium position. The energy level of the center is estimated to have a parabolic shape centered at a finite minimum energy. As the thermal energy in the lattice increases, the energy of the trapped charge will increase along the energy parabola. The trapped charge can raised be above the minimum of the energy state through the absorption of phonons.. When a center absorbs a photon of energy ($h\upsilon_1$), the localized charge is promoted vertically upward to an excited state. The charge will then thermally relax to the minimum of the excited state via the emission of lattice phonons. Then the charge may emit a photon of energy ($h\upsilon_2$) equal to the difference between the excited state minimum and the ground state at the configuration co-ordinate corresponding to the excited state minimum. For a detailed description of this process the reader is referred to *Semiconductor Devices* by Zamburo [2.8].

Due to the many allowed vibrational modes of a given energy state at a given temperature, absorption does not take place at one given energy. Instead the absorption

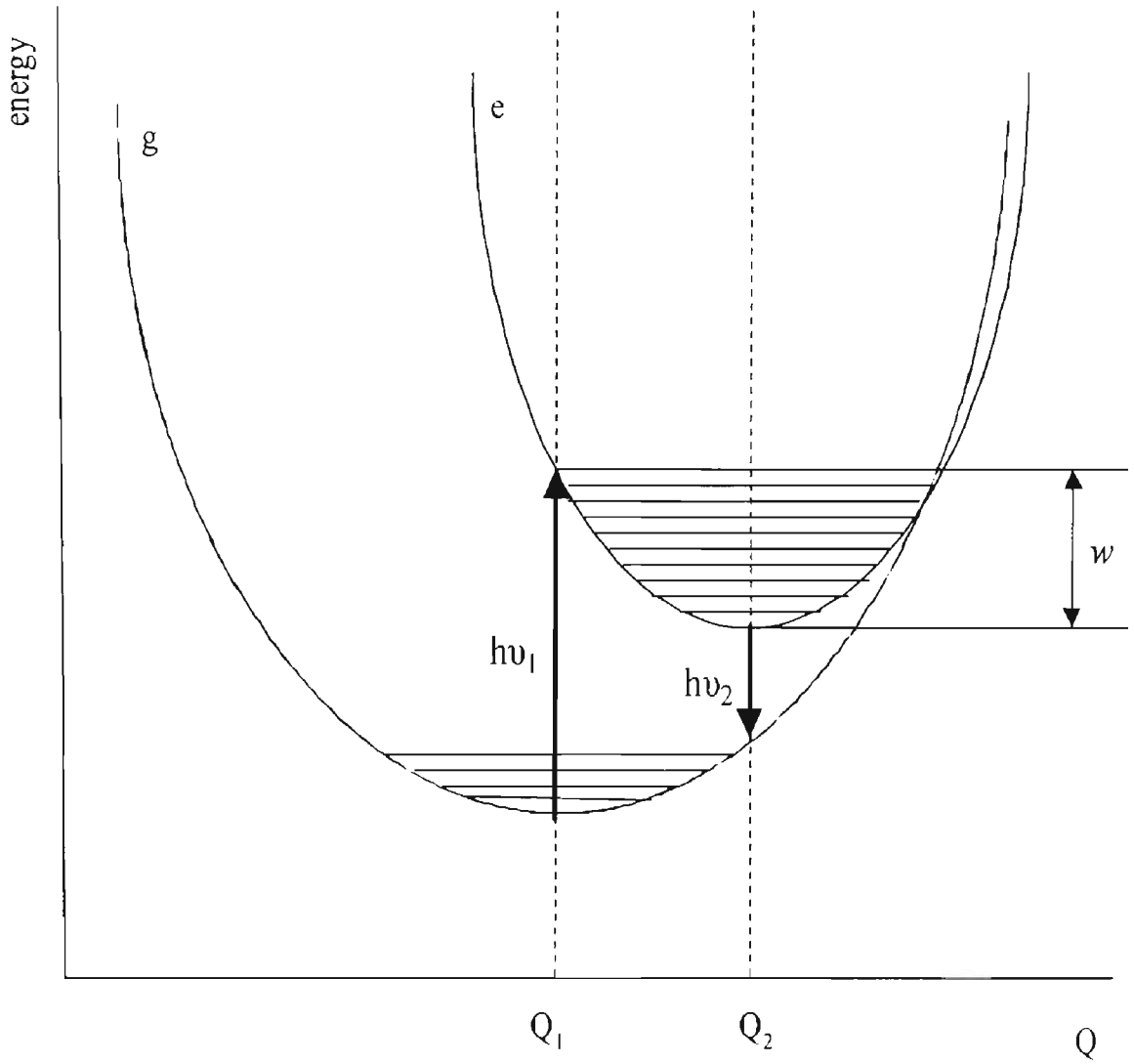

Figure 2.4: A cofigurational coordinate diagram of an electron trap. Optical excitation of an electron into an excited state (e) takes place at the mininimum of the ground state (g) Q_1 by a photon of energy $h\nu_1$ followed by a relaxation to the minimum of the excited state at Q_2 via emission of lattice phonons followed by relaxation to the ground state by the emission of photon of energy $h\upsilon_2$.

takes place over a continuos band of photon energies. As photons of increasing energy are allowed to illuminate a crystal, an absorption curve will be produced. The shape of the curve is dependent on the shape of the energy states and the number of vibrational modes available at a given energy.

It is possible to calculate the concentration of defect centers in a crystal from the strength of the absorption band through the use of Smakula's Formula [2.9]. This formula gives an expression for the shape of the absorption band in terms of the number of absorbing centers per cm^3. Solving this formula for the number of centers per cm^3 (N_c), we get the expression,

$$N_c = \left(\frac{n_i}{(n_i^2 + 2)^2} \right) \frac{An\kappa\alpha_{max}\Gamma}{f}. \qquad (2.28)$$

Where n_i is the index of refraction of the crystal, A = 0.87 x 10^{17}/ cm^3, κ is determined by the absorption lineshape and is $\approx$1, Γ is the full width half max (FWHM) of the absorption peak, f is the oscillator strength, and α_{max} is the maximum absorption value. Using this expression, we can measure the relative changes in defect concentration of a crystal during a TL measurement by measuring the absorption of the defect center while the crystal is heated. Given values for the index of refraction, FWHM, and oscillator strength of a material, we can substitute the measured change in the absorption into Smakula's formula and calculate the change in defect center concentration.

From above, we see that to be able to accurately measure the concentration of a particular defect, we must know the absorption characteristics of the defect. The shape, strength, and position of the absorption band are known to be temperature dependent [2.10]. The maximum value of the absorption band will decrease and shift to higher

energies, and the FWHM of the band will broaden. The band will have a shape that is dependent on the number of vibrational modes available at each energy level. Since a large number of these modes are typically available, the interaction of these modes with incident photons will be a random process with a gaussian shaped distribution producing a gaussian shaped absorption band. As photons of increasing energy are incident on the defect site of a crystal, the probability of the photon causing an absorption transition is given by

$$P_{abs}(E) = (\frac{C}{\pi k_b T_1}) * \exp[-\frac{Cx^2}{k_b T_1}](\frac{dx}{dE}) \tag{2.29}$$

where C is the coupling coefficient of the charge carriers in the defect with the crystal lattice, and x is the displacement of the charge in the defect from its equilibrium position, E is energy difference between the ground and excited states, and T_1 is the effective temperature. The effective temperature is given by the expression

$$T_1 = \frac{h\nu}{k_b} \coth[\frac{h\nu}{k_b T}] \tag{2.30}$$

where ν is the oscillator frequency of the defect [2.11]. From equations 2.29 and 2.30, the absorption band peak will shift to higher temperatures, and its intensity will decrease as the temperature is increased.

2.4 Properties of Al_2O_3:C

This research is focused on the study of Al_2O_3 for the purpose of gaining a better understanding of the processes taking place within the crystal during a TL measurement. Therefore we now discuss the relevant properties of Al_2O_3. In particular, the properties

of the TL glow curves in Al_2O_3:C and of the F and F+ center oxygen vacancies. The discussed properties of the TL and these vacancies will be compared with the current work in this thesis to gain an understanding of the role played by the F and F+ centers in the TL process in Al_2O_3:C.

2.4.1 Crystal Structure and Growth

The Al_2O_3:C crystal structure is shown in figure 2.4 and a is hexagonal close packed O^{2-} sublattice with Al^{3+} ions occupying two out of every three interstitial sites in the lattice. The O^{2-} ions occupy two equilateral triangles one above and one below the plane of the Al^{3+} ion. The Al-O bond lengths are 0.197 nm and 0.186 nm due to the slight distortion of the Al^{3+} sublattice [2.13]. Al_2O_3:C has a band gap of approximately 9.0 eV [2.12].

Al_2O_3:C used in this research is typically grown from the melt at a temperature of approximately 2050 °C. The crystals are grown in the method discussed in section 1.2, and as a result have a relatively high concentration of carbon impurities (100-5000 ppm). Also, for the samples used in this research, Mg and H were also introduced as additional dopants into the growth process for the purpose of further catalyzing the production of oxygen vacancies. Along with carbon other intrinsic impurities occur in small amounts (Ca ~ 30 ppm, Cr and Ti ~ 10 ppm, Ni and Si ~5 ppm, and Cu and Fe < 2 ppm) [2.9].

2.4.2 TL of Al_2O_3:C

TL glow curves for AL_2O_3:C (known commercially as TLD-500) show several peaks over the temperature range from room temperature to ~700 °C as shown in figure 2.5. A strong peak is seen centered at ~175 °C (known as the main peak) and weaker peaks

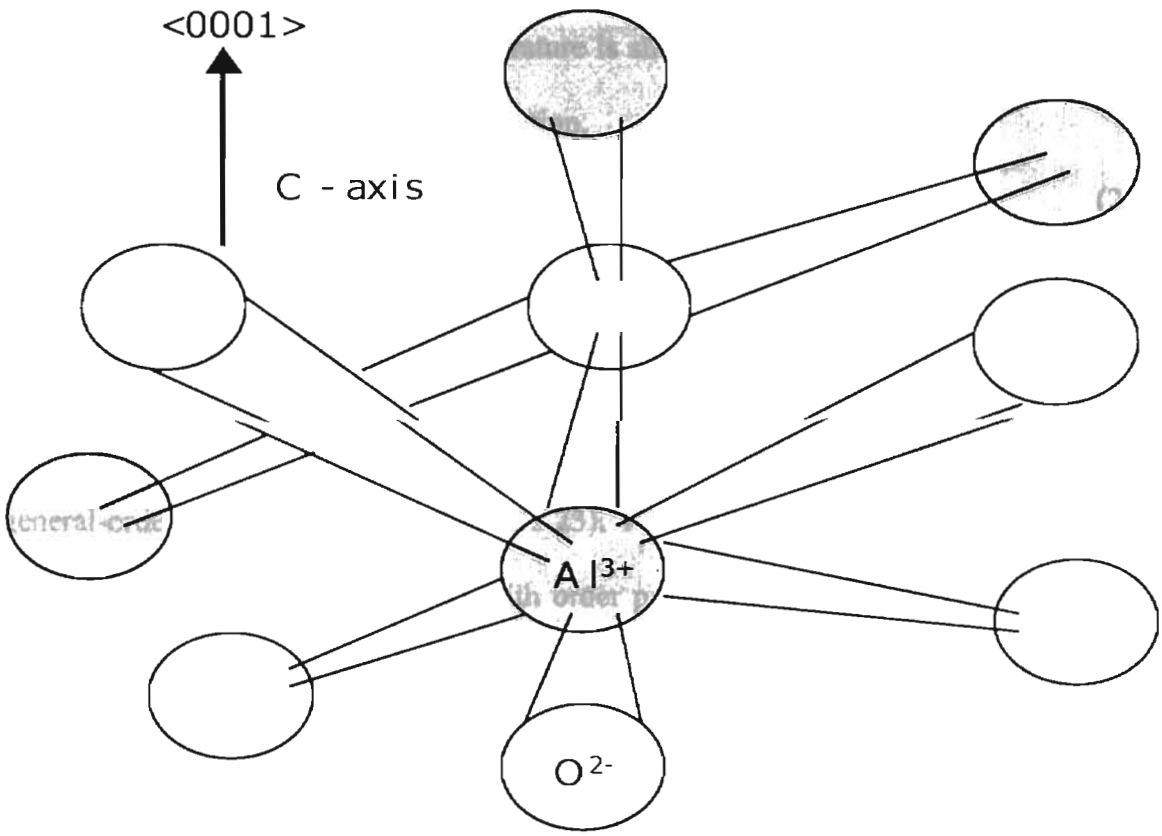

Figure 2.4: Schematic representation of the Al_2O_3 lattice showing the ions surrounding the Al^{3+} and O^{2-} ions.

appear at ~325 °C and ~475 °C. The efficiency of the luminescence in Al_2O_3:C is shown to be strongly temperature dependent above ~200 °C. Analysis done by Akselrod [2.14] and Kortov [2.15] shows that the luminescence efficiency is given by the equation

$$\eta(T) = \frac{1}{(1 + \tau\nu * \exp[\frac{-W}{k_b T}])} \tag{2.31}$$

with $\tau\upsilon \approx (3.8\pm1.5) \times 10^{12}$, $W \approx 1.1\pm0.05$ eV [2.14], and W is the activation energy for a nonradiative transition. As shown for the ~175 °C TL peak in figure 2.6, the intensity of the TL is reduced and the peak temperature is shifted to higher values. In this case the TL intensity would be given by the equation,

$$I_{TQ} = \eta(T) I_{TL} \tag{2.32}$$

where I_{TL} is given in general by equation 2.23. Along with this the shape of the TL peak is distorted producing a more symmetrical peak shape after correcting for thermal quenching. This has led to some conflicting analysis of the TL peaks when using the general-order equation for TL (equation 2.23). Kitis et. al. suggested that the uncorrected peaks appeared to fit to a TL peak with order parameter $b \approx 1.42$ [2.16] while Kortov suggested that the peaks fit to TL peaks with $b \approx 2$ [2.15]. However, when the peaks are corrected for thermal quenching, it is has been shown that the peaks are actually made up of several closely spaced first-order peaks that produce the overall TL peak [2.17]. Therefore the TL peaks in Al_2O_3:C are generally believed to be due to a distribution of traps that are thermally active over the temperature range of the peak. Along with the changes due to thermal quenching, the luminescence efficiency is affected by the heating rate of the measurement. According to the predictions of the kinetic analysis made earlier in the chapter, the luminescence intensity will increase as the heating rate is

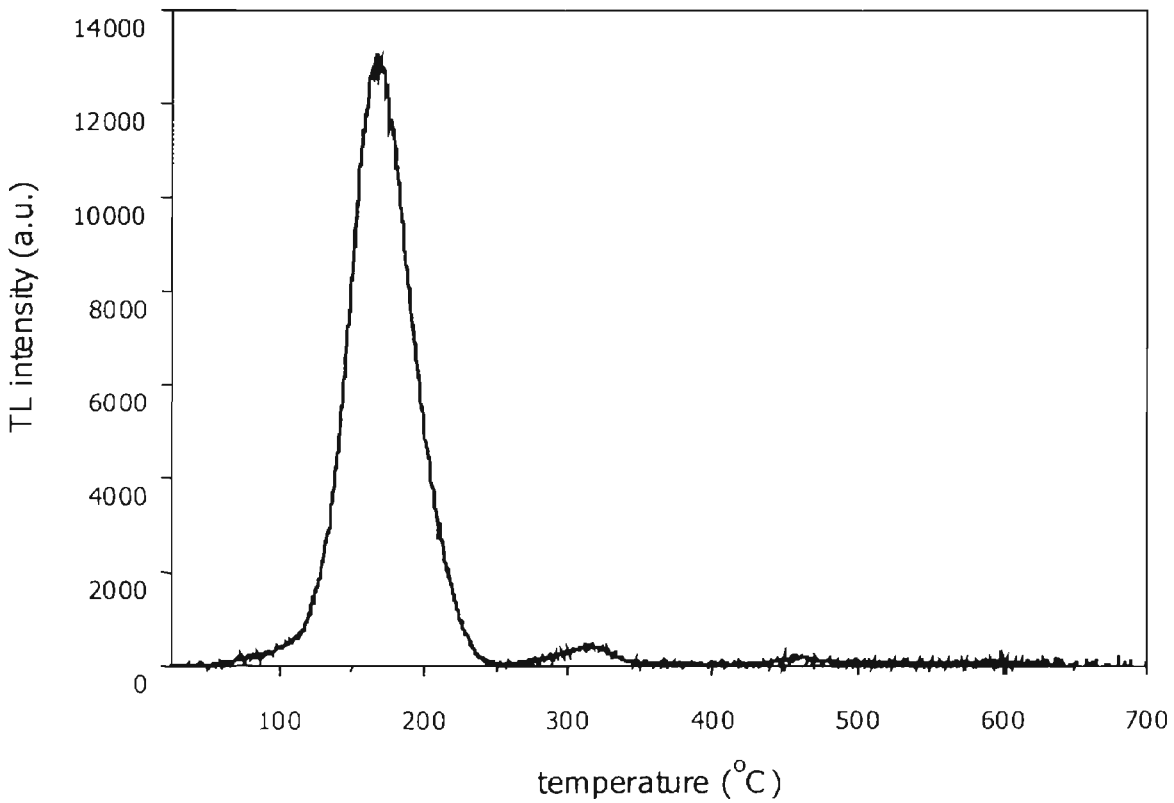

Figure 2.5: TL glow curve for Al_2O_3:C.

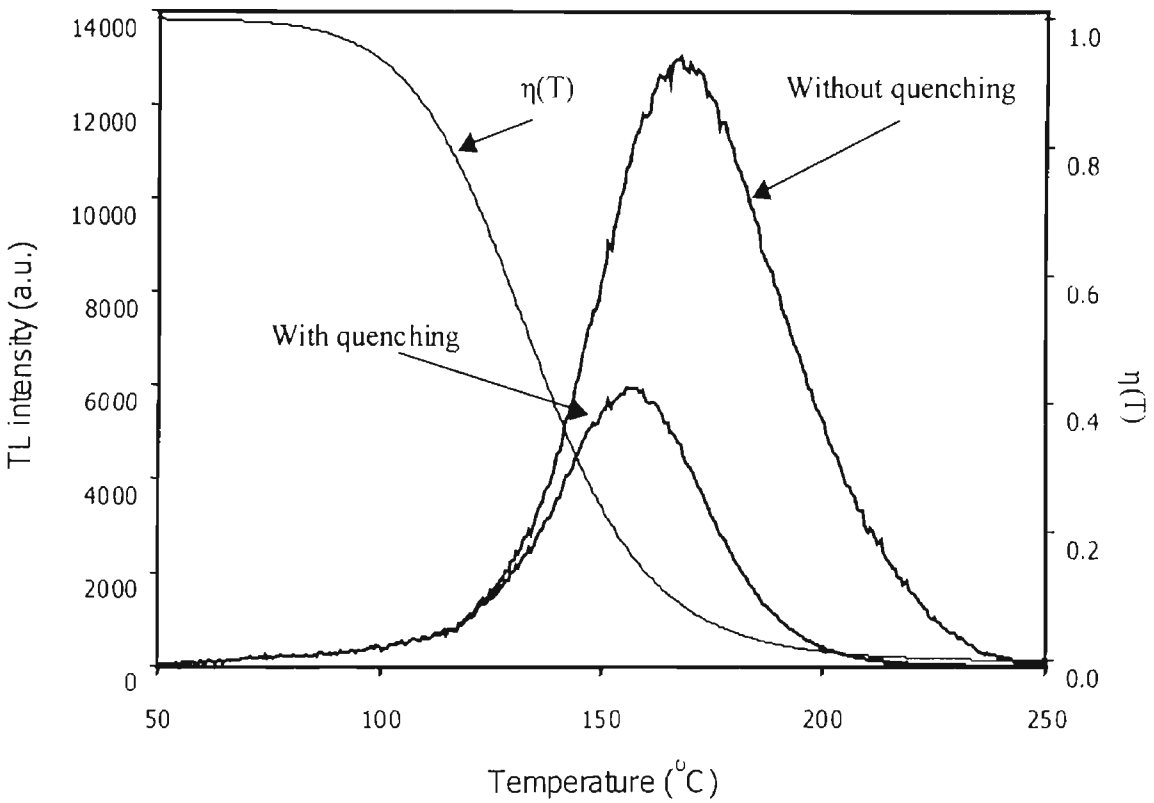

Figure 2.6: First order Randall-Wilkins glow peaks with and without the thermal quenching of luminescence intensity η(T).

increased. However, due to thermal quenching in Al_2O_3:C this has been shown not to be the case. For Al_2O_3:C, the expression for TL intensity must be modified to include the expression for thermal quenching. As the heating rate is increased, the TL peak will shift to higher temperatures and the numerical value of the efficiency changes accordingly. Therefore due to the behavior of the thermal quenching term given by equation 2.31 the TL peaks will decrease in intensity as the heating rate increases [2.14].

The emission spectrum for the TL peaks in Al_2O_3:C is mainly due to a single emission band centered at 420 nm. This spectrum is due to the relaxation of an excited F center. Also seen in other forms of Al_2O_3:C (such as Mg doped crystals) is an emission band centered as 326 nm due to the relaxation of an excited F+ center [1.5]. The F center emission is produced by the relaxation from the 3P excited state to the 1A ground state with a lifetime of ~35 ms [1.3]. The F+ center emission is produced during relaxation from the 2A or 2B excited states to the 1A ground state with a lifetime of $\leq$ 7 ns [2.18]. The relaxation and emission processes as well as the absorption processes to be discussed later in this chapter are shown in figure 2.7 [2.18, 2.19]. The production of F center emission is thought to be caused by the recombination of electrons with F+ centers according to the process [1.3],

$$F^{+} + e \Rightarrow F^{*} \Rightarrow F + h\nu_{420nm}. \tag{2.33}$$

In this process, the TL process would involve the release of a trapped electron that uses an F+ center as a recombination center. Conversely, the production of F+ center emission is believed to be caused by the recombination of a free hole with an F center according to the process [1.3],

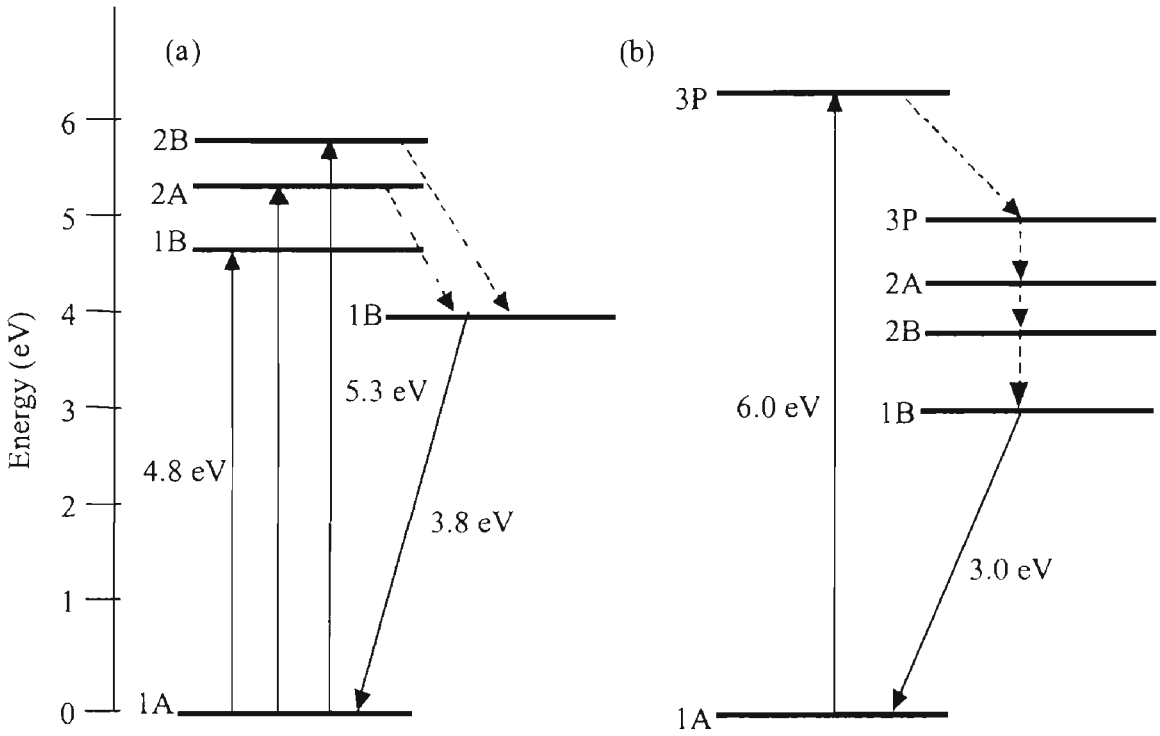

Figure 2.7: (a) F+ center transitions at 4.84 eV and 5.27 eV and emission of 3.8 eV, and (b) F center transition at 6.01 eV and emission at 3.0 eV.

$$F + h^+ \Rightarrow F^{+*} \Rightarrow F^+ + h\nu_{326nm}\,. \qquad (2.34)$$

In this case, the TL process would involve the release of a trapped hole that uses an F center as a recombination center. The TL in Al_2O_3:C depends strongly on the temperature at which the luminescence is being produced, as well as the heating rate used.

2.4.3 F and F+ centers in Al_2O_3:C

Transitions in neutral and singly charged anion vacancies (F and F+ centers) in Al_2O_3:C are the fundamental processes involved in the luminescence signal produced during TL. The F center is known to undergo a transition from 1A → 2P, with the 2P excited state lying in or near the conduction band, upon the absorption of a ~6 eV photon [2.20]. The F+ center is known to undergo a 1A → 1B transition upon the absorption of a ~4.8 eV photon and also a 1A → 2A transition upon the absorption of a ~5.3 eV photon neither of which lies in or near the conduction band [2.18]. The transitions of the F and F+ centers are shown in figure 2.7. The F and F+ center oscillator strengths were calculated by Evans and Staplebrook to be 1.33 and 0.66 respectively. Also, they measured FWHM for the F center of 0.78 ± 0.1 eV and for the F+ center transition at 4.8 eV of 0.41 ± 0.02 eV and at 5.3 eV of 0.32 ± 0.05 eV [2.18].

Upon inspection of the TL emission spectrum from Al_2O_3:C it can be seen that the main emission is at 420 nm due to the relaxation of F centers. From the model for the production of F center emission given in equation 2.33, it might be suspected that the production of luminescence would be dependent on the initial concentration of F+ centers. The sensitivity of Al_2O_3:C, in fact, has been shown to be sensitive to the concentration of F+ centers within the crystal[1.5, 2.20]. For samples with pre-existing

concentrations of F+ centers many orders of magnitude higher than of the radiation-induced F+ centers, the dose response has been shown to linear to higher temperatures as well as much more sensitive to changes in dose [1.5].

The F and F+ center emission measured during TL is known to be thermally quenched in Al_2O_3:C [2.14]. From the model of the production TL emission given by equations 2.33 and 2.34, the F and F+ center emission will be thermally quenched. The lifetime of the F center emission is shown to decay from a room temperature vale of ~35 ms to < 2 ms for temperatures above ~280 °C [2.14]. With the decay of the lifetime following the equation

$$\tau = \frac{\tau_0}{1 + \tau_0 \nu^* \exp[\frac{\Delta E}{k_b T}]}, \tag{2.34}$$

where $\Delta E \approx 1.1 \pm 0.05$ eV and $\tau_o \upsilon \approx (3.8 \pm 1.5) \times 10^{12}$. For the F+ center, the measurements were made of the integrated intensity due to the short lifetime (< 7 ns) of the center. Measurements of the intensity were made and the intensity was then corrected using equation 2.34 to account for the quenching of the emission lifetime. From these measurements values of $\Delta E \approx 0.602$ eV and $\tau_o \upsilon \approx 1.23 \times 10^5$ eV [2.22] were calculated.

The F and F+ center concentrations in Al_2O_3:C have been shown to exhibit a strong reciprocal relationship. That is to say that excitation of F center with 6 eV light has been shown to lower the concentration of the F center and increase the F+ center concentration [2.13, 2.20]. Also, when the crystal is exposed to ionizing radiation, the concentration of F centers is seen to increase and F+ centers to decrease [2.18, 2.21]. This supports the idea of the electrons being ionized into the conduction band by the irradiation are becoming trapped at the F+ centers to produce F centers. Conversely,

when the sample is illuminated with 6 eV light, the electrons are excited out of the centers to produce F+ centers. This reciprocal relationship supports well the ideas for recombination and the production of F center emission during TL given by equation 2.31.

2.4.4 Differences in TL for Mg and H Doped Al_2O_3:C

In this section are mentioned some of the differences observed in the TL, TSC signals by the addition of Mg and H dopants to Al_2O_3:C crystals like the ones used in this research. The addition of Mg and H as additional dopants to Al_2O_3:C during the growth process has several affects on the TL glow curves, TSC signals, and emission spectra.

The addition of Mg and H dopants to Al_2O_3:C has been shown to increase the concentration of F+ centers [2.21]. This increase leads to a change in the size, shape, and positions of the TL and TSC peaks. The TL peaks are much broader giving the appearance of being produced by a wider than Al_2O_3:C distribution of traps over the temperature range of the TL peak. Along with this the TL and TSC peaks are seen to shift in temperature along with the appearance of new peaks at ~75 ^{o}C, ~275 ^{o}C, and ~550 ^{o}C.

The TL emission shows much stronger F+ center emission at centered at 326 nm in the Mg doped samples. Also, for both Mg and H doped samples, the intensity of F center emission is increased substantially up to ~450 ^{o}C were the after which the emission is almost completely quenched. From these observations we note that the charge mobility, and the quenching term will affect the TL and TSC production in these samples differently, but the overall characteristics of the TL emission and TSC in these sample will generally behave in the same manner as Al_2O_3:C.

Chapter 3

Experimental Procedures and Results

3.1 Preparation of Experimental Samples

For this research, four samples of Al_2O_3:C were chosen that have strong F and F+ center absorption bands. These samples consisted of one crystal grown with hydrogen (Al_2O_3:C,H) as an additional dopant, and three samples grown with magnesium (Al_2O_3:C,Mg). The samples where grown by Dr. Mark Akselrod by the method mentioned in section 2.3.1 at Stillwater Sciences (Oklahoma) and at Medus (Russia). Along with carbon, hydrogen and magnesium were added to help catalyze the production of oxygen vacancies. Reducing growth conditions in the presence of carbon and hydrogen catalyzes the formation of oxygen vacancies in the crystal. The magnesium (Mg^{2+}) substitutes for aluminum (Al^{3+}) in the crystal [3.1]. This causes a charge imbalance in the sample, which is compensated for by the production of an oxygen vacancy filled with one electron (F+ center). The magnesium samples were grown with a decreasing amount of magnesium available to the melt as the rod was pulled. This results in a decreasing number of magnesium substitutions occurring along the length of the rod in the growth process. The three samples used were cut from different spots along the length of the rod resulting in decreasing F and F+ center concentrations in the three samples. The samples are labeled according to the concentration of vacancies with Mg-1

having the highest concentration, Mg-3 having the next highest level, and Mg-6 having only trace levels of magnesium. Mg-1 and Mg-6 were grown from the same melt at Stillwater Sciences and Mg-3 was grown at Medus. We expected that Mg-1 and Mg-6 will have similar properties, but Mg-3 will have slightly different OA, TL, TSC, and TL emission properties. For the hydrogen-doped sample, we use the label H-1.

For experimental purposes the samples were all cut to the size of about 1 cm^2 with thickness ranging from 0.101 to 0.066 cm. For the purpose of taking absorption measurements, the samples were all polished to the one micron level. The samples were pre-annealed at 700 °C to remove any trapped charge that may have pre-existed in the samples. The samples were given a saturation dose of approximately one kiloGray (kGy) of 1.75 MeV electrons from the electron beam of a Van de Graaf accelerator.

3.2 Optical Absorption Procedures and Results

The purpose of this research was to investigate the changes in the F and F+ centers in Al_2O_3:C during a TL measurement to determine the role the play in the thermoluminescence process. The monitoring of these centers was done by measuring the changes in optical absorption by the centers in the crystals during heating. From the amount of light absorbed by the center, the concentration of F and F+ centers in the sample can be calculated using Smakula's formula (equation 2.28). By correlating the changes in F and F+ center concentrations to TL, TSC, and TL emission measurements, we can gain an understanding of the role that these centers play in the production of luminescence in Al_2O_3:C.

3.2.1 OA Experiments

The optical absorption experiments were conducted using a Cary 5 spectrophotometer. An oven was placed inside of the spectrophotometer to heat the sample while the absorption was measured. The sample temperature was ramped at a linear rate of 0.33 °C/sec, and was controlled by an Omega Fuzzy Logic temperature controller. The heater was connected to a heat ramp that was connected to a computer that recorded the heating ramp and absorption. A schematic of the setup is shown in figure 3.1.

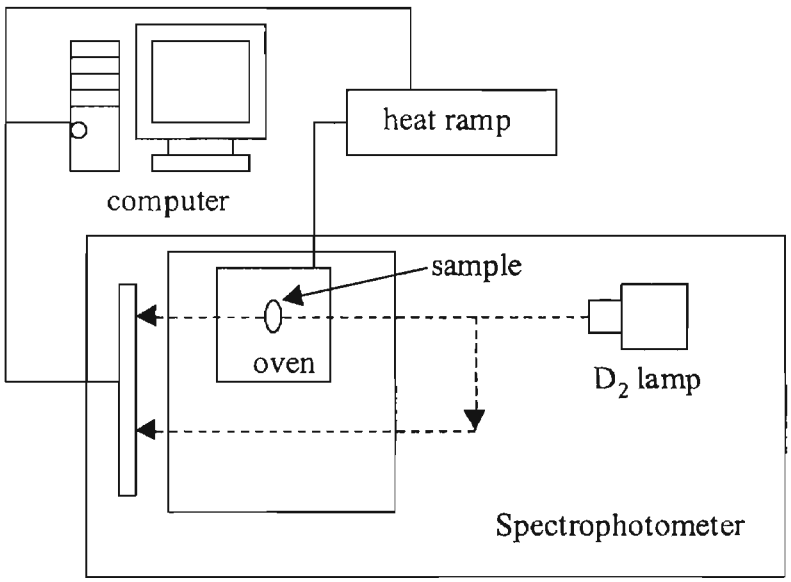

Figure 3.1: Diagram of optical absorption experimental setup.

The absorption spectra were taken at 50 °C as a function of the anneal temperature by the process known as pulse annealing [1.3]. The pulsed absorption spectra are shown in figures 3.2 to 3.5. The absorption spectrum of each sample was taken from 270 nm to 190 nm of an irradiated sample at 50 °C. The sample was then annealed to 75 °C and cooled to 50 °C and the spectrum taken again. This procedure was repeated as the anneal temperature was each time increased in 25 °C increments from 50 °C up to 700 °C. The

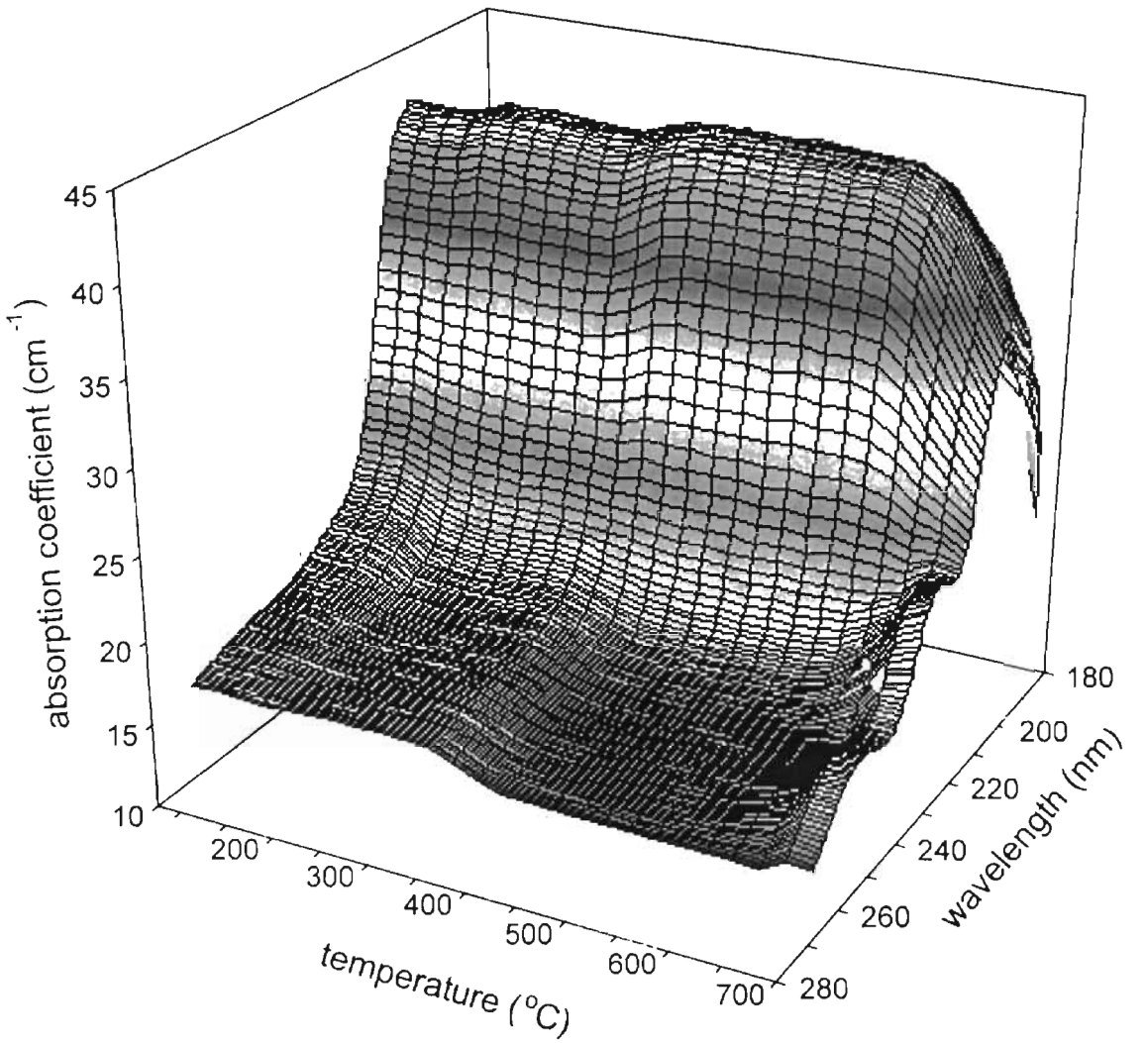

Figure 3.2: 3-D pulse annealed absorption spectrum for H-1.

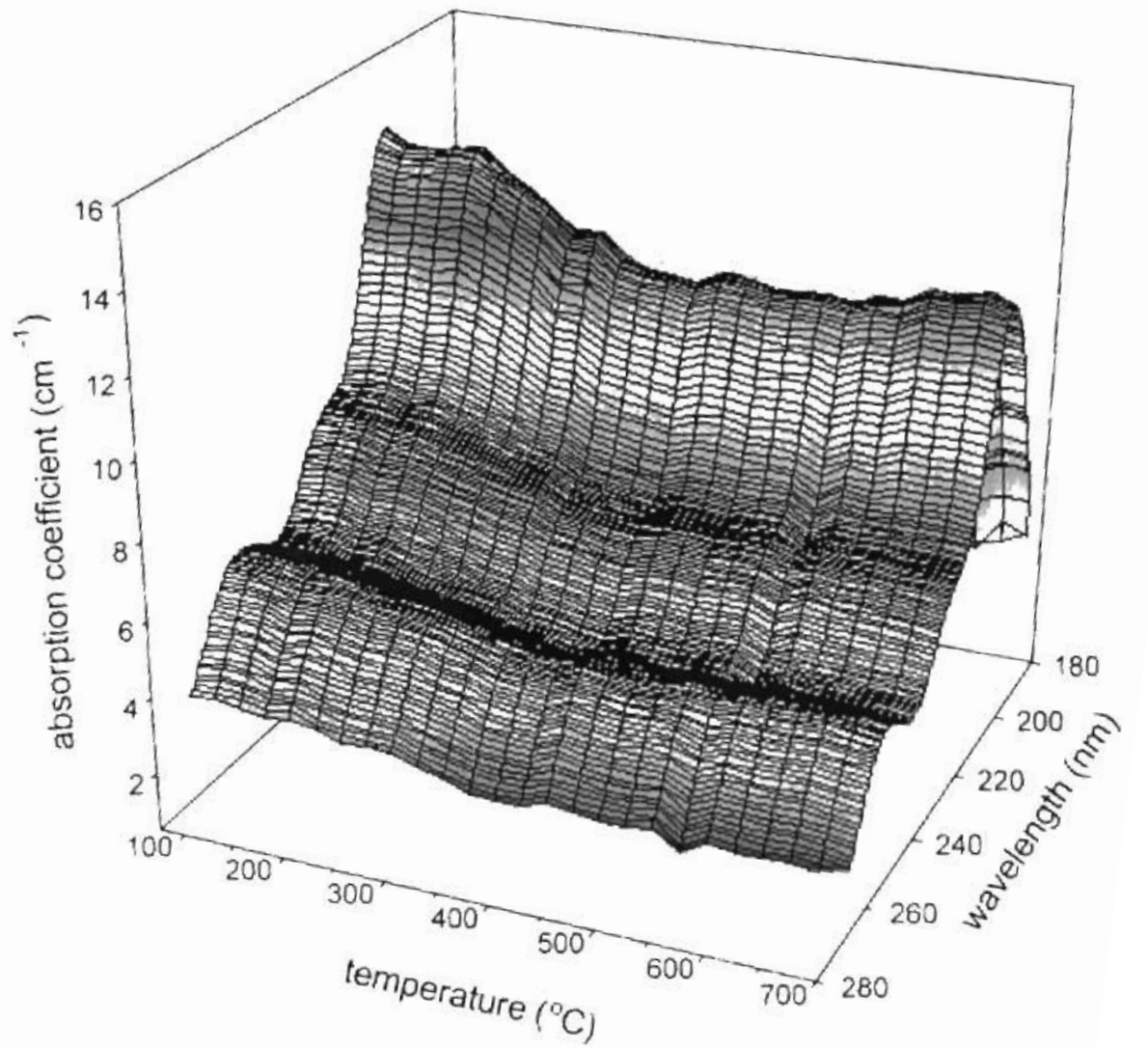

Figure 3.3: 3-D pulse annealed absorption spectrum for Mg-1

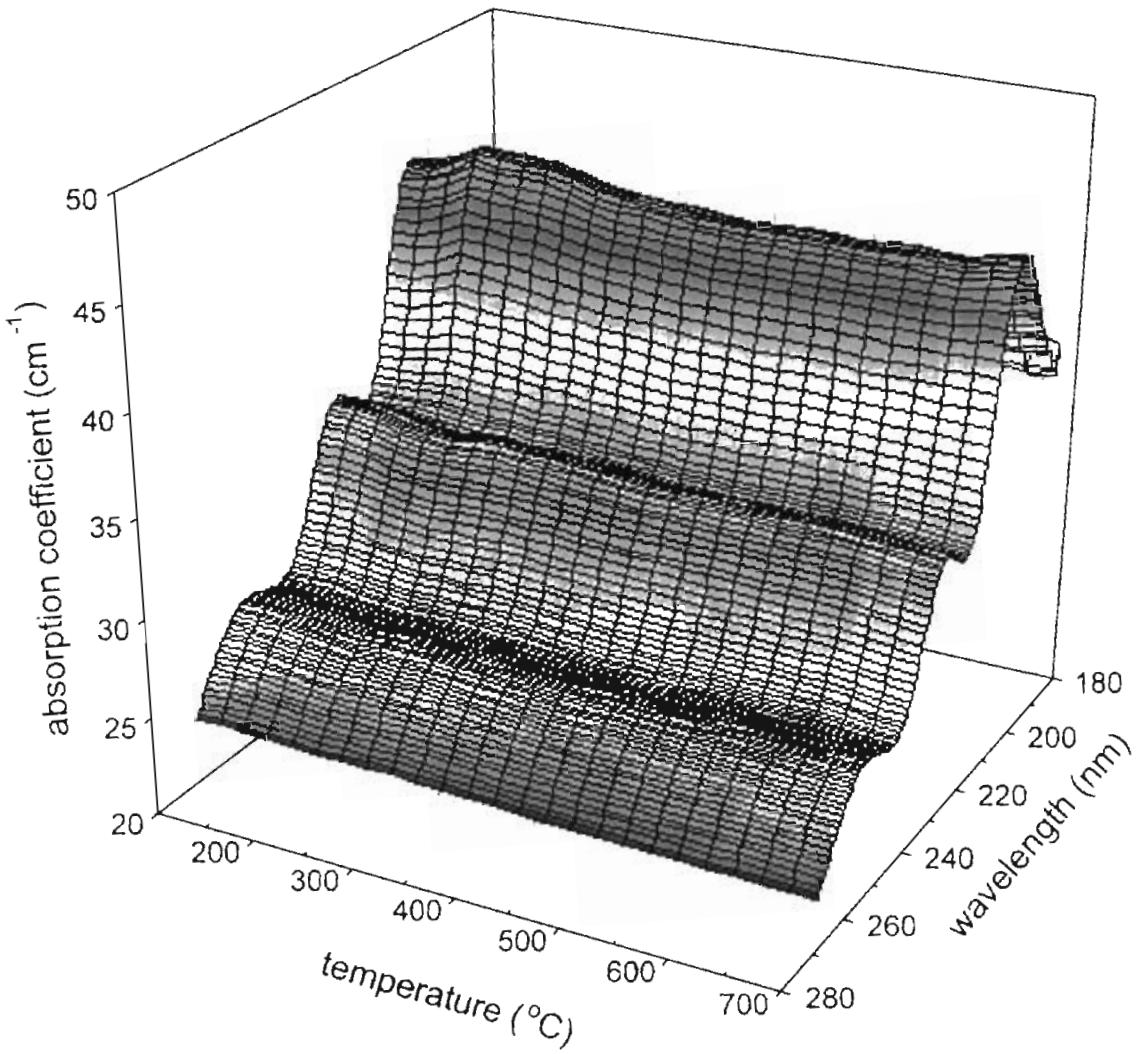

Figure 3.4: 3-D pulse annealed absorption spectrum for Mg-3.

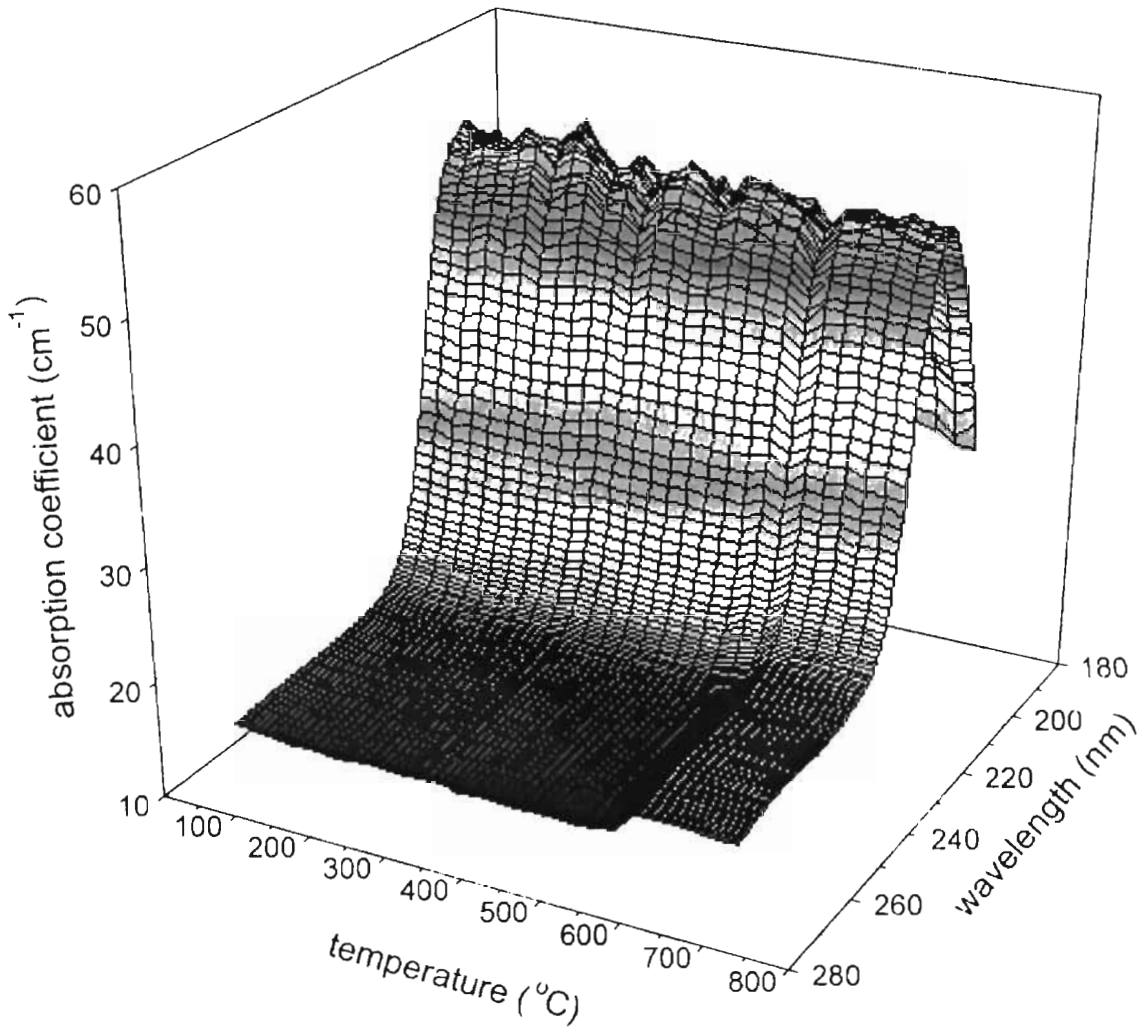

Figure 3.5: 3-D pulse annealed absorption spectrum for Mg-6.

absorption for each sample was plotted in three dimensions as a function of photon energy and anneal temperature.

The absorption spectra were taken over the wavelength range from 270 to 190 nm to determine the absorption bands for the F and F+ centers. The absorption spectra of the four samples are shown in figure 3.6. From the spectra obtained, absorption bands were seen centered at approximately 255 nm (4.85 eV), 235 nm (5.27 eV), and 205 nm (6.03 eV). As shown in figure 2.7, the 4.85 eV and 5.27 eV bands (as reported by Evans and Staplebrook [2.16], and Lee and Crawford [2.18]) were assigned to the 1A to 2B and the 1A to 2A transitions of an F+ center respectively [2.18, 2.16]. The 6.03 eV band was assigned to the 1A to 1P transition of an F center [1.5]. The samples were then irradiated, and the absorption at 4.85 or 6.03 eV (corresponding to F+ and F center absorption) was measured as the sample was heated at a rate of 0.33 °C/sec from 50 to 700 °C/sec. The sample was then cooled to 50 °C and an absorption scan of the annealed sample was measured as the sample was heated to 700 °C with an identical heating rate. The annealed absorption scan was taken for the purpose of removing the effects of heating on the absorption coefficient. The coefficient is seen to be attenuated as the sample is heated ad discussed in section 2.4.3. The annealed absorption scan was then subtracted from the irradiated absorption scan to remove any background changes in the absorption due to heating of the sample. After subtraction, the signal left would be only from the changes in the F and F+ center concentration due to irradiation of the sample. Therefore, the only effects presented in the background absorption scan are hose that were induced by radiation. Before the annealed scan was subtracted from the irradiated absorption scan, the absorption signal was smoothed to remove noise in the scan due to thermal effects.

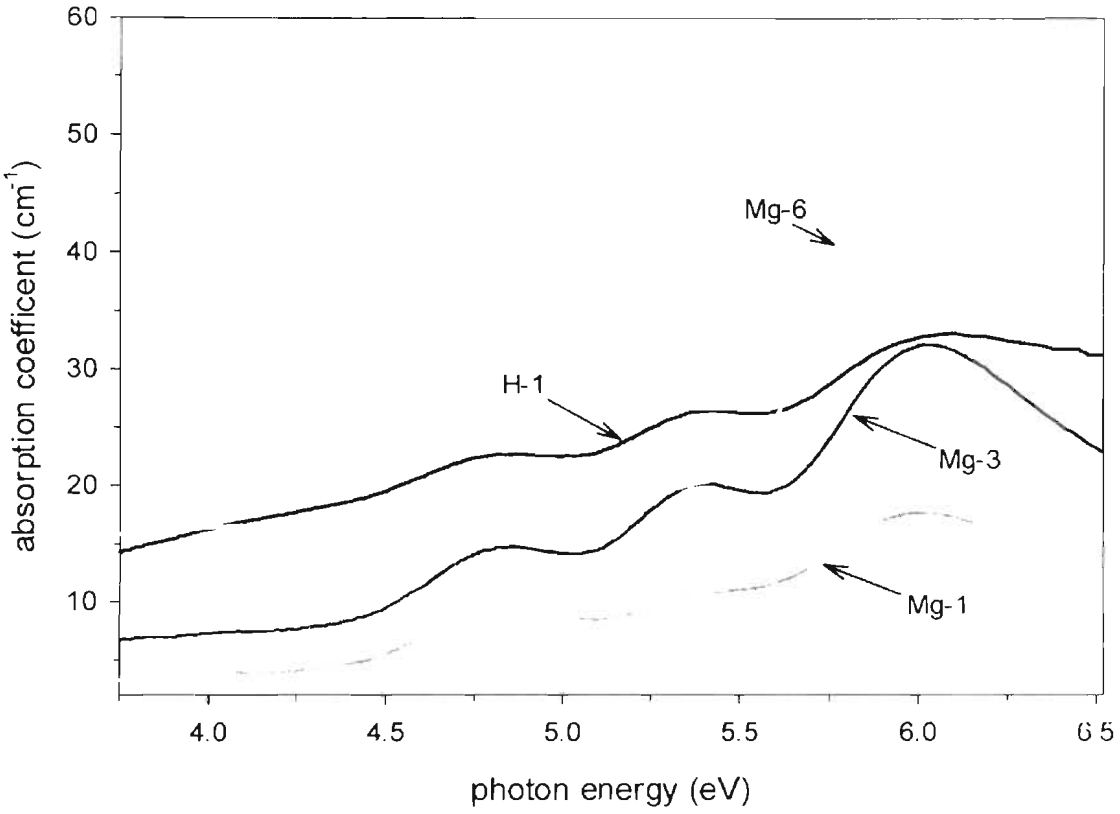

Figure 3.6: Absorption spectra for H-1, Mg-1, Mg-3, Mg-6 showing the F center bands and 6.03 eV and the F+ center bands at 4.85 and 5.27 eV.

For this technique, the fourier transform of the absorption scan is multiplied with the fourier transform of a gaussian transform function. The smoothed data is then obtained by taking the inverse fourier transform of the convolved data and gaussian transform fourier transforms. The smoothing process is given by the equation

$$D_{sm} = IFT[\sqrt{N} * FT(D_{raw}) * FT(G)] \qquad (3.1)$$

where D_{sm} is the smoothed data, D_{raw} is the raw data, G is the gaussian transform function, IFT is the inverse fourier transform, FT is the fourier transform, and N is the number of data points. The effects of the smoothing process is shown in figure 3.7 for the F+ center absorption of H-1.

The absorption spectrum of the samples after annealing at 700 °C were then deconvolved using gaussian peak shapes to represent the F and F+ center absorption bands to obtain the center position, the absorption coefficient, and the FWHM of the peaks. The initial concentrations of F and F+ centers were then calculated using these results. The absorption band centers, absorption coefficients, and FWHM calculated from the results of the deconvolution for the four samples are listed in table 3.1.

3.2.2 Optical Absorption Results

The deconvolution of the optical absorption data for the four samples showed good correlation the results of Evans and Staplebrook and Lee and Crawford mentioned above. From the deconvolution of the annealed H-1 absorption spectrum shown in figure 3.8, the F center peak position was calculated to be at 6.03 eV, the absorption coefficient to be 35.99 cm^{-1}, and the FWHM to be 0.784 eV. The F+ center absorption peaks were calculated to be centered at 4.83 and 5.35 eV, the absorption coefficients to be 17.41 and 16.48 cm^{-1} respectively, and the FWHM to be 0.588 and 0.465 eV respectively. Using

Sample	F center				F + center			
	Conc. ($\times 10^{17}$)	FWHM (eV)	Abs Coef. (cm^{-1})	Center (eV)	Conc. ($\times 10^{17}$)	FWHM (eV)	Abs Coef. (cm^{-1})	Center (eV)
H-1	1.35	0.784	35.99	6.03	0.986	0.588	17.41	4.83
						0.465	16.48	5.35
Mg-1	0.388	0.824	17.68	6.00	0.200	0.708	9.23	4.83
						0.411	5.21	5.37
Mg-3	2.01	0.801	17.71	6.01	1.41	0.729	9.18	4.84
						0.427	5.34	5.38
Mg-6	1.37	0.716	52.15	6.04	0.583	0.696	17.92	4.84
						0.423	10.36	5.35

Table 3.1: Table of calculated properties of samples used in research. Values reported for the F center correspond to the 1A→3P absorption transition. Values reported for the F+ center refer to the 1A→1B (top number) and the 1A→2B (bottom number) absorption transitions.

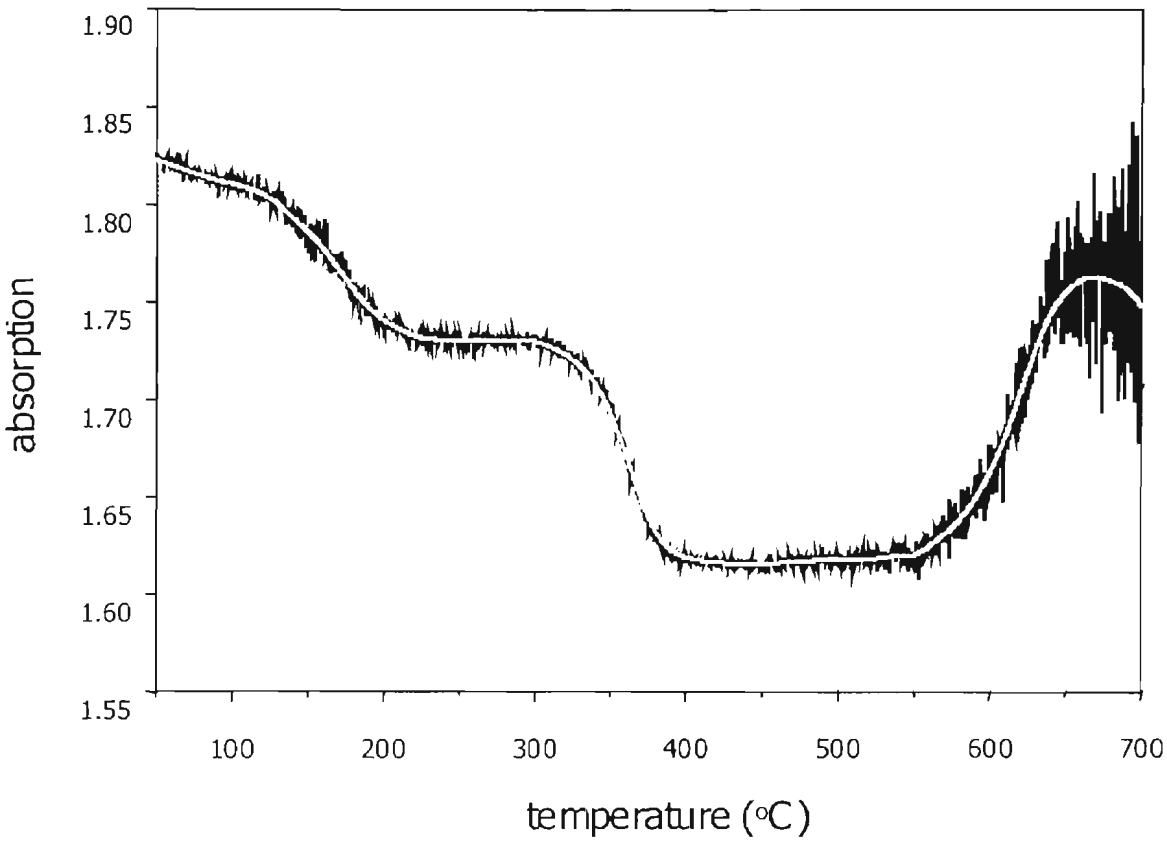

Figure 3.7: Fourier smoothing of F+ absorption data for H-1. The original data (black) is smoothed by the technique of equation 3.1. The smoothed data (gray) is plotted on top of the original data.

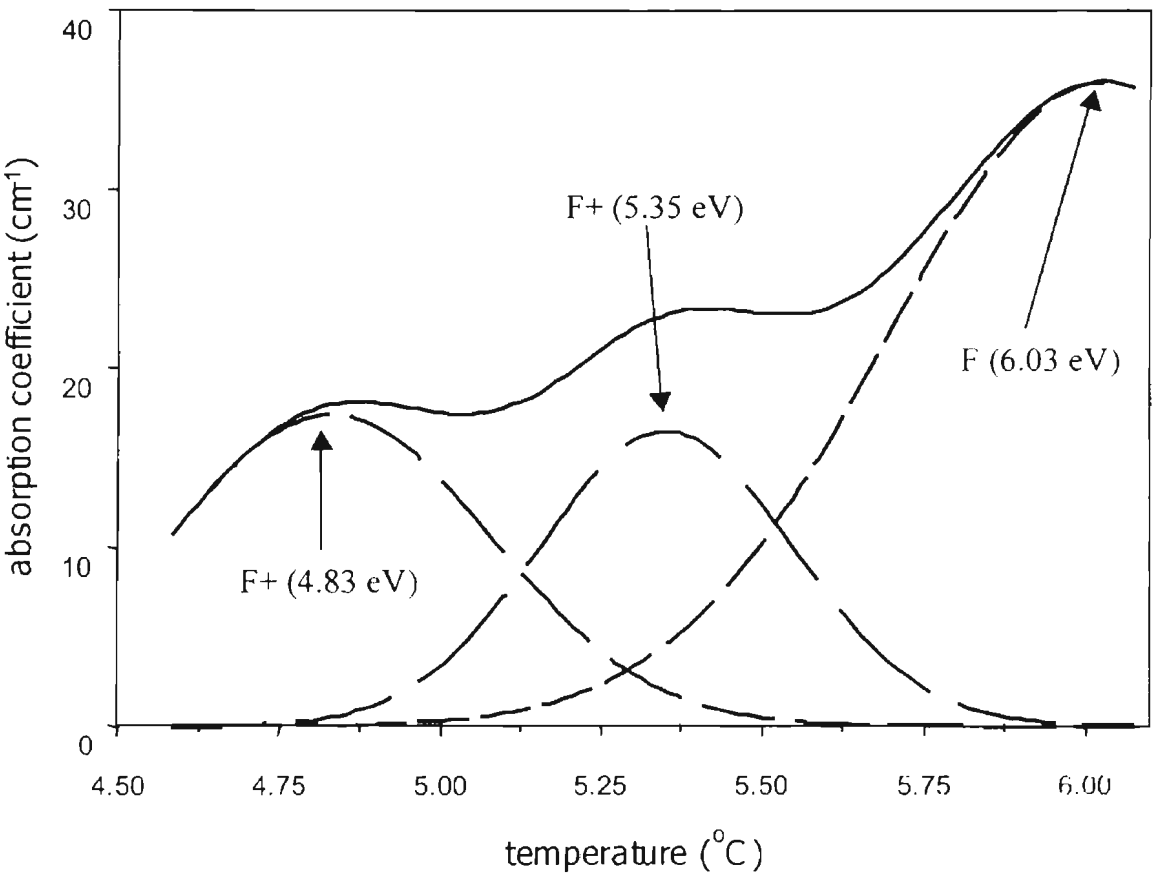

Figure 3.8: The deconvolution of the absorption spectrum for H-1 (solid) showing the fit of the F and F + center absorption bands (dashed) centered at 6.03 eV, 4.83 eV, and 5.35 eV to a gaussian distribution.

these values and an index of refraction of n_i = 1.665, an F center oscillator strength of 1.33, and an F+ center oscillator strength of 0.66 the concentrations of the centers were calculated [2.16]. From this the initial F and F+ center concentrations for the unirradiated H-1 crystal were calculated from equation 2.28 to be 1.35 x 10^{17} cm^{-1} and 0.986 x 10^{17} cm^{-1} respectively. From figure 3.9, a general anti-correlation in the F and F+ center concentrations is observed for sample H-1 during heating. For example, the F center concentration for H-1 increased slowly from about 150 °C to about 200 °C. The F center increase correlated to a decrease of about the same size in the F+ center concentration through the same temperature range. Another increase in the F center and subsequent decrease in F+ center concentration, each of approximately the same size was measured from about 300 to 400 °C. Finally, from approximately 500 to 700 °C, the F center concentration decreased and the F+ center concentration increased. For this step in concentration, The F+ increased only roughly half as much as the F center decreased. Also shown in figure 3.9 is the comparison of the F and F+ center concentrations from the step anneal measurements. From these measurements we see that the calculated values of the F and F+ center concentrations is somewhat less than for the single wavelength measurements. However, there was good agreement between temperature ranges during which the changes in concentration occurred, and the step sizes for the changes for the two types of measurements.

From the deconvolution of the Mg-1 absorption spectrum shown in figure 3.10, the F center absorption peak was calculated to be at 6.01 eV with an absorption coefficient of 11.94 cm^{-1} and a FWHM of 0.681 eV. The F+ center peak positions were calculated to be at 4.83 and 5.36 eV with absorption coefficients of 4.52 and 4.82 cm^{-1}

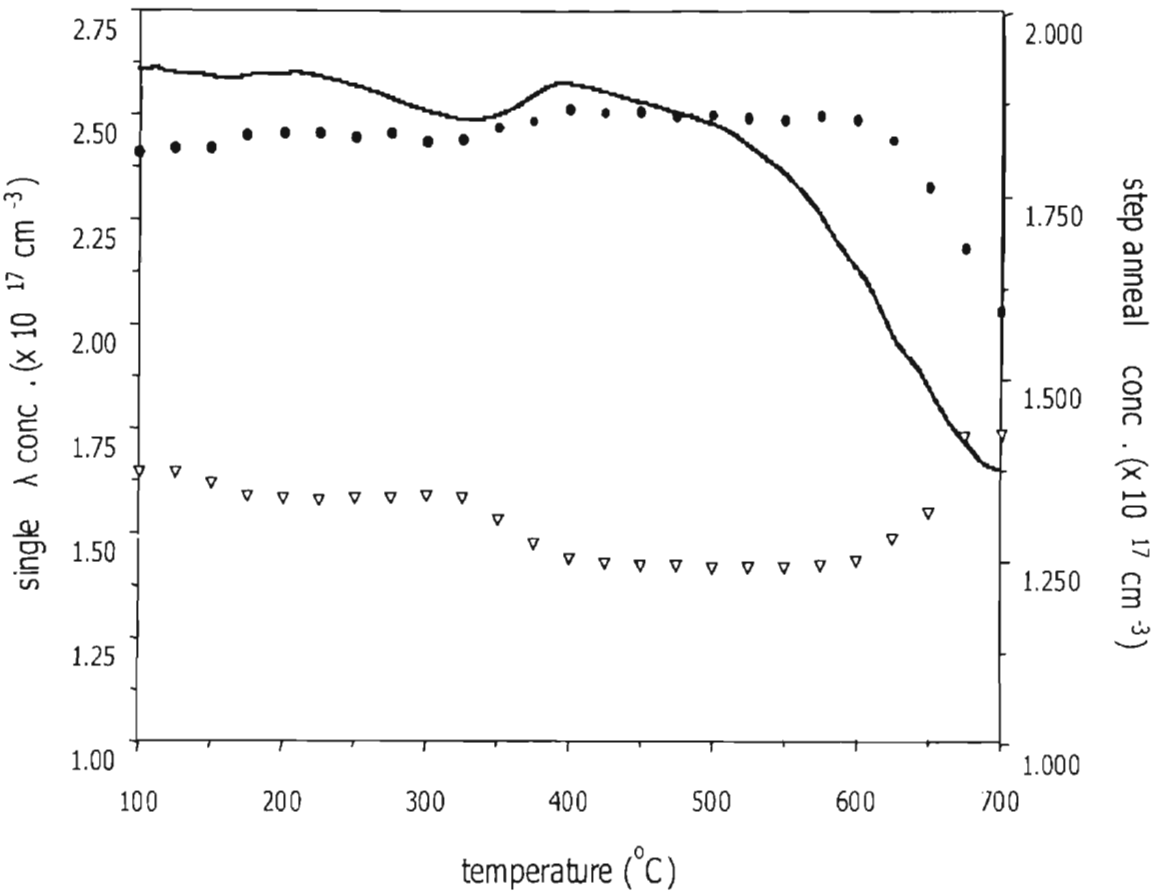

Figure 3.9: The changes in F (black) and F+ (gray) center concentration from single wavelength absorption scans and F (circles) and F+ (triangles) concentration from pulsed anneal absorption scans for H-1 as a function of temperature. An anti-correlation in the F and F+ center concentration is observed over several temperatures ranges for both experiments.

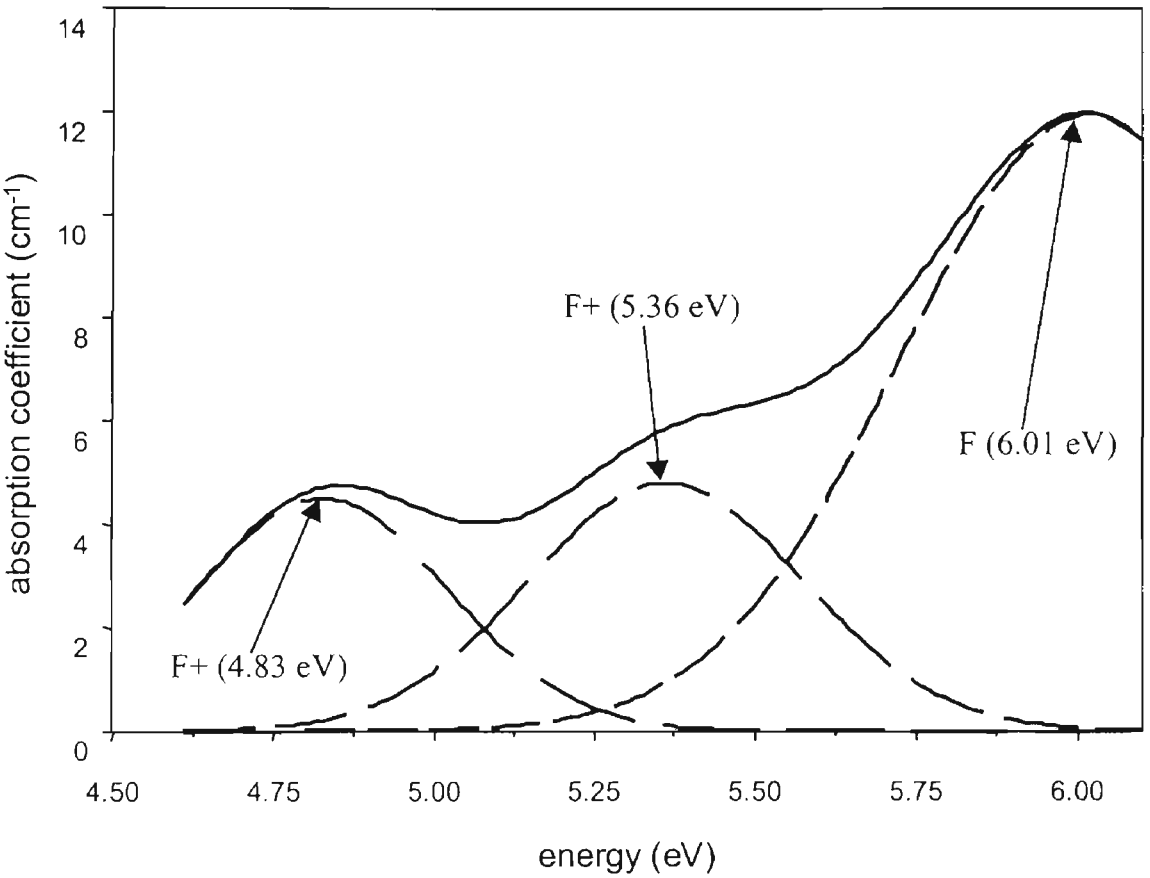

Figure 3.10: The deconvolution of the absorption spectrum for Mg-1 (solid) showing the fit of the F and F + center absorption bands (dashed) centered at 6.00 eV, 4.83 eV, and 5.37 eV to a gaussian distribution.

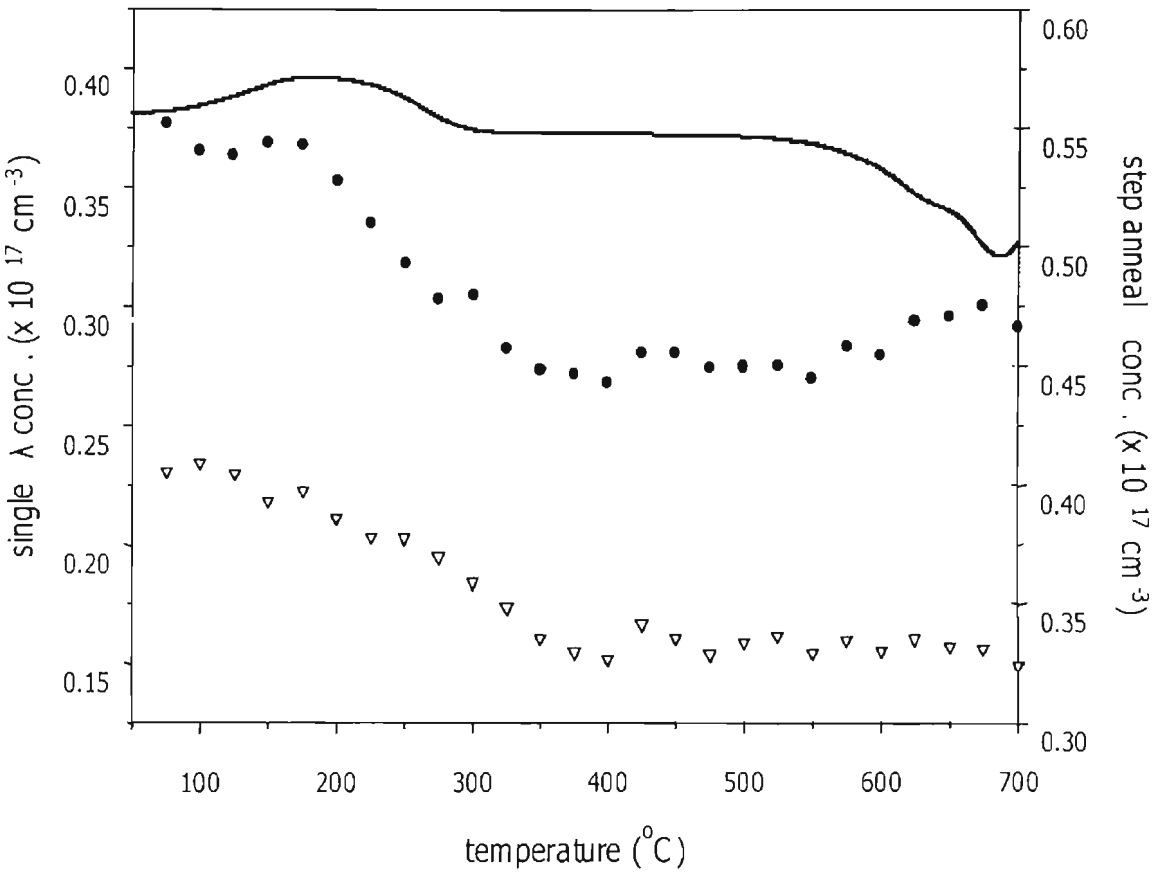

Figure 3.11: The changes in F (black) and F+ (gray) center concentration from single wavelength absorption scans and F (circles) and F+ (triangles) concentration from pulsed anneal absorption scans for Mg-1 as a function of temperature. An anti-correlation in the F and F+ center concentration is observed over several temperatures ranges for both experiments.

respectively and FWHM of 0.460 and 0.502 eV respectively. From these measurements, the F and F+ center concentrations of unirradiated Mg-1 were calculated from equation 2.28 to be 0.388 x 10^{17} for the F centers and 0.200 x 10^{17} for the F+ centers. From figure 3.11, we see that during heating the F center concentration increased in the range from about 100 °C to 175 °C which correlated to a decrease of about twice as much in the F+ center concentration. From 175 °C to about 300 °C there is a decrease in the F center concentration correlating to a slight increase in the F+ center concentration. The concentrations of both the F and F+ centers remain approximately constant until about 525 °C when the F center concentration is seen to decrease until about 700 °C. The F+ center concentration in this range is seen to undergo an increase at about 525 °C followed by a decrease at about 560 °C, then another increase at about 600 °C. From about 630 °C to 660 °C, the F+ center concentration decreases correlating to a decrease in the negative slope of the F center concentration curve. Finally, the F+ center concentration increases from about 660 °C through 700 °C. Also, comparing the calculated concentrations from the step anneal measurements, we see that the F and F+ changes in F and F+ centers both showed a decrease in the range from 175 °C to 300 °C. After this change, the concentrations remained roughly constant for the rest of the measurement. This showed bad correlation to the single wavelength absorption measurements, and the general anti-correlation between the F and F+ center concentrations were not observed in this measurement.

From the deconvolution of the Mg-3 absorption spectrum shown in figure 3.12, the F center peak position was calculated to be at 6.02 eV, the absorption coefficient to be 45.42 cm^{-1}, and the FWHM to be 0.926 eV. The F+ center peak positions were calculated

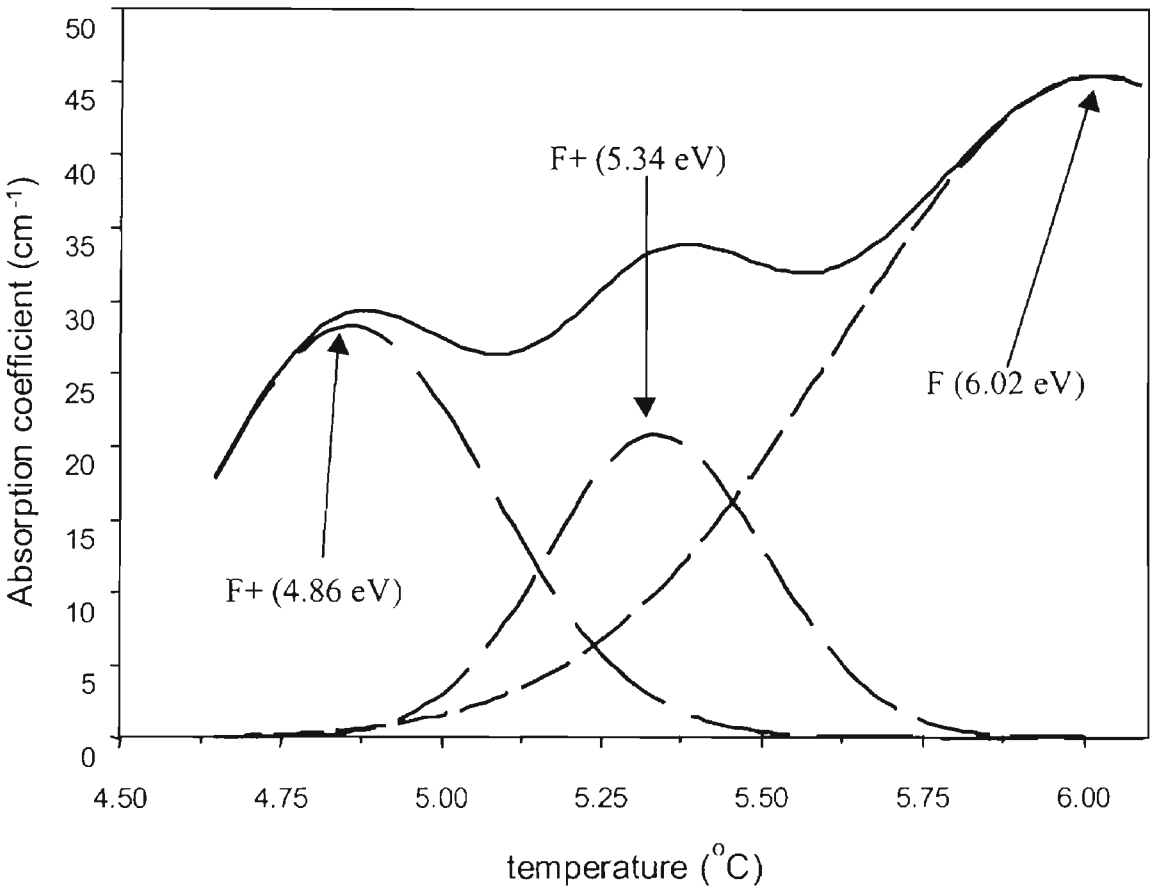

Figure 3.12: The deconvolution of the absorption spectrum for Mg-3 (solid) showing the fit of the F and F + center absorption bands (dashed) centered at 6.01 eV, 4.83 eV, and 5.38 eV to a gaussian distribution.

to be at 4.86 and 5.34 eV, the absorption coefficients to be 28.26 and 20.81 cm^{-1} respectively, and the FWHM to be 0.519 and 0.403 eV respectively. From these measurements, for Mg-3 before irradiation the F and F+ center concentrations were calculated from equation 2.28 and found to be 2.01 x 10^{17} cm^{-1} and 1.41 x 10^{17} cm^{-1} respectively. The calculated properties for Mg-3 are listed in table 3.1.

Shown in figure 3.13, during heating the concentration of the F centers in Mg-3 increased from about 125 °C to 180 °C, which corresponded to a decrease in the F+ center concentration of about the same size. Then, from about 180 °C to 325 °C, there is a rapid decrease in F center concentration accompanied by a rapid increase of about the same size in F+ center concentration. After this, from about 325 °C to 550 °C The F center concentration continues to steadily decrease, while the F+ center concentration stays rather constant. Finally, from about 550 to 700 °C, the F center concentration increases while the F+ center concentration shows a sudden decrease at about 625 °C. The changes shown in the step anneal measurements show good correlation to the changes in the single wavelength measurements in both the temperature range of occurrence and size of concentration change.

From the deconvolution of the Mg-6 absorption spectrum shown in figure 3.14, the F center peak position was calculated to be at 6.02 eV with an absorption coefficient of 52.14 cm^{-1} and a FWHM of 0.679 eV. The F+ center peak positions were calculated to be at 4.84 and 5.29 eV with absorption coefficients of 14.76 and 16.12 cm^{-1} and FWHM of 0.410 and 0.487 eV respectively. Using these measurements, for Mg-6 the unirradiated F center concentration was calculated from equation 2.28 to be 1.37 x 10^{17} cm^{-3} and the F+ center concentration to be 0.583 x 10^{17} cm^{-3}. The calculated properties

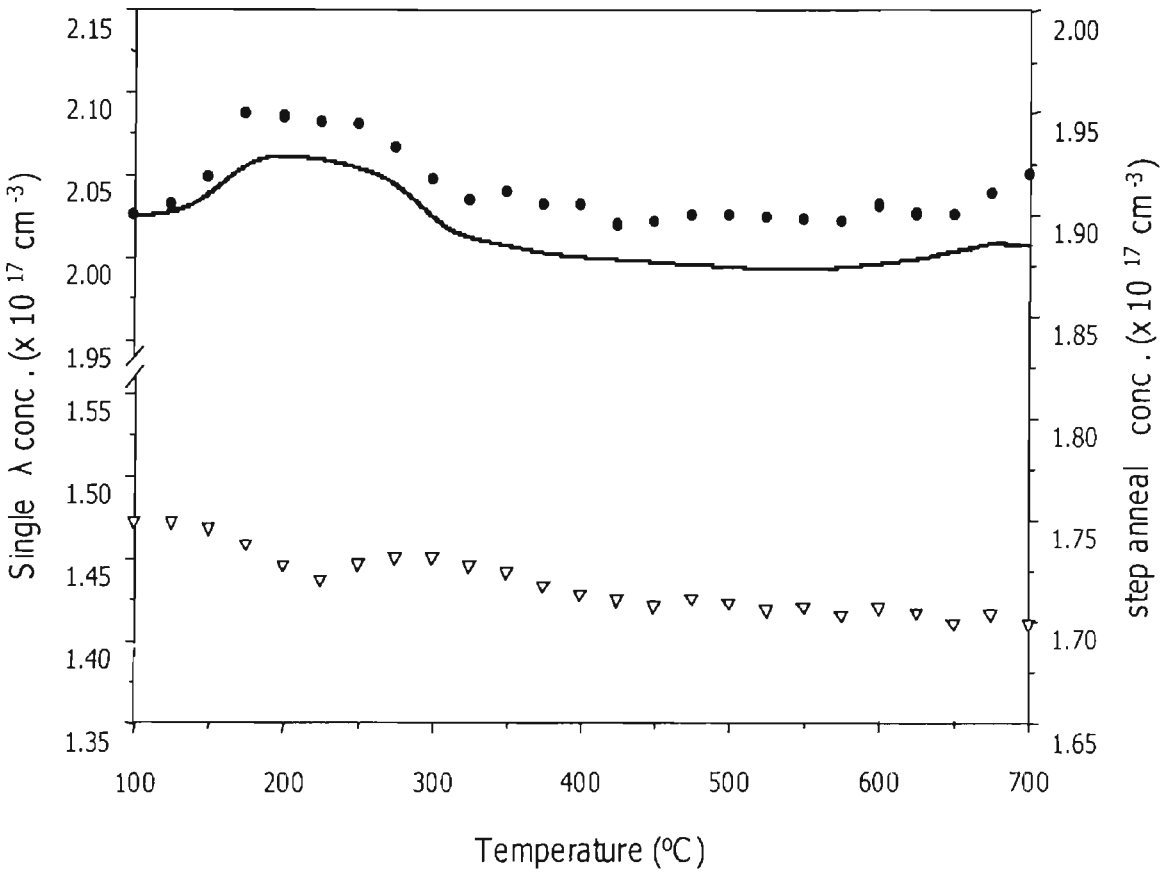

Figure 3.13: The changes in F (black) and F+ (gray) center concentration from single wavelength absorption scans and F (circles) and F+ (triangles) concentration from pulsed anneal absorption scans for Mg-3 as a function of temperature. An anti-correlation in the F and F+ center concentration is observed over several temperatures ranges for both experiments.

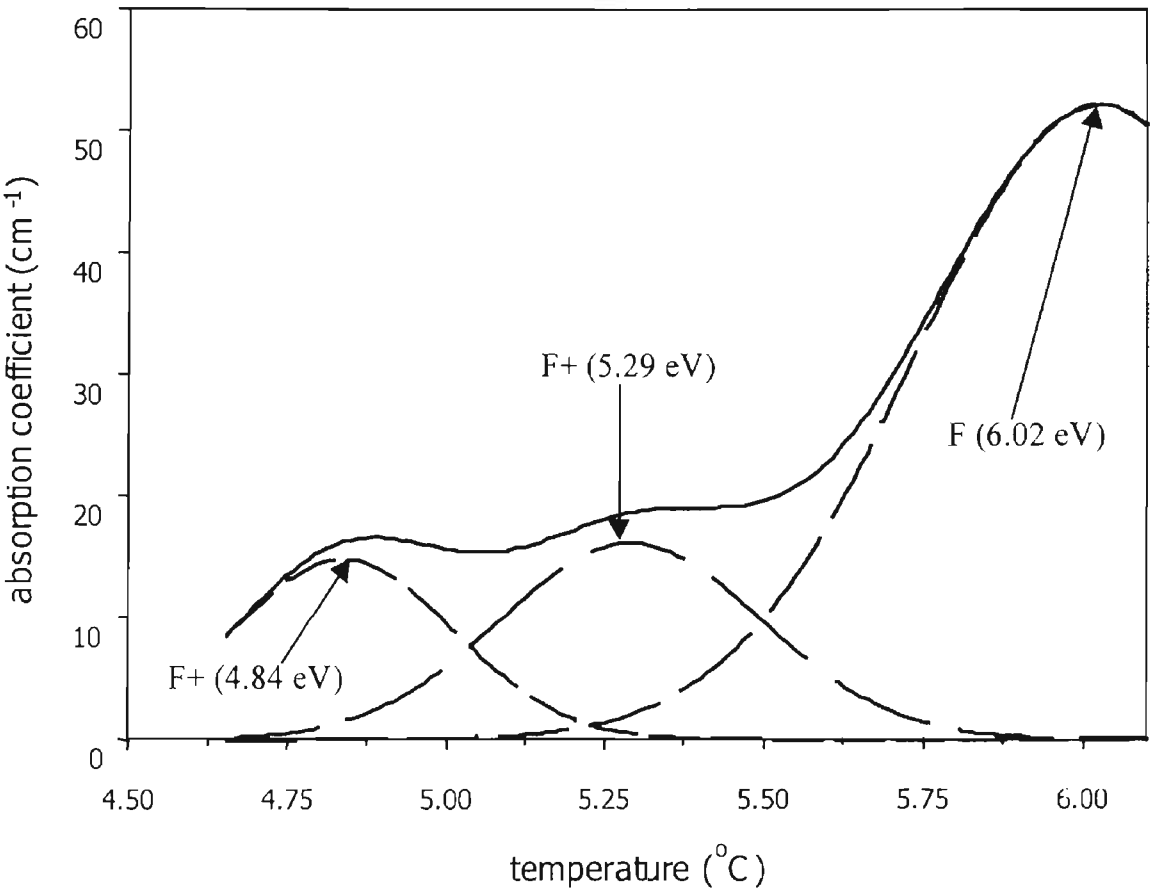

Figure 3.14: The deconvolution of the absorption spectrum for Mg-6 (solid) showing the fit of the F and F + center absorption bands (dashed) centered at 6.02 eV, 4.84 eV, and 5.29 eV to a gaussian distribution.

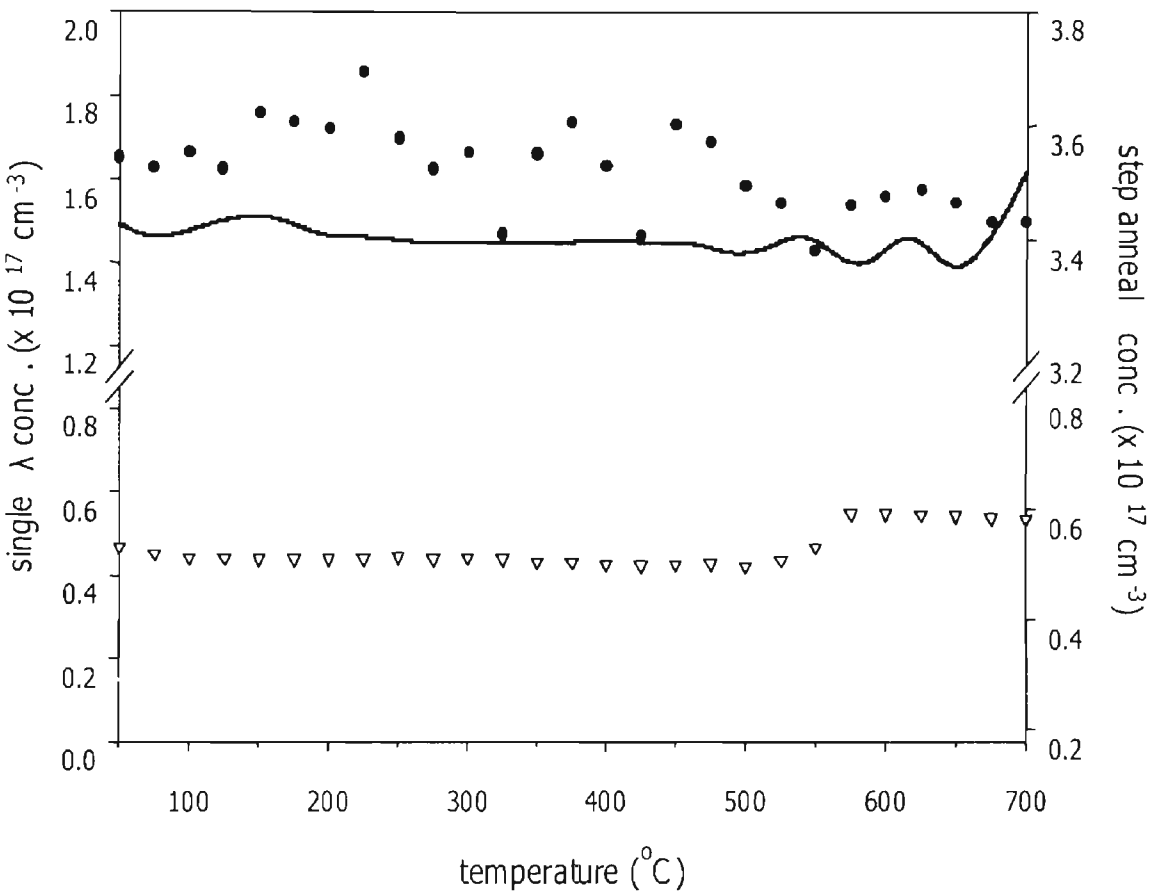

Figure 3.15: The changes in F (black) and F+ (gray) center concentration from single wavelength absorption scans and F (circles) and F+ (triangles) concentration from pulsed anneal absorption scans for Mg-6 as a function of temperature. An anti-correlation in the F and F+ center concentration is observed over several temperatures ranges for both experiments.

for Mg-6 are listed in table 3.1. As shown in figure 3.15, during heating the F center concentration decreased from about 100 °C to about 160 °C, which correlated to a decrease in the slope of the F+ center concentration curve. The F center concentration then decreased from 160 °C to about 210 °C that correlated to an increase in the slope of the F+ center concentration curve. The concentration of the F centers stayed relatively constant until about 500 °C when the concentration was seen to increase and decrease several times in over the temperature range of about 500 to 700 °C. This correlated to small changes the F+ center concentration and a large increase in the concentration at about 650 °C. The pulse annealed measurements showed rather noisy results for the F center concentrations, but the overall trend of the concentration is seen to be increasing from 50 °C to about 225 °C and then decreasing for the rest of the measurement.

TL and TSC measurements were used to determine the thermally stimulated luminescence and conductivity properties of the irradiated samples. These measurements gave us information about the temperature at which charges are thermally released from traps, intensity of luminescence and conductivity produced during this process. Along with this information, the TL emission spectra were also measured for the irradiated samples to determine the emission bands produced during TL. This information was then to the results from OA and TL emission to better characterize the emission process during TL.

3.3 TL and TSC Procedures and Results

TL and TSC measurements were performed to determine the correlation between the TL and TSC peaks and TL peaks and F and F+ center concentration changes.

3.3.1 TL, Emission, and TSC Experiments

A schematic of the TL and TSC setups is shown in figure 3.16. For the measurement of TL and TSC, the irradiated samples were heated at a rate of 0.33 °C/sec from 50 to 700 °C. TL measurements were taken using the automated RISØ TL/OSL reader systems. A full description of the RISØ TL/OSL reader system can be found in the paper *The Automated RISØ TL Dating Reader System* by L. Bøtter-Jensen [3.2]. The TL emission was measured by passing the luminescence through an American Holographic inc. spectrograph model no. 100S to spatially separate emission spectrum. The emission was then passed to an EG&G OMA diode array camera model no. 1024-1241UV, and the resulting signal was then recorded by a computer. Also, for the TL emission measurements the temperature of the samples was ramped at a linear rate of 0.33 °C/sec using an Omega Fuzzy Logic Temperature controller. The temperature during heating was measured by a thermocouple that was connected to the bottom of the sample holder on the opposite end as the heating element. The sample, however, was mounted toward the top of the holder next to the heating element. Because of this, it is believed that the temperature recorded by the thermalcouple was lower than the actual temperature of the sample. Because of this we expect that the emission will be shown to occur at a lower temperature than it actually did. For TSC, electrodes were deposited on either side of the samples. This was done by evaporating a thin film of titanium onto the sample followed by a thicker film of palladium. The titanium-palladium electrodes were used to reduce the background signal measured across the sample before the measurement is made. As shown in figure 3.16, these electrodes consisted of a central circle of titanium-palladium and a thin ring on the outer edge of sample. The outer edge was in contact with the

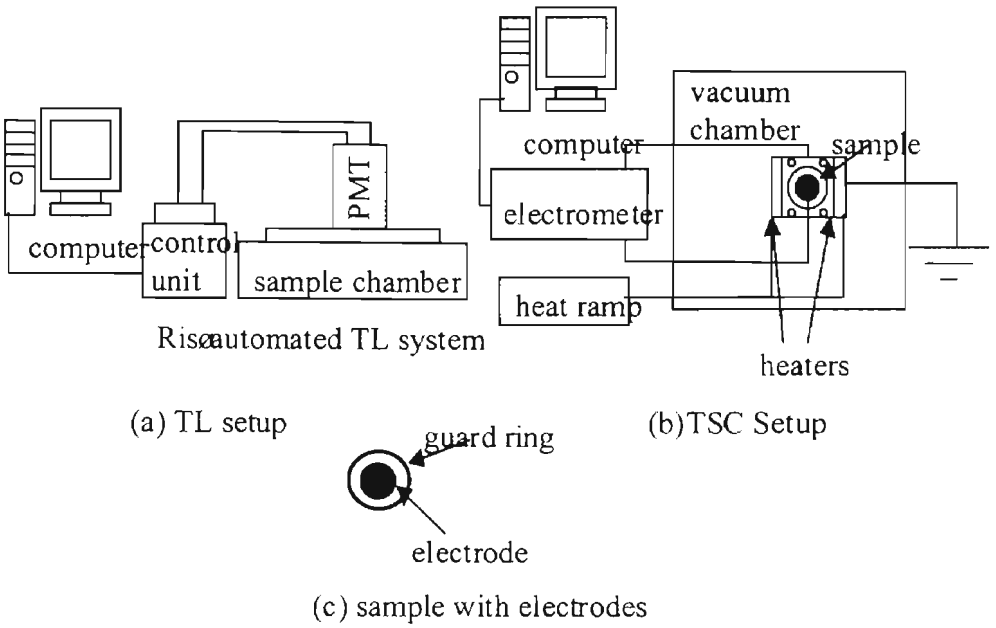

Figure 3.16: (a) Diagram of the TL experimental setup, and (b) diagram of TSC experimental setup (c) Diagram of electrodes for TSC.

sample holder to ground the sample with the holder and eliminate surface currents that may build up on the sample and distort the signal during measurements. The samples were then irradiated and placed under vacuum with a 100 V bias placed across the sample. They were then heated and the current produced across the sample was measured and recorded by a computer.

3.3.2 TL and TSC results

The TL glow curve, emission spectrum, and TSC curve from H-1 are shown in figure 3.17. The TL results from the four different samples showed a large variety in the properties of their glow curves as shown in figures 3.17 to 3.20. Sample H-1 showed several peaks, the first of which was centered at ~180 °C. Also, there is a second peak centered at ~410 °C and a third peak centered at ~630 °C. We see that while the 180 °C peak is rather intense, and has a rather symmetrical shape, the 310 °C and 630 °C peaks

have relatively low intensities, and are very anti-symmetrical with the low temperature side having a much more gradual slope than the high temperature side. This feature of the glow curve is due to thermal quenching at high temperatures. This effect is not only retarding the rise in the luminescence intensity, but it is also causing the luminescence to fall off more rapidly. The TL emission spectra for H-1 showed strong F center emission centered at 420 nm for the 180 °C TL peak and weaker emission (due to thermal quenching) centered at 420 nm for the 310 °C peak. The emission was shifted about 30 °C lower than the TL peaks due to the problem with the temperature mentioned earlier. The TSC data for H-1 shows a strong peaks at ~ 200 °C, ~310 °C, 410 °C and a peak at ~520 °C. The TSC peaks occur at temperatures that do not correspond to the TL peaks. Instead, they seem to occur about 20 to 40 °C after the TL peaks. This shift between the TSC and TL peaks is due to the thermal quenching of the TL peaks as shown in equations 2.24 through 2.27. Therefore, the 200 °C TSC peak is associated with the 180 °C TL peak, and either or both of the 310 °C and 410 °C TSC peaks with the 410 °C TL peak. Also, the TSC peaks may have been shifted due to the temperature dependent nature of the freed charge mobility ($\mu(T)$). The TL glow curve, emission spectrum, and TSC curve for Mg-1 are shown in figure 3.18. For Mg-1, the TL glow curve shows a peak centered at ~140 °C. This peak appears as a shoulder on the peak centered at ~220 °C. Also, peaks were observed at ~400 °C and ~550 °C. The temperature shifted TL emission spectrum shows a small F center emission peak at ~70 °C centered at 420 nm and a relatively large F center peak at ~170 °C and a smaller F+ center emission peak at ~ 175 °C centered at 325 nm. The TSC curve shows peaks at ~150 °C, and ~300 °C. Accounting for thermal quenching effects and the temperature shift in the mobility, the 150 °C TSC peak is

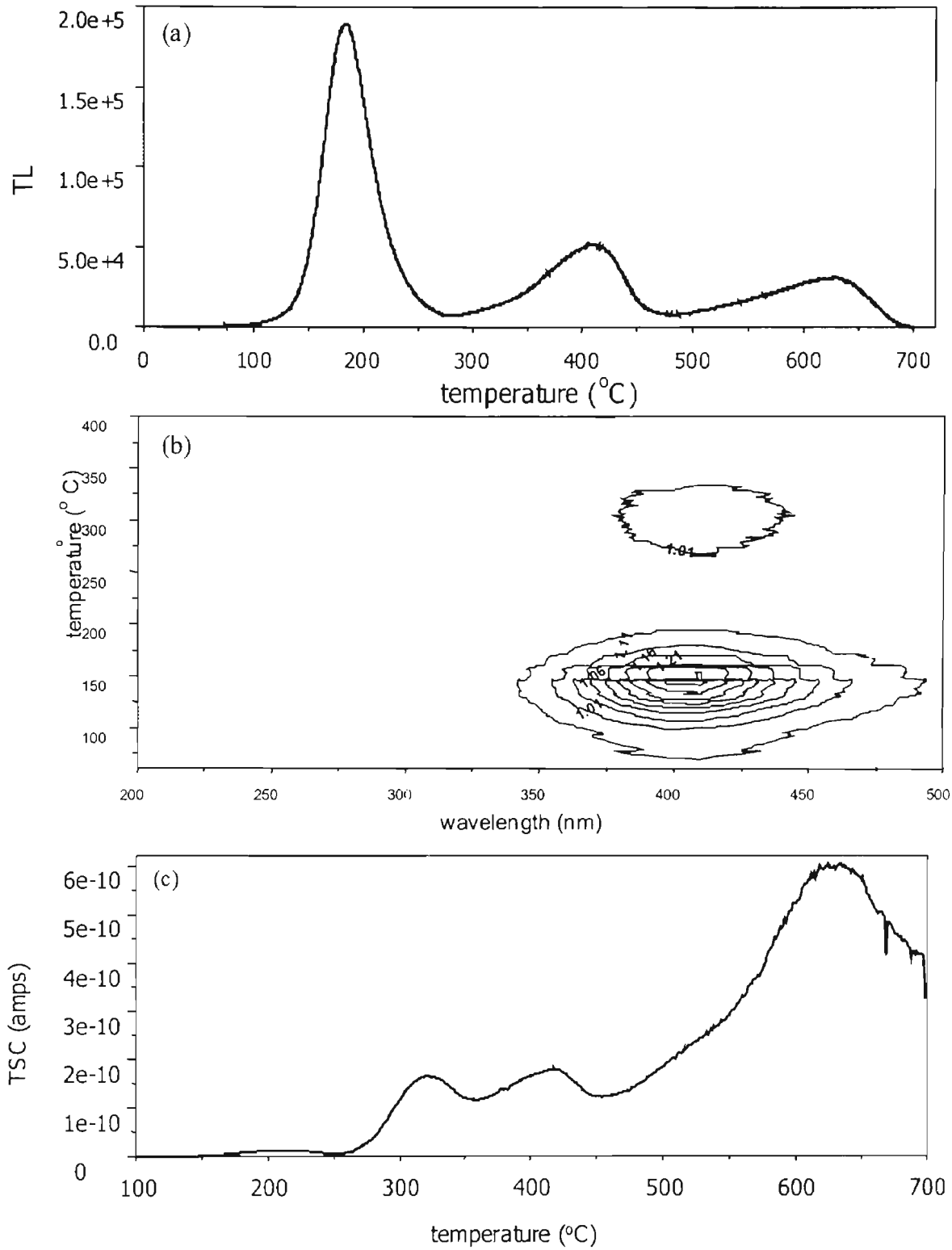

Figure 3.17: (a) TL glow curve for H-1 showing the peaks at ~180 °C, ~410 °C, and ~630 °C. (b) TL emission spectra showing peaks centered at ~160 °C and ~315 °C and at ~420 nm. (c) TSC curve showing conductivity peaks at ~200 °C, ~310 °C, 410 °C and possibly at ~520 °C.

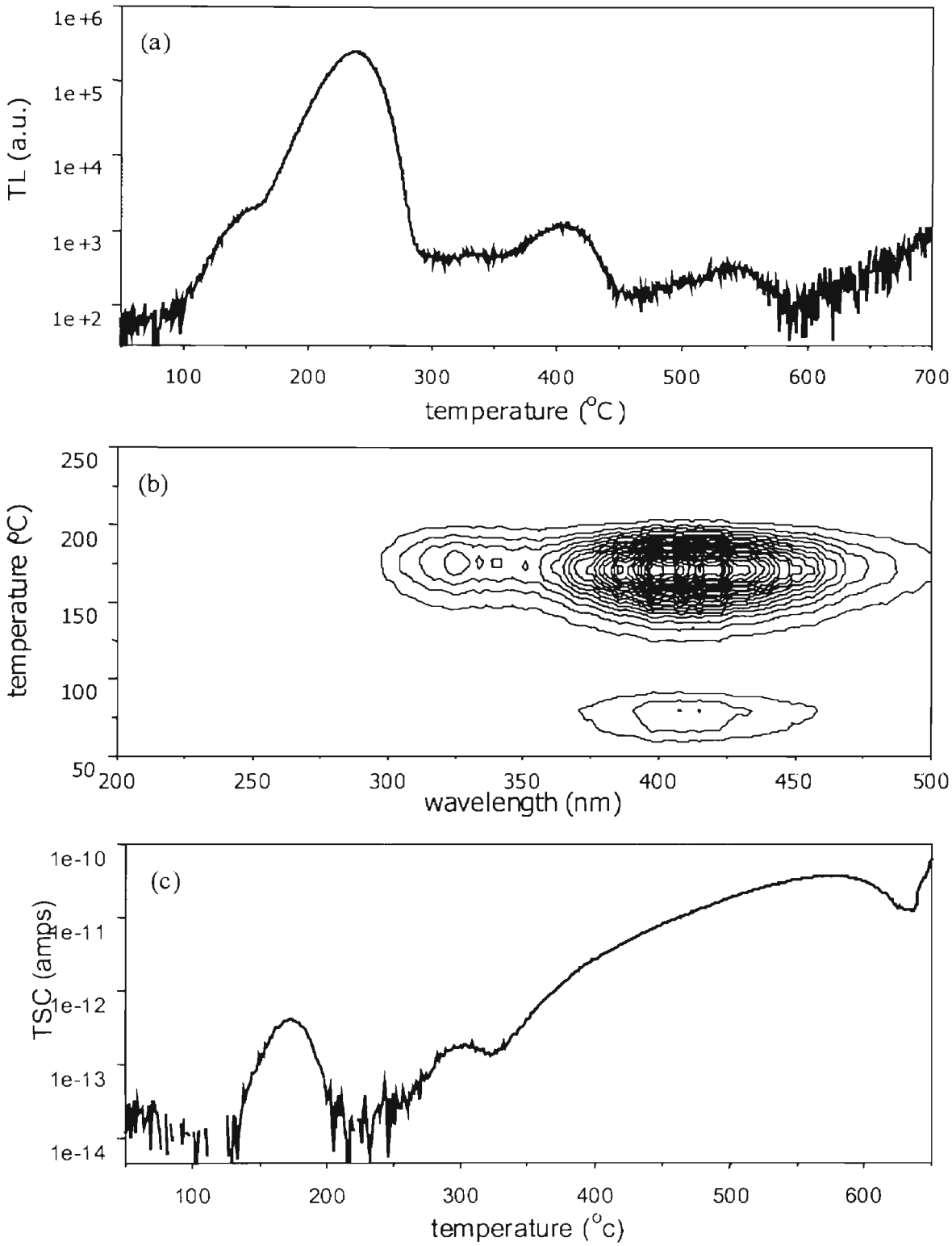

Figure 3.18: (a) TL glow curve for Mg-1 showing peaks centered at ~150 °C, ~225 °C, ~400 °C, and ~540 °C. (b) TL emission spectrum showing F center emission at ~75 °C, and F and F+ center emission at ~175 °C. (c) TSC curve showing peaks centered at ~175 °C, ~300 °C, and ~550 °C.

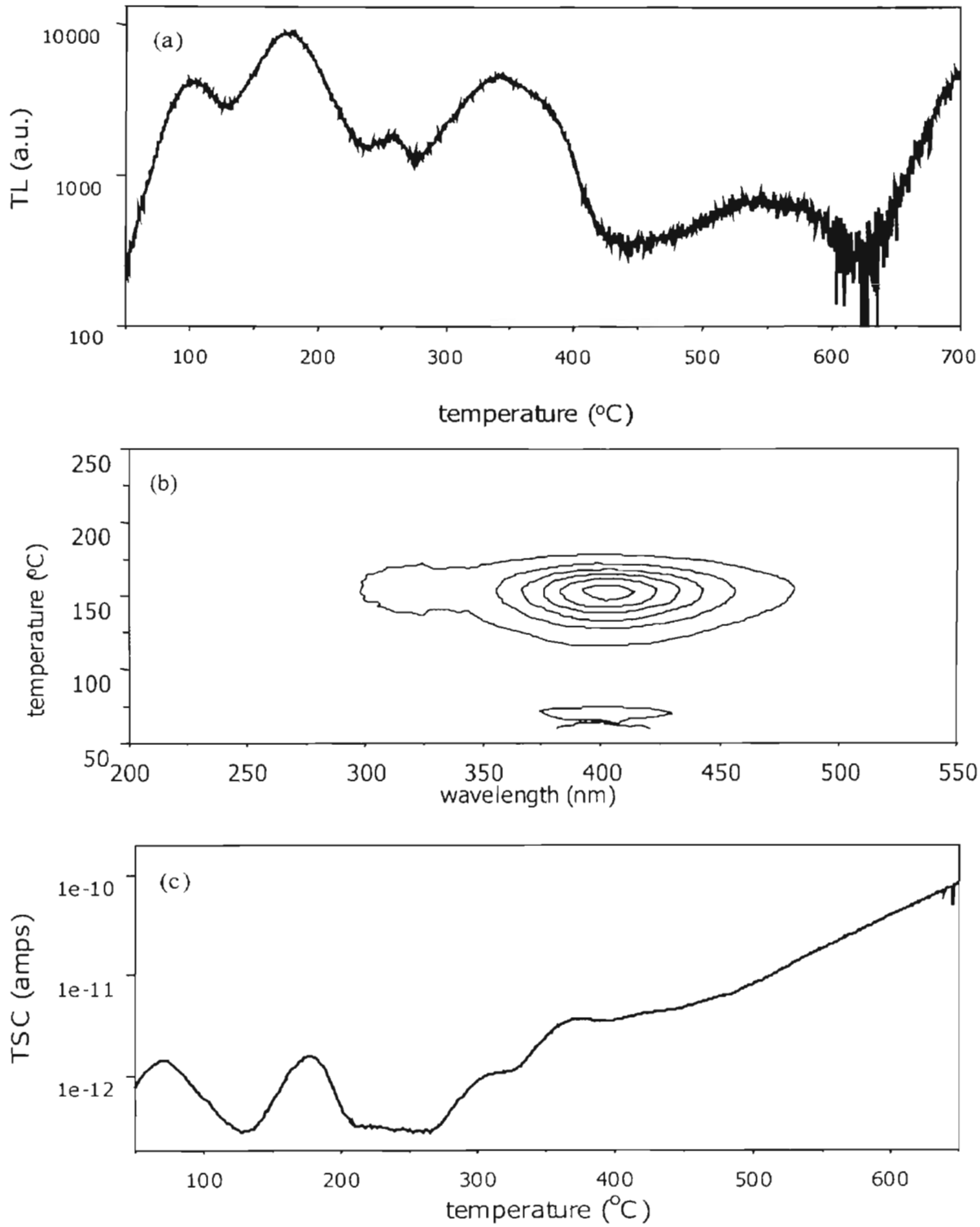

Figure 3.19: (a) TL glow curve for Mg-3 showing peaks centered at ~75 °C, ~160 °C, 340 °C, and 550 °C. (b) TL emission spectrum showing F center emission at ~75 °C and ~180 °C, and F+ center emission ~180 °C. (c) TCS curve showing peaks at ~75 °C, ~180 °C, ~300 °C, ~375 °C, and ~420 °C.

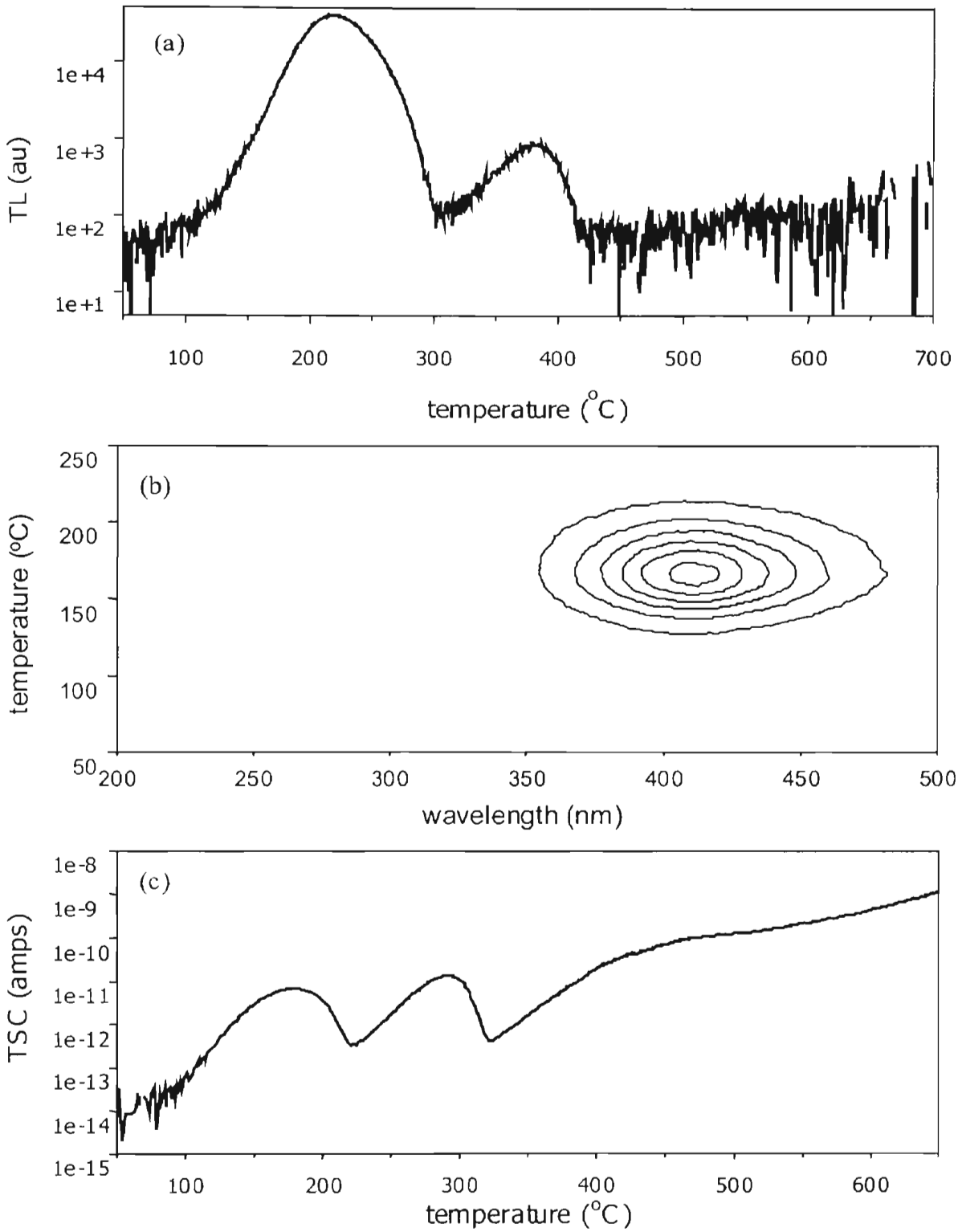

Figure 3.20: (a) TL glow curve for Mg-6 showing peaks centered at ~210 °C and 375 °C. (b) TL emission showing F center emission at ~160 °C centered at 420 nm. (c) TSC curve showing peaks at ~180 °C, ~290 °C, and 460 °C.

associated with the 140 °C TL peak. The 300 °C TSC peak is associated with a possible TL peak around 325 °C, and the changes in the slope of the TSC curve through the range of 350 °C to 410 °C with the 400 °C TL peak.

The TL glow curve, emission spectrum, and TSC curve for mg-3 is shown in figure 3.19. For Mg-3, the TL glow curve showed a small peak at ~75 °C, a relatively large peak at ~180 °C, a peak at ~340 °C, and a peak at ~550 °C. The TL emission spectrum shows a small F center emission peak at ~75 °C and a relatively large F center emission peak at ~175 °C both of which are centered at 420 nm. Also we see a small F+ center emission peak at ~180 °C centered at 325 nm. The TSC curve shows a peak at ~75 °C associated with the 75 °C TL peak. Also seen is a TSC peak at ~180 °C associated with the 180 °C TL peak, TSC peaks at ~310 °C associated with the 310 °C TL peak, and TSC peaks at ~375 °C and ~ 420 °C associated with the 420 °C TL peak.

For Mg-6 the TL glow curve shows a large peak centered at ~210 °C and a relatively small peak centered at ~375 °C. The TL emission spectrum shows a single F center emission peak at ~180 °C centered at 420 nm. The TSC curve shows a peak centered at ~180 °C and ~290 °C associated with the 210 °C TL peak. The TL glow curve, emission spectrum, and TSC curve for Mg-6 is shown in figure 3.20.

Relatively good agreement is seen between the TL glow curve and TSC curve from the samples. In general each TL peak can be correlated to a TSC peak that occurs at slightly higher temperatures. This gives good evidence that radiative recombination is occurring via recombination processes that involve the conduction band. The shift in the occurrence of the TSC peaks is noticed to be different in all of the samples. This leads to the interpretation that the temperature dependence of the charge mobility is different in

each sample. Also this might lead to the conclusion that the type of charge being released into the delocalized bands are different, and what we are actually seeing is a mixture of electrons and holes being released and recombining. This conclusion follows from the fact that the charge mobility is dependent upon such factors as the recombination lifetime (n_c/τ) and the charge carrier concentration (n_c, n_h) of the individual samples [3.3].

Chapter 4

Discussion of Results and Conclusions

4.1 Discussion of Results for H-1

4.1.1 Comparison of TL and TSC

Figure 4.1 shows the comparison of the TL and the TSC curves for sample H-1 prepared, according to the experimental conditions described in chapter three. The position of the TSC peaks are shown to be in good correlation with the position of the TL peaks. This leads to the conclusion that the TL process involves the release of charge carriers into the delocalized bands as shown in figure 2.2. The delocalized charges then recombine producing luminescence. We see from the sizes of the TL and TSC peaks that the 410 °C and 630 °C peaks are much smaller than their TSC counterparts at 310 °C, 410 °C, and 625 °C. This is due to thermal quenching of the TL peak intensities seen in Al_2O_3:C. From the discussion of section 2.4.2 (specifically equations 2.24-2.27), we expect the TL peaks to be shifted to lower temperatures than the TSC peaks without considering thermal quenching. However, for the most part, the TL and TSC peaks occur at approximately the same temperature throughout the duration of the measurement. From figure 4.1 we see that the 180 °C TL peak position is somewhat lower than its corresponding TSC peak centered at 200 °C (as expected). For the other TL peaks however, we do not see this type of temperature shift. In fact, the 410 °C TL peak is

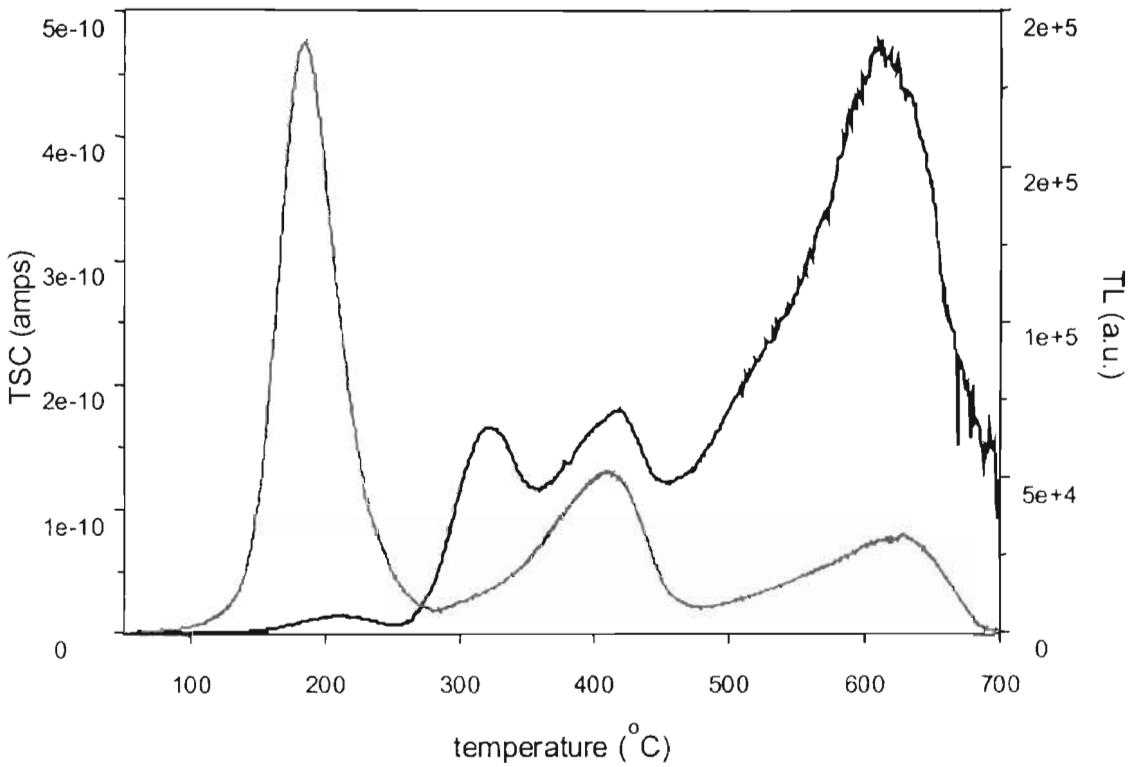

Figure 4.1: Comparison of the TL glow curve and TSC signal form H-1. Good correlation is seen between the positions of the TL and TSC peaks, and thermal quenching is evident by the decrease in the size of the TL peaks relative to the TSC peaks.

matched almost perfectly with the peaks of the corresponding TSC signals at 310 °C and 410 °C. Then we see that the 630° C TL peak is actually centered at a slightly higher temperature than the corresponding TSC peak centered at 625 °C.

The positions and sizes of the TL and TSC peaks are dependent on many factors. We must remember, that TL and TSC peaks in Al_2O_3:C are known to be made up of a distribution of smaller peaks that add up to produce the overall peak [4.1,4.2]. The size and position of a given TL peak is dependent on the distribution and the amount of overlap of the smaller peak components. From equations 2.6, 2.8, and 2.24 we see that the TL and TSC can be written

$$I_{TL} = \eta n_c n_h A_r \tag{4.1}$$

$$I_{TSC} = VAe\mu n_c \tag{4.2}$$

where all terms are the same as previously defined. For TL, we see that the peak position and size will depend on the temperature dependence of the thermal quenching function (η), the concentration of charge in the delocalized bands (n_c), the concentration of recombination centers (n_h), and the transition coefficient of free holes (A_r). For η, we see from equation 2.31 that the quenching effects only influence the TL peak positions in the temperature ranges that the quenching curve is changing. That is to say that when $d\eta/dT \neq 0$. We see from figure 2.6, if we use the values of $\tau\upsilon$ and W reported by Akselrod et. al. [2.14] for Al_2O_3:C, that thermal quenching only will only affect the position of the TL peak in the temperature range of approximately 100 °C to 200 °C. For n_h, we see from equation 2.6 that the TL is dependent on the negative rate of recombination ($-dn_h/dT$). However as seen in the samples studied in this research, the

initial concentration of recombination centers for both electron recombination (n_h) and hole recombination (n) is much greater than the change in the concentrations of these of centers due to irradiation ($n_h \rangle\rangle \Delta n_h$). From this, we conclude that the concentration of recombination centers remains approximately constant during heating ($dn_h/dT \approx 0$). For A_r, we see that it is weakly temperature dependent due to the fact that it is the product of the thermal velocity (v) and the capture cross sections (σ) of the free holes as given by the equation

$$A_r = v\sigma \tag{4.3}$$

where A_r is given in units of $cm^{-3}*sec^{-1}$. From the analysis of Rose [4.3], σ is shown to be proportional to T^2, and the most widely excepted value for v is given by

$$v = (\frac{3k_bT}{m^*})^{\frac{1}{2}} \tag{4.4}$$

where m^* is the effective mass of the charge carrier [4.4]. Making these substitutions into equation 4.1 we can correct the position of the TL peak due to the temperature dependence of A_r. Taking values of m^*= 0.256 MeV for the rest mass of an electron [4.5], and $\sigma = (1/T^2)$ for A_r, the shift of a TL peak, with a peak temperature of 50 °C, due to the temperature dependence of A_r would be approximately 0.5 °C. This shift is negligible compared to the greater than 100 °C temperature ranges of the overall TL peaks of the samples used in this research. Therefore we will take A_r to be a constant in our measurements. From this, we conclude that the change in the TL intensity during heating will depend on the changes in the concentration of free charges in the delocalized bands and the changes in the thermal quenching function during heating as shown by

$$\frac{dI_{TL}}{dT} = \frac{d\eta}{dT} n_c n_h A_r + \eta \frac{dn_c}{dT} n_h A_r . \tag{4.4}$$

We see from equation 4.4 that at temperatures outside of the range of influence for η (~100–200 °C) the first term is approximately zero. At these temperatures, we expect that the TL peak intensity will occur when $dn_c/dT = 0$. For TSC, we see from equation 4.2 that the size and position of the peaks will depend on the temperature dependence of the charge mobility (μ), and the voltage (V) across the sample. In general, μ is found to be proportional to the temperature ($\mu \propto T^{\alpha}$), where α may be positive or negative. However, from data taken by Agersnap Larsen et. al. [4.6], suggests that μ in Al_2O_3:C is approximately constant. However, we consider it still quite possible that μ might exhibit some temperature dependence in our samples. For our purposes, we shall consider the voltage (V) across the sample to be constant, even though the space charges in the sample may exhibit some temperature dependence as charge is de-trapped during heating. For now we have no way of monitoring this, and thus we will consider V to be a constant. From these conclusions, we expect the change in the TSC intensity from equation 4.2 to be given by the equation

$$\frac{dI_{TSC}}{dT} = VAe \frac{d\mu}{dT} n_c + VAe\mu \frac{dn_c}{dT} . \tag{4.5}$$

When we are at temperatures were $d\eta/dT \approx 0$ and if $d\mu/dT = 0$, we will expect the TL and TSC peaks to occur at the same temperature. When $d\eta/dT < 0$, we expect that the TL peaks will be shifted to lower temperatures than the TSC peaks. Also, if μ exhibits a temperature dependence, we expect the TSC peaks to be shifted to higher temperatures if $\mu(T) \propto T^{\alpha}$, and we expect them to be shifted to lower temperatures if $\mu(T) \propto T^{-\alpha}$.

For H-1, we see that the 180 °C TL peak is shifted to lower temperature than its corresponding TSC peak. At this temperature, we see that $\frac{d\eta}{dT} < 0$ and therefore would expect the TL peak to be shifted to lower temperatures than its corresponding TSC peak. The 410 °C TL peak is centered at approximately the same temperature as its corresponding TSC peak, and the 310 °C peak appears to correspond to a TL peak that appears as a tail on the front side of the 410 °C TL peak. Also, the 630 °C peak appears to be shifted slightly lower than its TSC counterpart, but the shift is small enough that it is within the uncertainties of the temperature measurements. Therefore we neglect the shift of the 630 °C peak. The fact that these TL and TSC peaks correspond well suggests that the mobility is possibly exhibiting an inversely proportional temperature dependence ($\mu(T) \propto T^{-\alpha}$). However, this is difficult to conclude due to the peak overlap of the individual peaks that make up the overall TL peaks. Therefore, we can draw no solid conclusions about the temperature dependence of the mobility for H-1 and make only the statement that the possibility exists of an inversely proportional temperature dependence.

4.1.2 Comparison of TL with the F and F+ Center Concentration

The temperature dependence of the F+ center concentration is shown in figure 4.2 in comparison with the TL glow curve. The F+ center concentration is seen to decrease in correlation with the 180 °C TL peak. The F+ center concentration decreases again over a temperature range of 300 °C to 400 °C correlating to the 410 °C TL peak and increases from about 550 °C to 700 °C correlating to the 630 °C TL peak. The decrease in the F+ center concentration around 180 °C and 410 °C coincides with an increase in the F center concentration in the same temperature ranges as shown in figure 3.9. This leads to the

conclusion that the 180 °C and 410 °C TL peaks in H-1 are produced by the release of trapped electrons that recombine at F+ centers to produce an excited F center which relaxes producing an emission band centered at 420 nm as shown in equation 2.33. This conclusion is further supported by the TL emission spectrum shown in figure 3.17. We see an emission band centered at 420 nm. We expect that this emission lies in the same temperature ranges as the 180 °C and 410 °C TL peaks; the dependence in temperature is due to the error introduced by experimental setup, as discussed in section 3.3.1. The increase in the F+ center concentration from about 550 °C to 700 °C and coincides with a decrease in the F center concentration in the same temperature ranges as shown in figure 3.9. This leads to the conclusion that the 630 °C TL peaks in H-1 are produced by the release of trapped holes that recombine at F centers to produce excited F+ centers that relax to produce an emission band centered at 326 nm as shown in equation 2.34. The emission spectrum in this temperature range could not be measured due to limitations in the heating range of the TL emission experimental setup.

From equation 2.6 we see that the TL intensity should be proportional to the negative derivative of the concentration of recombination centers (n_h) in the crystal ($I_{TL} \propto -dn_h/dT$). For the case of H-1 we have concluded that the recombination centers are either the F+ centers (for the 180 °C and 410 °C peaks) or the F centers (for the 630 °C peak). Figure 4.3 shows a comparison of the positive peaks produced by the negative derivative of the F+ center concentration ($-dn_{F^+}/dT$) and the negative derivative of the F center concentration ($-dn_F/dT$) to the TL glow curve for H-1. The concentration derivative peaks are centered at lower temperatures than the TL peaks. However, overall, we see good correlation between the TL peaks and the peaks produced

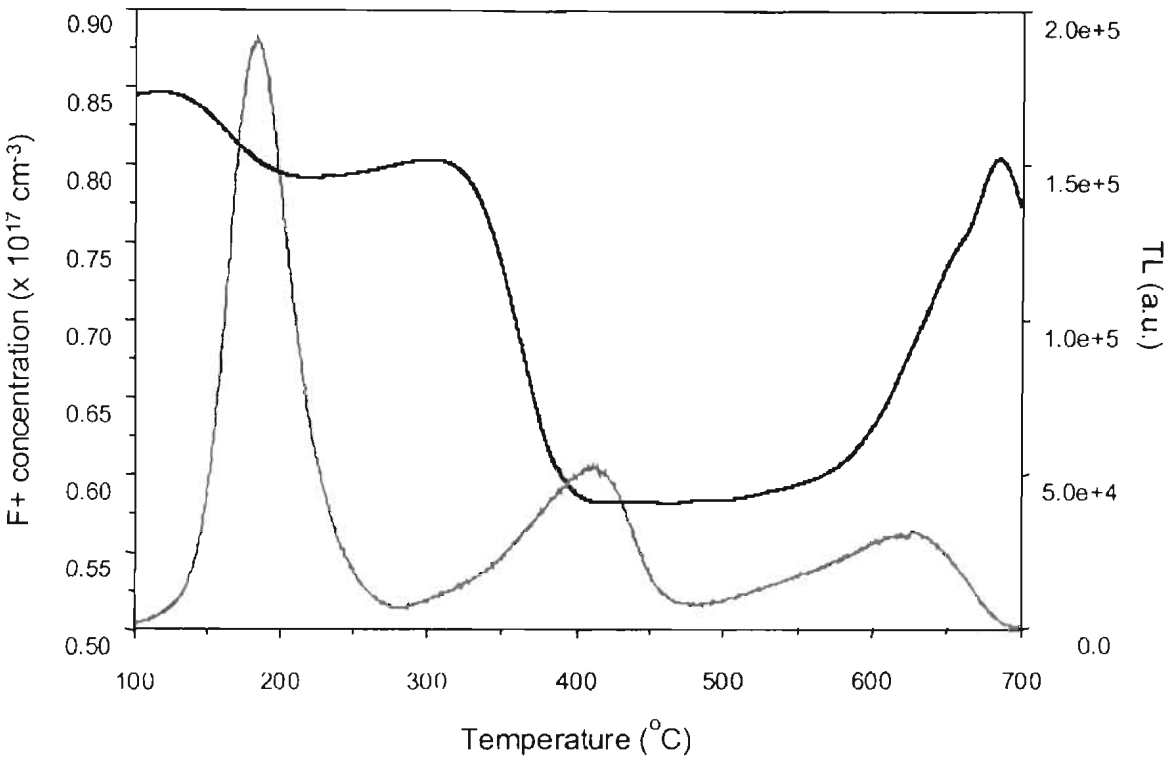

Figure 4.2: Comparison of the TL glow curve and F+ center concentration for H-1. Good correlation is seen between the positions of the TL peaks and the changes in the F+ center concentration.

by differentiating the F and F+ center concentrations with respect to temperature. The F center concentration derivative peak at 630 °C shows several sharp peaks due to the noise in the data that was then smoothed and then differentiated. This results in the high frequency noise at high temperatures being smoothed into several steps in the data that are differentiated to produce several sharp peaks.

The fact that the peaks of the derivative of the recombination center concentration are at lower temperatures than the TL peaks suggests that recombination at the F and F+ centers might not be the only type of recombination occurring during TL. This conclusion is also suggested by the differences in the concentration changes of the F and F+ centers over the temperature ranges of the TL peaks as seen in figure 3.9. If another recombination process is occurring during the TL process, F centers may be lost or created without the production or loss of an F+ center or vice versa resulting in the changes in the F and F+ center concentrations being different. If the process didn't involve recombination at F+ centers, then the derivative of the F+ center concentration would not be affected. However if this involved the production of F centers and F center emission, it would add to the TL peak causing the TL peak maximum to be shifted to a higher temperature. Such a process might involve a negatively charged F center such as

$$F^- + h^+ \rightarrow F + h\nu_{420nm} \quad . \tag{4.6}$$

Also if the process involves the production of F+ centers and F+ center emission, it might involve a doubly ionized F center (F++) such that

$$F^{++} + e^- \rightarrow F^+ = h\nu_{326nm} \quad . \tag{4.7}$$

The process described in equation (4.6) involves the production of an F center without

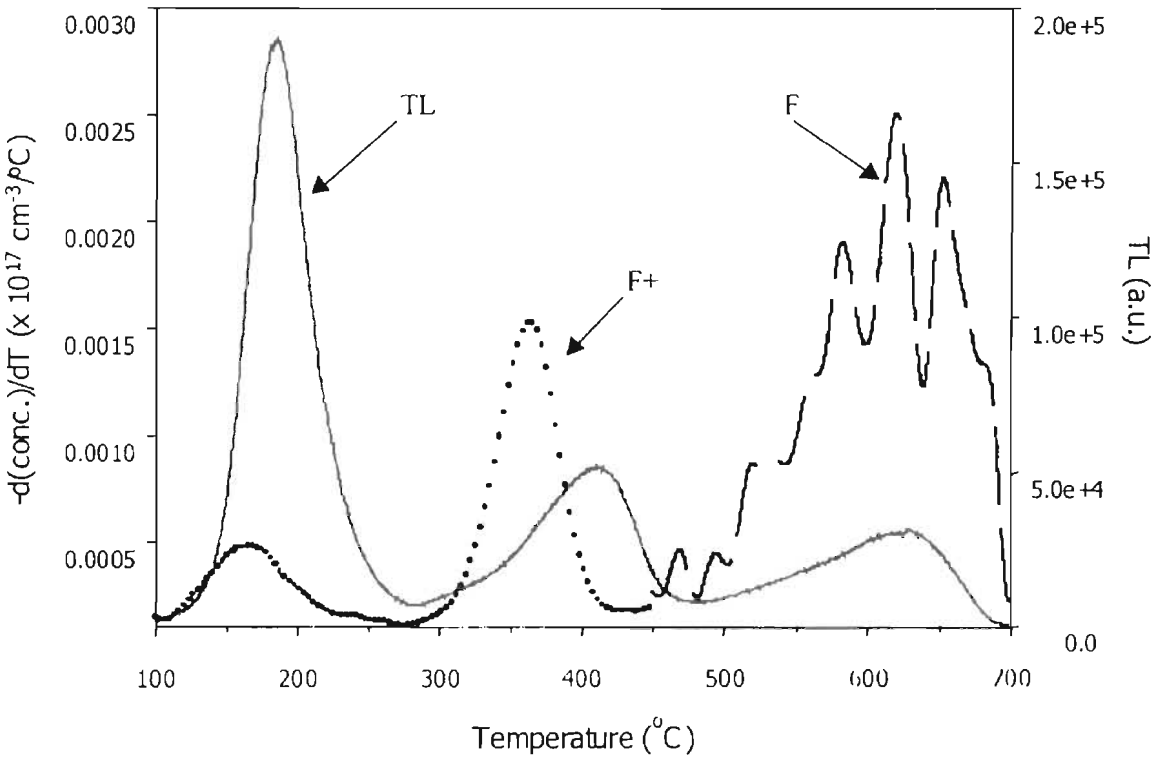

Figure 4.3: Comparison of TL intensity (solid gray) and the negative derivative of the concentration of recombination centers for H-1. The 180 °C and 410 °C TL peaks are compared to recombination at F+ centers (dotted lines), and the 630 °C TL peak is compared to recombination at F centers (dashed lines).

the loss of an F+ center, and the process described in equation (4.7) involves the production of an F+ center without the loss of an F center. These ideas might give some insight into the differences in the size of changes in the F and F+ center concentrations, and in the differences in the position of the peak maximums for the TL and derivative of the recombination centers in H-1.

4.2 Discussion of Results for Mg-1, Mg-3, and Mg-6

4.2.1 Comparison of TL and TSC

Figure 4.4 shows the comparison of the TL and the TSC data for sample Mg-1 prepared according to the experimental conditions described in chapter three. We see that the 175 °C TSC peak is shifted slightly higher than the TL peak centered at approximately 150 °C due to thermal quenching in this temperature range. The 300 °C TSC peak is shifted quite substantially from the 225 °C TL peak (if they are at all connected), and the large TSC peak that is centered at 575 °C is shifted above the TL peak centered at 540 °C. This suggests that the charge mobility for Mg-1 is possibly directly proportional to the temperature ($\mu(T) \propto T^{n}$). However, due to peak overlap we are unable to make a definite conclusion about the charge mobility.

Figure 4.5 shows the comparison of the TL to the TSC measurement for sample Mg-3. We see from the sizes of the TL and TSC peaks that the 340 °C TL peak is much smaller than its TSC counterparts at 300 °C and 360 °C. The 180 °C TL and its TSC counterpart are centered at about the same temperature. As seen for H-1, we expect to see the TL peak shifted to lower temperatures than its TSC counterpart as seen from the discussion of section 2.4.2 and due to thermal quenching. The lack of shift suggests that

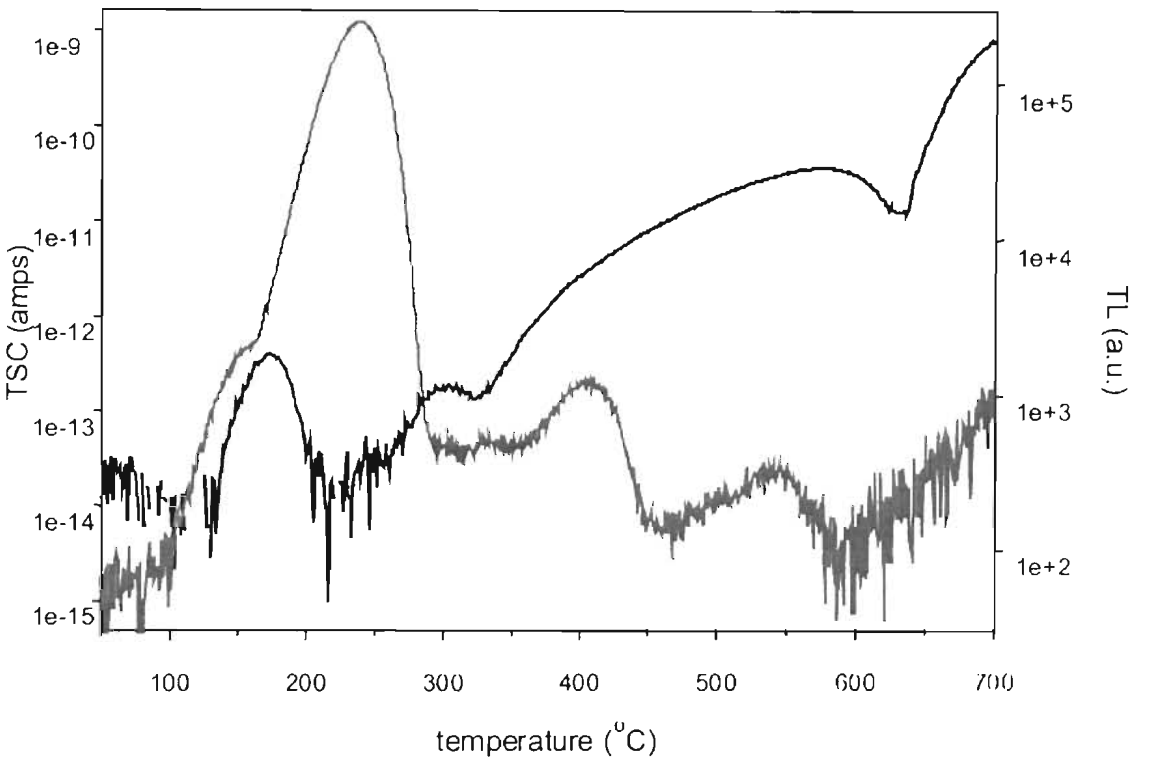

Figure 4.4: Comparison of the TL glow curve and TSC signal form Mg-1. Good correlation is seen between the positions of the TL and TSC peaks, and thermal quenching is evident by the decrease in the size of the TL peaks relative to the TSC peaks.

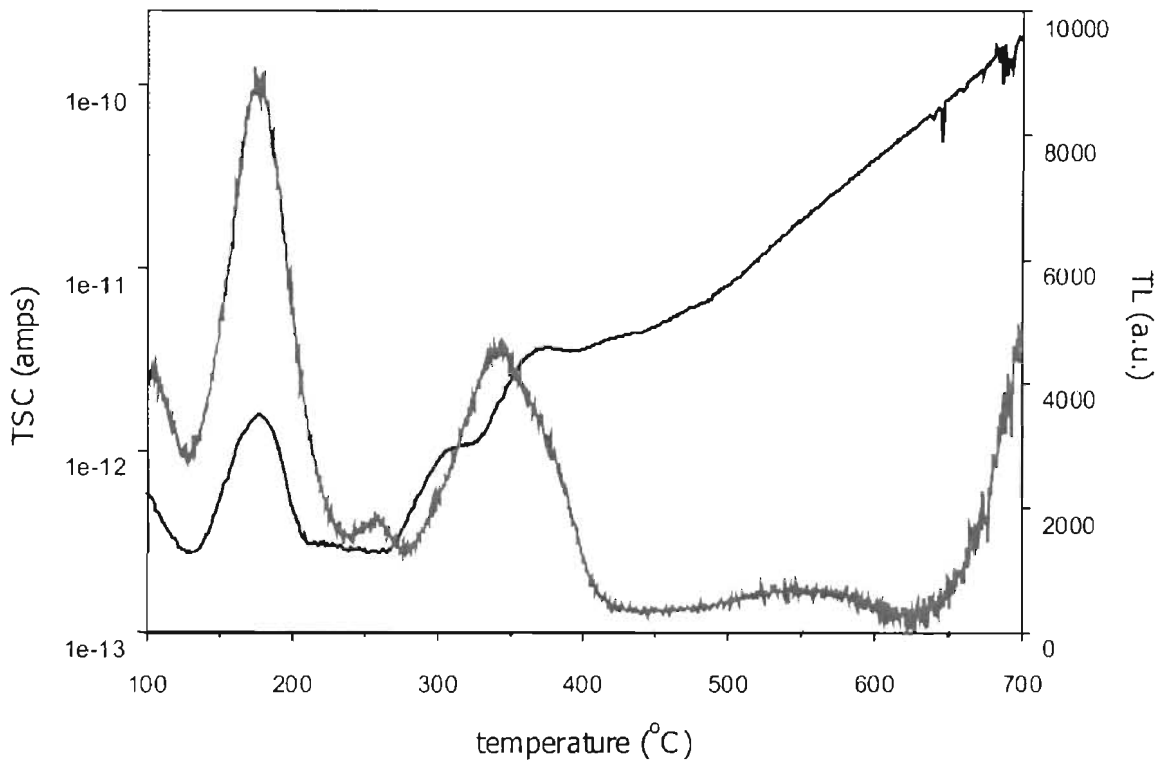

Figure 4.5: Comparison of the TL glow curve and TSC signal form Mg-3. Good correlation is seen between the positions of the TL and TSC peaks, and thermal quenching is evident by the decrease in the size of the TL peaks relative to the TSC peaks.

the charge mobility is inversely dependent on the temperature, but no conclusion can be made because we do not know the details of the individual peaks that make up the overall 180 °C TL peak. The 310 °C TL peak appears to correlate to the 300 °C and 375 °C TSC peaks. The two separate TSC peaks offer good evidence that the TL peak is made up at least two smaller TL peaks that overlap to produce the 310 °C TL peak. The TSC signal shows no distinct peak in the region of the 550 °C TL. There might be a TSC peak correlated with this TL peak, however the high background signal at these temperatures will cover up any signal produced by the release of trapped charges.

Figure 4.6 shows the comparison of the TL and the TSC measurements for sample Mg-6 prepared according to the experimental conditions described in chapter three. The 210 °C TL peak is somewhat shifted to lower temperatures than the TSC peaks at 180 °C and 290 °C. This is good evidence of that the 210 °C TL peak is made up of at least two smaller peaks. Also, the 375 °C TL peak is shifted to lower a temperature than it 460 °C TSC counterpart. This shifting of the TL peaks to lower temperatures is in agreement with the discussion of section 2.4.2. Also this could suggest that the charge mobility for Mg-6 is possibly directly proportional to the temperature, but we must also consider this shift is occurring due to the overlap of the peaks.

4.2.2 Comparison of TL with the F and F+ Center Concentration

The comparison of the F+ center concentration as a function of temperature with the TL glow curve for Mg-1 is shown in figure 4.7. The decrease in F+ center concentration until 150 °C and increase until 250 °C in the F+ center concentration coincides with an increase and then decrease in the F center concentration in the same temperature ranges as shown in figure 3.11. This leads to the conclusion that the 150 °C TL peak in Mg-1 is

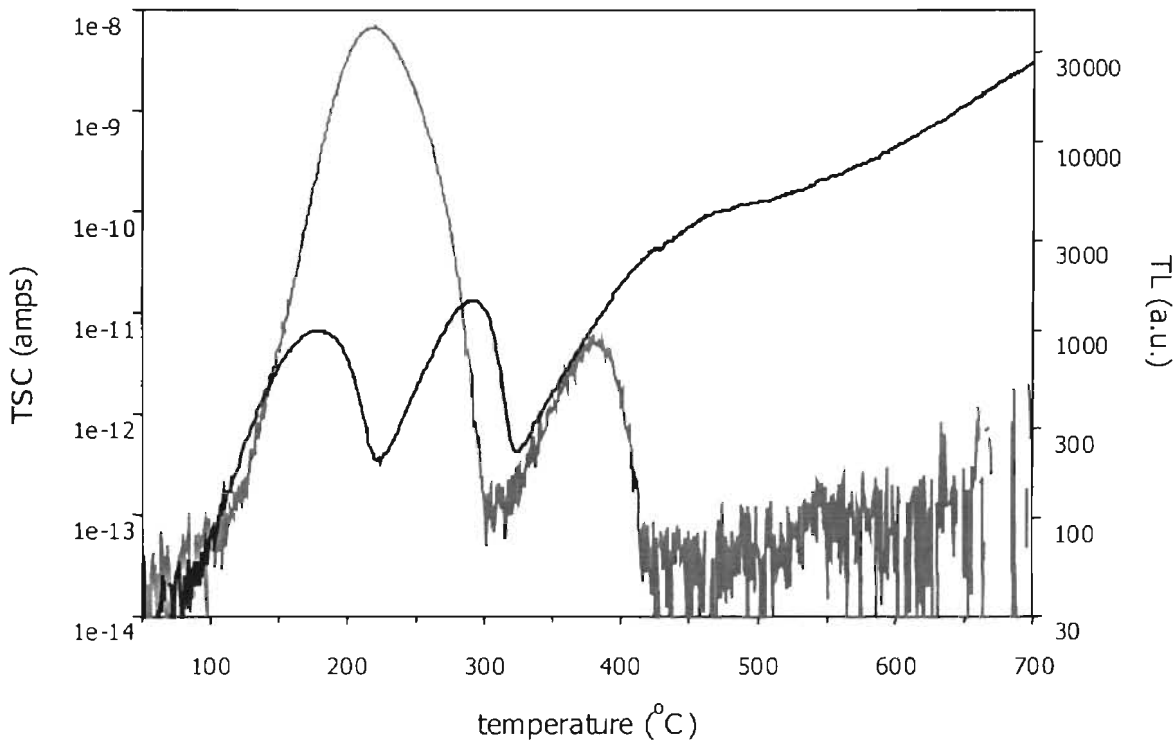

Figure 4.6: Comparison of the TL glow curve and TSC signal form Mg-6. Good correlation is seen between the positions of the TL and TSC peaks, and thermal quenching is evident by the decrease in the size of the TL peaks relative to the TSC peaks.

produced by electron recombination with F+ centers. The increase in the F+ center concentration from about 150 °C to 250 °C leads to the conclusion that the 225 °C TL peak in Mg-1 is produced by hole recombination at F centers. From figure 3.18, we see an emission band centered at 420 nm correlating to the 150 °C TL peak after temperature correction as well as a strong F+ center emission band. The appearance of both emission bands in this temperature range suggests that both F and F+ center recombination is occurring. We see that there is no significant change in the F+ or F center concentrations correlating to the 400 °C TL peak. We then assign the production of the 400 °C TL peak to recombination processes not involving the F and F+ centers. The 540 °C TL peak correlated to an increase and then a decrease in the F+ center concentration, which we assign to recombination of holes with F centers and recombination of electrons with F+ centers. The increase in the TL signal from 600 °C out to 700 °C is assigned recombination of electrons with F+ centers.

The comparison of the F+ center concentration as a function of temperature to the TL glow curve for Mg-3 is shown in figure 4.8. This leads to the conclusion that the 180 °C peak is produced by a combination of electron and hole recombination processes at F+ and F centers to produce F and F+ center emission bands. This conclusion is further supported by the TL emission spectrum shown in figure 3.19 were we see both F and F+ center emission bands. The production of the 340 °C TL peak in Mg-3 is assigned to both the recombination of electrons at F+ centers and recombination of holes at F centers. Also, we conclude that the 540 °C TL peak is produced by F center recombination processes that do not involve the F+ center, and the TL signal seen from 650 °C to 700 °C is produced by a both F and F+ center recombination processes.

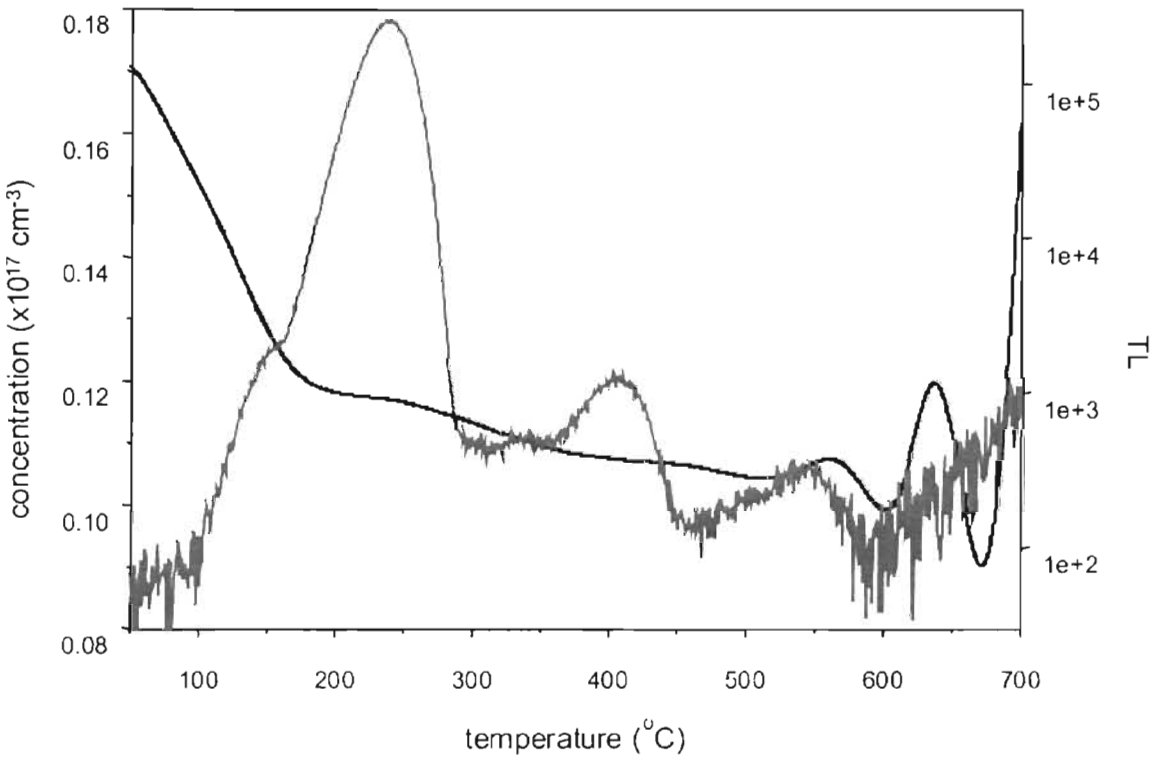

Figure 4.7: Comparison of the TL glow curve and F+ center concentration for Mg-1. Good correlation is seen between the positions of the TL peaks and the changes in the F+ center concentration.

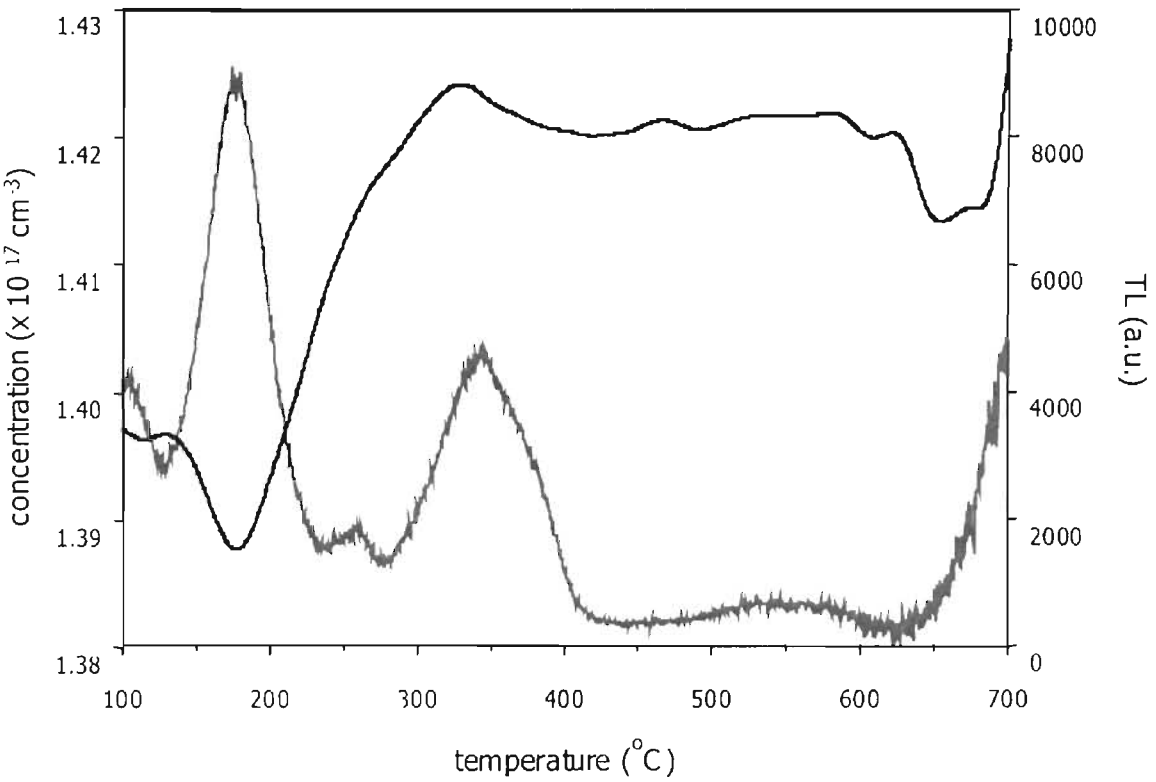

Figure 4.8: Comparison of the TL glow curve and F+ center concentration for Mg-3. Good correlation is seen between the positions of the TL peaks and the changes in the F+ center concentration.

The comparison of the F+ center concentration as a function of temperature to the TL glow curve for Mg-6 is shown in figure 4.9. The overall changes in the F and F+ center were very small in Mg-6, and did not show a general anti-correlation as in the other samples. We also see poor correlation to the change in the F+ center concentration and the TL peaks for this sample. From the comparison made in figure 4.9, we make the conclusion that the 210 °C TL peak in is produced by recombination of electrons and holes with F+ and F centers respectively. This conclusion is in contrast to the TL emission spectrum shown in figure 3.18, which shows only a large F center emission peak centered at 420 nm. We conclude, that the 375 °C TL peak is not produced by a process involving both F and F+ centers as described by equation 2.34. Instead, it could be produced by a process such as the one described by equation 4.3. The remaining increases in F+ centers do not correlate to a decrease in F center concentration or a TL peak. Therefore we conclude that the recombination occurring is nonradiative and not of the type described by equation 2.34.

For the case of Mg-1 we have concluded that the recombination centers are either the F+ centers (for the 150 °C, 225 °C, and 540 °C TL peaks and 700 °C TL signal) or the F centers (for the 225 °C and 540 °C TL peaks). Figure 4.10 shows a comparison of the positive peaks of the negative derivative of the F+ center concentration ($-dn_{F_+}/dT$) and of the negative derivative of the F center concentration ($-dn_F/dT$) to the TL glow curve for Mg-1. We see, as for H-1, that the concentration derivative peaks are shifted to lower temperatures than the TL peaks. The TL peaks for Mg-1 appear to be produced by both electron and hole recombination processes. As seen by the 225 °C and 540 °C TL peaks, and the 600 °C to 700 °C TL signal, both electron and hole recombination processes are

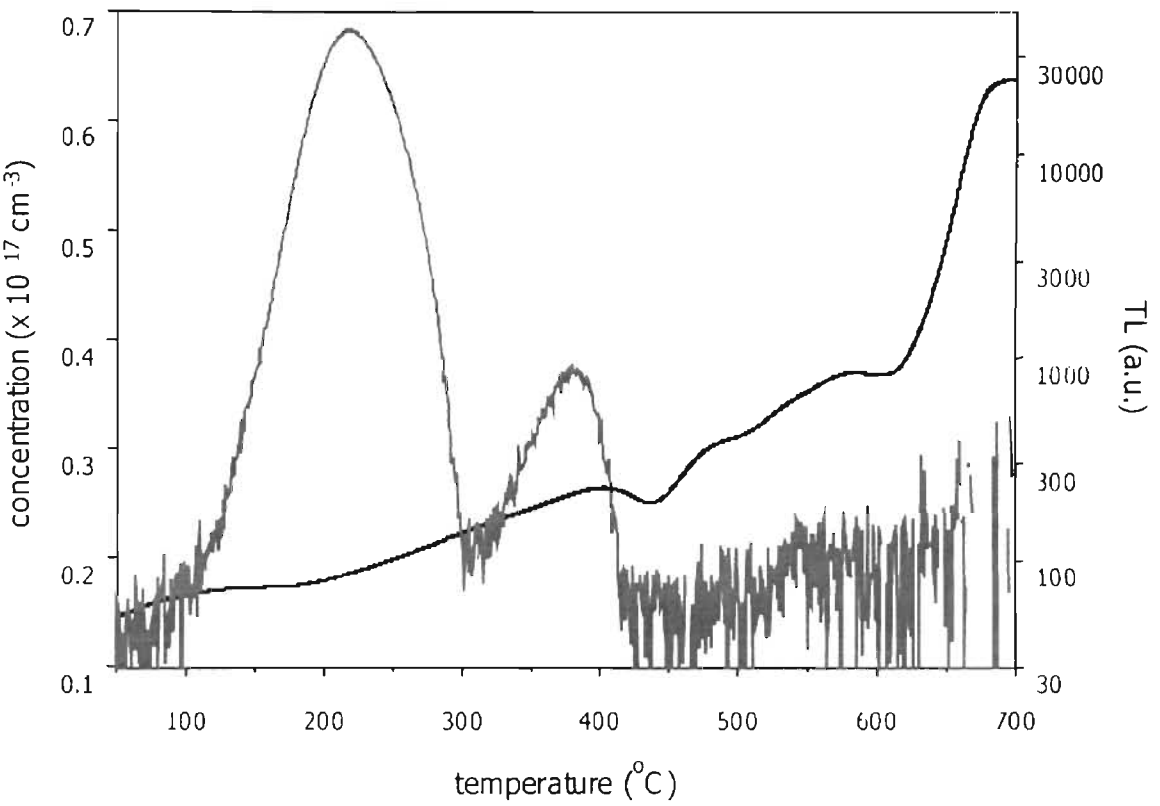

Figure 4.9: Comparison of the TL glow curve and F+ center concentration for Mg-6. Good correlation is seen between the positions of the TL peaks and the changes in the F+ center concentration.

involved in the production of the overall TL peak. Also, several small peaks in the F + center concentration derivative indicate that several distinct recombination processes are occurring producing smaller TL peaks that overlap to form the overall TL peak. As suggested by the comparison of F+ concentration to the TL for Mg-1 we see no peak for the F or F+ center concentration derivative for the 400 °C TL peak. Because of this, along with the recombination processes described by 2.33 and 2.34, we also recognize that alternative processes of recombination must be occurring in Mg-1. Any number of additional processes, such as the ones mentioned in equations 4.6 and 4.7, could be contributing to the TL peaks.

For the case of Mg-3 we have concluded that the recombination centers are either the F+ centers (for the 180 °C, 340 °C, and 550 °C peaks) or the F centers (for the 180 °C, 340 °C, 550 °C peaks). Figure 4.11 shows a comparison of the positive peaks produced by taking the negative derivative of the F+ center concentration ($-dn_{F+}/dT$) and of the F center concentration ($-dn_{F}/dT$) to the TL glow curve for Mg-3. We see good correlation between the TL peaks and the peaks produced by differentiating the F and F+ center concentrations, and we again notice the shift to lower temperatures of the concentration derivative peaks as seen in H-1 and Mg-1. Several F and F+ center derivative peaks appear in the temperature range of the 340 °C and 550 °C TL peaks leading to the conclusion that they are made up of several smaller peaks distributed over the temperature range of the TL peaks. Also, along with F and F+ center recombination processes described by equations 2.33 and 2.34, we noticed recombination processes involving the F center (correlating to the 550 °C TL peak) that did not involve the F+ centers. One possible conclusion is that a recombination process such as the one

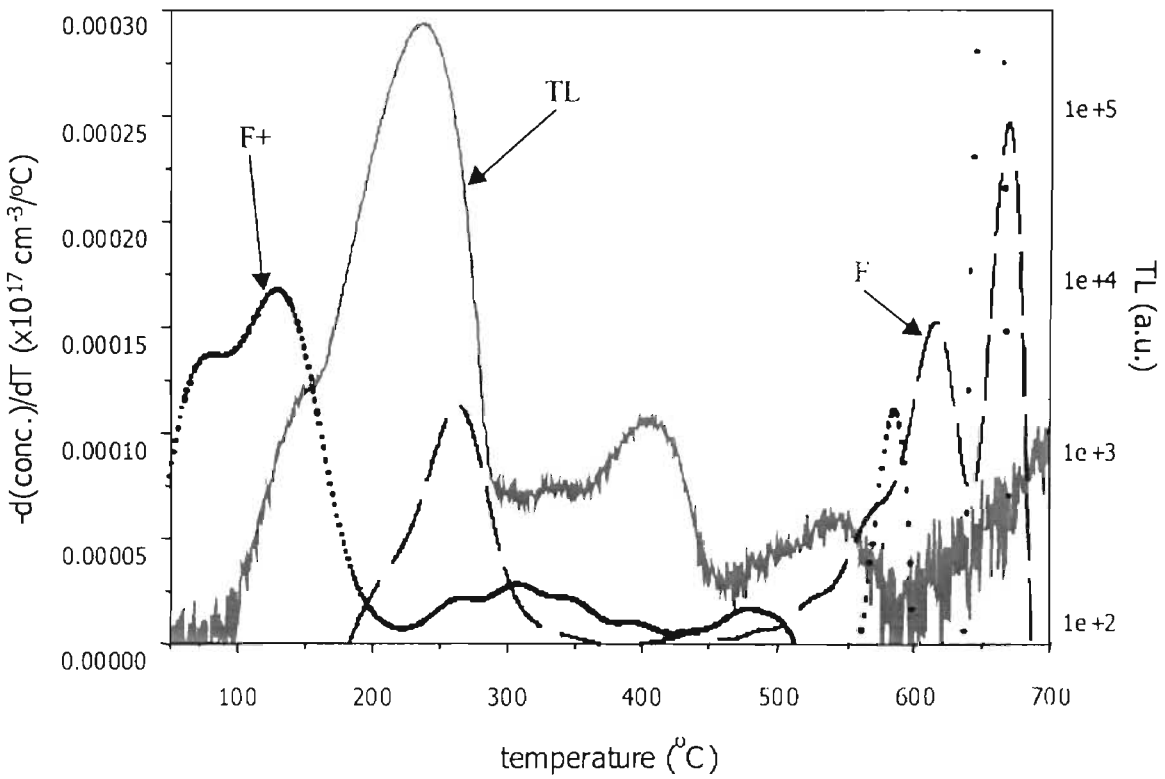

Figure 4.10: Comparison of TL intensity (solid gray) and the negative derivative of the concentration of recombination centers for Mg-1. The 150 °C, 225 °C, 540 °C, TL peak and 700 oC TL signal are compared to recombination of electrons with F+ centers (dotted lines), and the 225 °C and 540 °C TL peak and 700 °C TL signal are compared to recombination of holes with F centers (dashed lines).

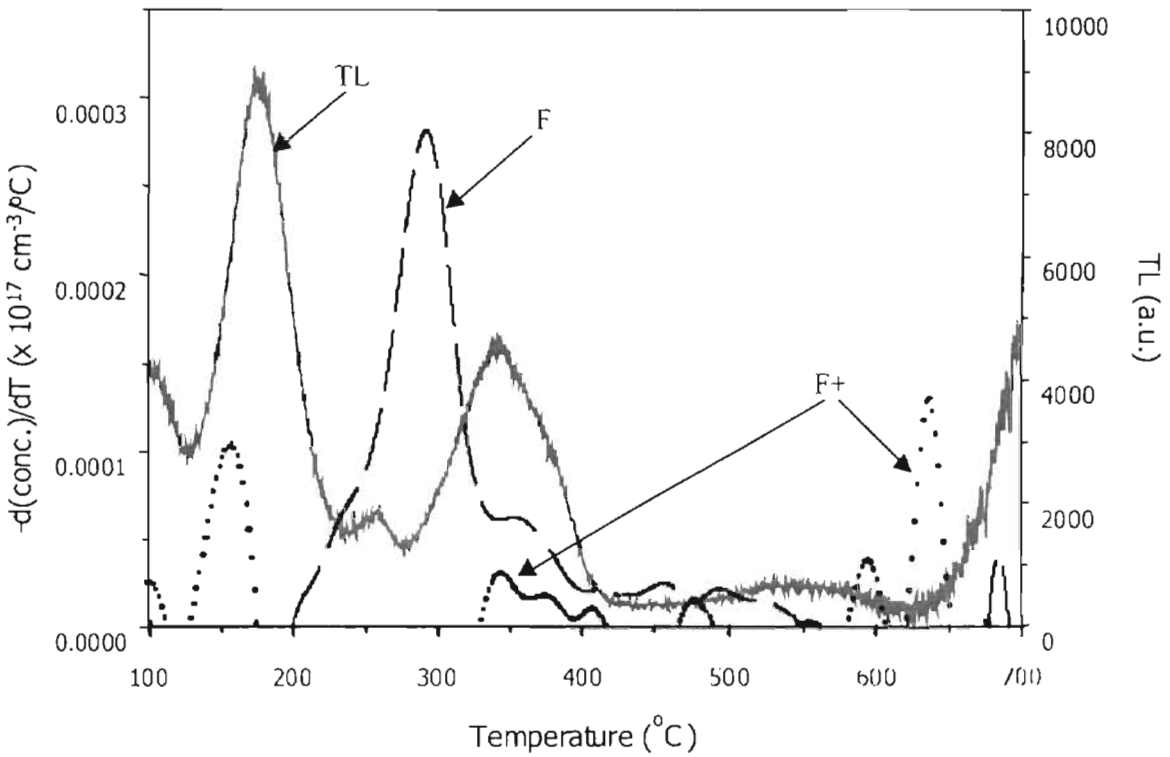

Figure 4.11: Comparison of TL intensity (solid gray) and the negative derivative of the concentration of recombination centers for Mg-3. The 175 °C, 340 °C, 550 °C TL peak and 700 °C TL signal are compared to recombination of electrons with F+ centers (dotted lines). The 180 °C, 340 °C, and 550 °C TL peak and 700 °C TL signal are compared to recombination of holes with F centers (dashed lines).

described by equation 4.2 is occurring.

For the case of Mg-6, we do not see good results in the correlation of the changes in the F and F+ center concentration to the TL peaks. Therefore we do not expect good correlation between the TL peaks and the peaks of the concentration derivatives. Figure 4.12 shows this comparison for the negative derivative of the F+ center concentration ($-dn_{F+}/dT$) and of the F center concentration ($-dn_F/dT$) and the TL glow curve for Mg-6. The F center concentration derivative peaks occur within the temperature range of the 210 °C TL peak suggesting hole recombination that produces an F+ center emission band. This is contrary to the TL emission of Mg-6 shown in figure 3.20. which shows only an F center emission peak in this temperature region. No derivative concentration peak appears in the temperature range of the 375 °C peak. This leads us to believe that this TL peak is not produced by recombination at F or F+ centers.

4.5 Conclusions

From the presented work, we see that the F and F+ centers play an important role in the production of luminescence during the TL process for the samples studied in this research. The TL process was seen to involve the release of trapped charge into the delocalized bands and recombination at F or F+ centers. All samples showed the correlation of TSC peaks to the TL peaks. All the samples also showed thermal quenching of the intensity of the high temperature TL peaks. Also sample H-1 and Mg-1 showed evidence that the TL peaks in the range from approximately 100 °C to 200 °C showed a shift to lower temperature than the TSC peak due to the effects of the thermal quenching. From the shift in the TL peaks we suggest the possibility that the charge mobility is proportional to the temperature for Mg-1 and Mg-6 and inversely

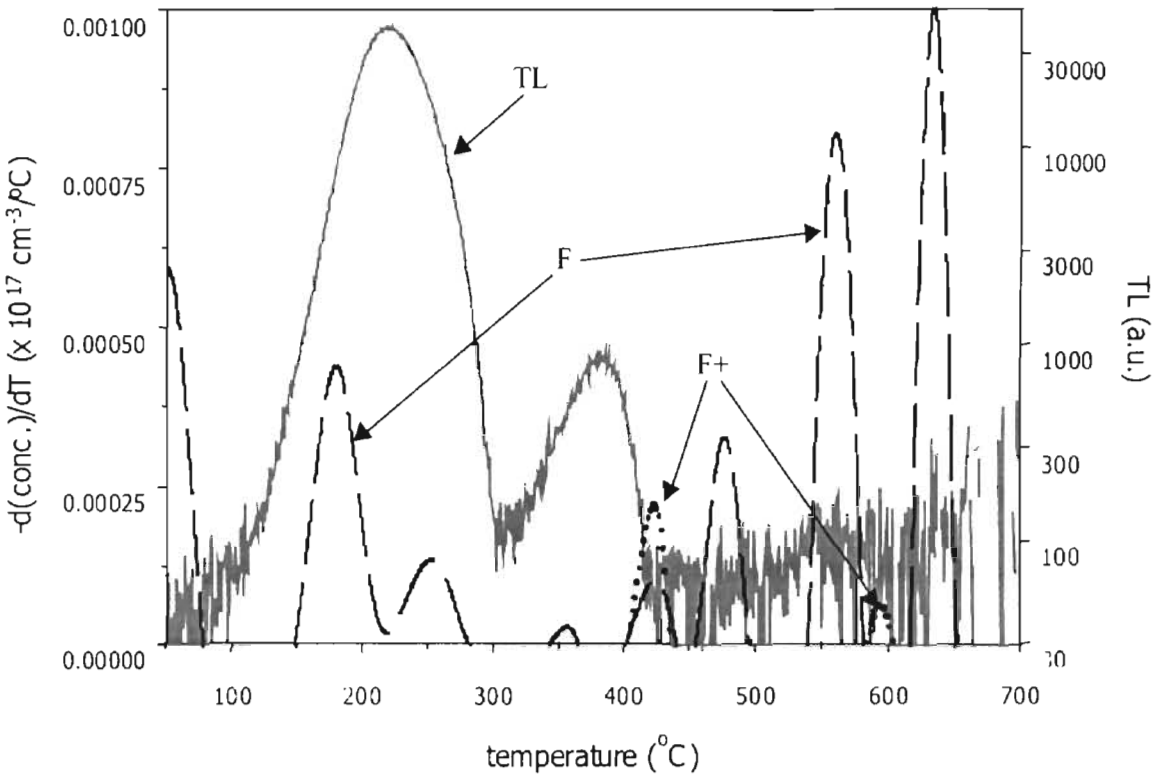

Figure 4.12: Comparison of TL intensity (solid gray) and the negative derivative of the concentration of recombination centers for Mg-6. The 210 °C TL peak is compared to recombination of holes with F centers (dashed lines). The 375 °C TL peak is not seen to correlate to recombination at F and F+ centers. Changes in F and F+ (dotted lines) center concentrations at higher temperatures are not seen to correlate to any TL peaks.

proportional to the temperature for H-1 and Mg-3. However, we cannot draw a definite conclusion as to the temperature dependence of the charge mobility since we do not know the details of the individual TL peaks that make up the overall TL peaks.

The change in the F+ center concentration is shown to correlate well to the TL peaks in samples H-1, Mg-1, and Mg-3. However, the TL peaks and the changes in F+ center concentration are not seen to correlate well for Mg-6. From the results of samples H-1, Mg-1, and Mg-3, we see that the TL peaks are made up of a distribution of both hole and electron recombination processes giving rise to both F and F+ center emission. This leads to the conclusion that both holes and electrons are being released and radiatively recombining to produce the TL peaks. Therefore, we can see that the TL peaks in Al_2O_3:C can not be accurately analyzed by the simple first, second, or general order techniques discussed in chapter 2. Instead the peaks would need to be deconvolved into the smaller peaks produced by each individual recombination process that makes up the overall TL peak. This is consistent with the conclusions of Agersnap Larsen et. al. [4.1] and Walker et. al. [4.2]. The concentration of the F and F+ centers showed an anti-correlation during heating. However, the size of the changes in the F and F+ centers was not always equal. We see from this that recombination processes other than the ones described by equations 2.33 and 2.34 are occurring in the samples. This might be explained by equation 4.6 and 4.7. These equations present the idea that recombination at centers other than F or F+ centers can take place within the samples to produce an F or F+ center. If these processes were to take place, the concentration of one center would increase without the concentration of the other decreasing. In all of the samples we saw the TL peaks occurring at higher temperatures than the concentration derivative peaks.

This might also be caused by recombination processes such as the ones given by equations 4.6 and 4.7 occurring in the samples that are adding the TL peaks. This leads to the conclusion that recombination at centers other than F and F+ centers are occurring or perhaps energy from recombination at an unknown center is being transferred to the F center to produce F center emission when it relaxes. Also, just as likely is the possibility that energy is transferred to the F+ center to produce F+ center emission when it relaxes. The exact nature of any recombination process other than the ones studied in this research are not known at this time, and any statement made about these processes is merely a suggestion.

4.5 Further Work

The results presented in this thesis lead to the conclusions that although the primary recombination processes involve electron and hole recombination with F and F+ centers respectively, alternative processes must also be taking place during TL. To gain a complete understanding of the recombination process in Al_2O_3:C, these alternative processes must be identified. To do this, it would be important to measure the emission spectrum of Al_2O_3:C from room temperature to 700 °C. This would give more evidence of the type of recombination process occurring for the higher temperature TL peaks. Also, the emission in over a broader range of emission wavelengths would be helpful in determining other types of recombination processes occurring during TL. It would also, to perform simultaneous measurements of TL and optical absorption. This might resolve any differences in the heating rate that might occur between two separate measurements.

Bibliography

[1.1] McKeever S.W.S, *Thermoluminescence of Solids*, Cambridge University Press (1985), Cambridge U.K.

[1.2] Horowitz Y., *Thermoluminescence and Thermoluminescent Dosimetry*, vol. 2, CRC Press (1984), Boca Raton Florida.

[1.3] McKeever S.W.S., Mosovitch M., Townsend P.D., *Thoermoluminescence Dosimetry Materials: Properties and Uses*, Nuclear Technology Publishing (1995), Ashford England.

[1.4] Akselrod M.S., Kortov V.T., Gorelova E.A., Rad. Prot. Dosim., **47**, 159-164 (1993).

[1.5] McKeever S.W.S., Akselrod M.S., Colyott L.E., Agersnap Larsen N., Polf J.C., Whitley V, Rad. Prot. Dosim., **84** No. 1-4, 163-168 (1999).

[2.1] Barr L.W., Lidiard A.B. (1970), Physical Chemistry – an Advanced Treatise, **10,** 165, Academic Press, New York.

[2.2] Randall J.T. and Wilkins M.H.F., Proc. Roy. Soc. London, **A184**, 366 (1945).

[2.3] Chen R. and S.W.S. McKeever, *Theory of Thermoluminescence and Related Phenomena*, World Scientific Publication, Singapore (1997)

[2.4] Bohm M. and Scharman A., Phys. Stat, Sol., (a) **4**, 99 (1971).

[2.5] Chen R., Kriastianpoller N., Davidson Z., and Visocekas J., Lumines., **23**, 293, (1981).

[2.6] Garlick G. F. J. and Gibson A. F., Proc. Roy. Soc. London, **A60**, 574 (1945b).

[2.7] Rasheedy M.S., J. Phys.: Condensed Matter, **5**, 633 (1993).

[2.8] Zambuoro M., *Semiconductor Devices*, McGraw-Hill Book Company (1989), New York New York.

[2.9] Stoneham A.M. and Hayes W., *Defects and Defect Processes in Nonmetallic Solids*, Wiley Interscience Publications, New York City, New York (1985).

[2.10] Levy P.W., Phys. Rev., **123**, 1226-1233 (1961).

[2.11] Summers G. P., Rad. Prot. Dosim., **8** No. ½, 69 (1984).

[2.12] Akselrod M.S., Agersnap Larsen N., Whitley V., McKeever S.W.S., Journ. App. Phys., **84** No. 6, 3364 (1998).

[2.13] Kotov V.S., Milman I.I., Kirpa V.I., Lesz J., Rad. Prot. Dosim., **55** 279 (1994).

[2.14] Kitis G., Papadopoulus S., Charalambous S., Tuyn J., Rad. Prot. Dosim., **55** 183 (1994).

[2.15] Agersnap Larsen N., Doctorate of Philosophy Thesis, Niels Bohr Institute, University of Copenhagen (1997).

[2.16] Evans B.D. and Staplebrook M., Phys. Rev. B, **18** No. 12, 7089 (1978).

[2.17] Summers G.P., Advances in Ceramics: Structure and Properties of MGO and Al_2O_3 Ceramics, **10**, 25 (1983).

[2.18] Lee K.H. and Crawford J.H. Jr., Phys. Rev. B, **15** No. 8, 4065 (1977).

[2.19] Akselrod M.S. and Goreleva E.A., Nucl. Tracks Radiat. Meas., **21**, 143 (1993).

[2.20] Whitley V.H., Doctorate of Philosophy Thesis, Oklahoma State University, (2000).

[3.1] Kulis P.A., Springs M.J., Tale I.A., Vainer V.S., Valbis J.A., Phys. Stat. Sol. (b), **104**, 719 (1981).

[3.2] Bøtter-Jensen L., Nucl. Tracks Radiat. Meas., **14**, 177 (1988).

[3.3] Bohm M. and Shcarmann A., Phys. Stat. Sol. (A), **4**, 99 (1971).

[4.1] Agersnap Larsen N., Bøtter-Jensen L., McKeever S.W.S, Rad. Prot. Dosim., **84** No.1-4, 87 (1999).

[4.2] Walker F.D., Colyott L.E., Agersnap Larsen N., McKeever S.W.S., Rad. Meas., **26** No. 5, 711 (1996).

[4.3] Rose A., *Concepts in Photoconductivity and Allied Problems*, Interscience (1963), New York.

[4.4] Lax M., Phys. Rev., **119**, 1502 (1960).

[4.5] Whitley V.H., and McKeever S.W.S., Journ. App. Phys., **87** no. 1, 249 (2000).

[4.6] Agersnap Larsen N., McKeever S.W.S., private communications, 1999-2000

VITA

Jerimy Clifford Polf

Candidate for the Degree of

Masters of Science

Thesis: THE ROLE OF OXYGEN VACANCIES IN THERMOLUMINESCENCE PROCESSES IN Al_2O_3:C

Major Field: Natural and Applied Sciences

Biographical:

Personal Data: Born in Liberal, Kansas, on June 30, 1974, the son of Dewey and Sherrilyn Polf.

Education: Graduated from Liberal High School, Liberal Kansas in May 1992; received Bachelors of Science degree in Applied Physics form Oklahoma State University, Stillwater, Oklahoma in May 1998. Completed the requirements for the Masters of Science degree with a major in Photonics at Oklahoma State University in May 2000.

Experience: Employed in the field of construction from 1992 until 1994 and due to this experience decided to go to college. Employed as an undergraduate Physics teaching and research assistant from 1996 to 1997, and a graduate research assistant for Dr. Stephen McKeever from 1998 to present.

Professional Memberships: Optical Society of America, Society of Physics Students, Phi Kappa Tau National Fraternity, and the Stillwater "Groovers."